Polish Academy of Sciences
Institute of Physics

Piotr Sankowski

THEORY OF SPIN-DEPENDENT PHENOMENA IN LAYERED STRUCTURES BASED ON (Ga,Mn)As

Ph.D. Dissertation

Supervisor
dr hab. Perła Kacman
Institute of Physics
Polish Academy of Sciences

May 2008

Author's declaration

Aware of legal responsibility I hereby declare that I have written this dissertation myself and all the contents of the dissertation have been obtained by legal means.

Date Author's signature

Supervisor's declaration

This dissertation is ready to be reviewed.

Date Supervisor's signature

Pracę tą dedykuję
Uli.

Contents

Chapter 1

Introduction

Gallium arsenide doped with manganese is a flag member of the group of semiconductors which at low temperatures exhibit ferromagnetism. These so called diluted ferromagnetic semiconductors are mainly III-V compounds with part of the cations substituted by magnetic ions. Since the discovery of such materials at the 90-ties of previous century, the ferromagnetic p-type (Ga,Mn)As is by far the most studied and best understood. For (Ga,Mn)As also the highest temperature of the transition to the ferromagnetic phase (173 K) has been achieved [70].

In this dissertation we present a theory, which allows to describe the interlayer coupling between the (Ga,Mn)As layers as well as the spin-dependent transport in all-semiconductor magnetic tunnel junctions (MTJ). In the diluted ferromagnetic semiconductor (Ga,Mn)As the ferromagnetism is hole-mediated and results from energy gain upon the redistribution between hole spin sub-bands [16]. Thus, the whole complexity of the (Ga,Mn)As valence bands resulting from strong spin-orbit interactions has to be taken into account in the calculations of the band spectrum of these multilayers. In our model a multi-orbital empirical tight-binding approach is used to describe correctly the band structure and energy spectrum in the studied multilayer systems. In contrast to the standard $k \cdot p$ method [53, 8], this theory allows to describe properly the band dispersion in the entire Brillouin zone as well as the interfaces and inversion symmetry breaking.

1.1 Interlayer Exchange Coupling

The discovery of the interlayer exchange coupling (ICE) is inherently connected with the discovery of gigantic magnetoresistance (GMR) effect. The GMR effect manifests itself as decrease in electrical resistance in the presence of a magnetic field [2]. However, the origin of this phenomena was latter [52] credited to the previously discovered [25] interlayer exchange coupling. The IEC structures are usually composed

out of two magnetic layers separated by nonmagnetic spacer. The interlayer exchange coupling leads to a spontaneous antiferromagnetic or ferromagnetic ordering of the magnetic layers. In the case of GMR effect, the magnetic layers are antiferromagnetically coupled by ICE, but when an external magnetic field is applied both layers align with the field and the device resistance decreases, as shown on Fig. 1.1.

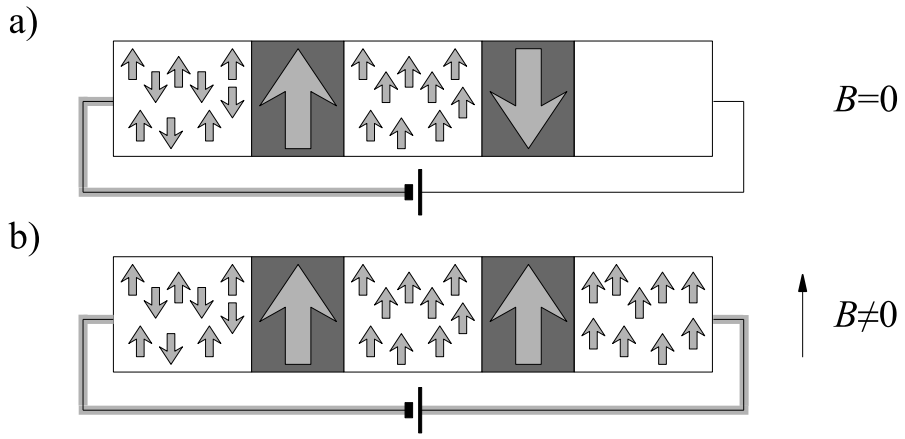

Figure 1.1: GMR device with ferromagnetic layers in (a) the antiferromagnetic spontaneous configuration (b) the ferromagnetic configuration in non-zero magnetic field. In a) the spin-polarized current cannot pass through the magnetic layers and the device resistance is higher.

In order to quantify the above effect the magnetoresistance ratio has been introduced. In the literature the ratio is given in two different ways as shown in the next equations. The optimistic GMR ratio is given as:

$$GMR_o = \frac{R_{AFM} - R_{FM}}{R_{FM}} = \frac{I_{FM} - I_{AMF}}{I_{AFM}}, \tag{1.1}$$

where R_X denotes resistance of configuration X or I_X denotes current flowing through the device in configuration X. In contrast the pessimistic GMR ratio is defined as:

$$GMR_p = \frac{R_{AFM} - R_{FM}}{R_{AFM}} = \frac{I_{FM} - I_{AMF}}{I_{FM}}. \tag{1.2}$$

Throughout this dissertation we use only the first optimistic definition of MR. When needed the pessimistic ratio can be derived using the following equality:

$$GMR_o = \frac{1}{1 - GMR_p} - 1. \tag{1.3}$$

The structures considered in [25, 2] are all metallic, and so have a high density of states on Fermi level. In such a case the dominant contribution to the IEC comes from magnetic "information" transfer via electrons in the spacer layer. This mechanism is analogical to the mechanism responsible for the RKKY interactions,

which lead to the spin dependent changes of the density of states due to the quantum interference of conduction electron waves [9]. It has been also proven that similar mechanism, however mediated by valence-band electrons, leads to long range magnetic correlations also when there are no free carriers in the system [4]. The IEC transmitted by valence-band electrons, determined within this model, correlates antiferromagnetically the spins at the two interfaces bordering each nonmagnetic layer of the SL. According to the experimental findings, such spin-spin interactions cause zero net magnetic moment in the case of AFM EuTe/PbTe SL [37] and an AFM coupling between successive FM EuS layers in EuS/PbS SL [35, 65]. The strength of the IEC diminishes quickly (exponentially) with the distance between the spins, i.e., with the thickness of the nonmagnetic spacer layer and actually doesn't depend on the magnetic layers' thickness. In Refs [65] and [11] a thorough examination of the experimental results, especially of the temperature and magnetic field dependence of the SQUID magnetization, guided the authors to the conclusion that such IEC describes correctly all the neutron-scattering and magnetic observations in EuS/PbS structures with ultrathin (ca 1.2 nm thick) PbS spacers. The traces of the coupling observed by neutron scattering in samples with relatively thick spacers have been noted. However, the coupling has been accredited to the weak but slowly decomposing contribution from the dipolar interactions [35, 11].

In contrast, in the (Ga,Mn)As-based semiconductor ferromagnetic/nonmagnetic systems interlayer coupling of opposite FM sign was observed. Similar results have been obtained by different means: by magnetic measurements [1, 12, 14], neutron diffraction [67] and polarized neutron reflectometry [36]. The (Ga,Mn)As-based structures are very different from EuS-based structures. First of all, in contrast to the simple rock-salt crystal structure of EuS-based SL, they crystallize in zinc blende structure. Moreover, PbS is a narrow gap, whereas EuS is a wide gap semiconductor. In EuS/PbS SL the spacer layers form deep wells in the energy structure of the multilayer – here, the band structures of the magnetic ((Ga,Mn)As) and nonmagnetic (GaAs, (Al,Ga)As) materials are either very similar or the spacer layers introduce potential barriers for the carriers. It should be noted, however, that in EuS-based structures the wider energy gap of the spacer material does not lead to different character of IEC, but results only in a reduction of the coupling' strength and range. This was shown by theoretical studies of the coupling between EuS layers separated by YbSe and SrS insulators [58] and confirmed by neutron reflectivity experiments in EuS/YbSe SL [34]. Finally, the system is no longer a magnetic electrically neutral semiconductor, but diluted magnetic semiconductor, where the ferromagnetism is carrier-induced [16] and requires a large concentration of holes. This and all other differences may considerably affect the IEC and lead to the observed IEC sign.

In Refs [1] and [12] the observed much weaker IEC in samples with high (30%) Al content in the (Al,Ga)As spacer led the authors to the conclusion that the coupling between the FM layers is mediated by the carriers in the nonmagnetic layer. Recently,

it was also shown that introducing extra holes by Be-doping of the GaAs spacer increases the interlayer coupling [14]. In order to explain the spin correlations between (Ga,Mn)As layers the RKKY mechanism and the models tailored for metallic systems were invoked in Refs. [32, 6].

1.2 Magnetic Tunnel Junctions

In early 1970s Tedrow and Meservey [69] showed a possibility of spin sensitive transport between two ferromagnetic (FM) films resulting from the spin conservation in electron tunneling. Soon after Jullière put forward a quantitative model, in which the resistance of a tunnel junction consisting of two FM layers separated by a thin insulator depended strongly on the relative orientation of the magnetizations in the FM leads, i.e., the tunnel magnetoresistance (TMR) effect was discovered [31]. These two findings started intensive experimental and theoretical studies of the spin tunneling and showed its tremendous potential for applications as, e.g., nonvolatile magnetic memory elements, read heads, field sensors and other spintronic devices. At the end of the century the efforts paid off with high TMR values at room temperature achieved repeatable in various trilayer structures of metallic ferromagnets [47, 54] and with fabrication of magnetic tunnel devices [5, 71]. Despite these achievements, several features of spin polarized tunneling remain not fully explained up to now. In particular, a rapid decrease of TMR with increasing bias voltage, which hampers the functionality of the devices, is observed in all FM metal/insulator tunnel junctions – this so called "bias anomaly" was not implied by the simple Jullière model and although many different phenomena (like the emission of magnons or scattering at impurities or defects) were invoked to account for the effect, none of these attempts was fully conclusive [47, 17]. The MR ratio (1.1) defined for GMR is used in analogical way for the TMR effect, and again we use here only the optimistic definition.

In contrast to the metalic structures all-semiconductor magnetic tunnel junctions offer potential for precise control of interfaces and barrier properties, particularly in the case of III-V compounds, for which epitaxial growth of complex heterostructures containing ferromagnetic (Ga,Mn)As or (In,Mn)As layers is especially advanced [44]. Intensive studies of such multilayers with modulated magnetization have proven that most of the phenomena essential for realizing functional spintronic devices can be observed also in these all semiconductor MTJs. The III-V ferromagnetic *p*-type semiconductor (Ga,Mn)As with its high spin polarization [16] appeared to b the most promising material. First of all an efficient electrical injection of spin polarized carriers – spin injection from *p*-(Ga,Mn)As into non-magnetic semiconductor has been achieved for spin polarized holes [49]. Later, injection of spin polarized electrons was demonstrated by employing interband tunneling from the valence band of (Ga,Mn)As into the conduction band of an adjacent *n*-GaAs in a Zener-Esaki

diode [40, 29, 39]. Recently, a very high spin polarization of the injected electron current (*ca* 80%) was obtained in such devices [18, 39]. Moreover, many other phenomena related to spin-dependent tunneling were observed in (Ga,Mn)As-based structures, e.g., the spin-dependent resonant tunneling [48] and the tunneling magnetoresistance (TMR) effect. The research on TMR was carried out by various groups and resulted in an increase of the observed TMR ratio from about 70% reported by Tanaka and Higo [68] to values higher than 250% [45, 13, 21]. Both effects, the TMR and the spin polarization of tunneling current in the Zener-Esaki diode in the GaMnAs-based structures exhibit the same phenomena observed previously in metallich TMR structures – "bias anomaly", i.e., the rapid decrease with the increase of the applied bias. Recently, it was also reported that the magnetoresistance of the (Ga,Mn)As-based tunnel junctions is very sensitive to the direction of applied magnetic field. This so called tunnel anisotropic magnetoresistance (TAMR) effect was observed when the saturation magnetization direction was changed in-plane [24, 55, 22], as well as when it was turned perpendicular to the magnetic layer [22, 23].

1.2.1 Zener-Esaki Diode

For the design and fabrication of novel spintronic devices, a detailed understanding of spin polarized Zener tunneling in (Ga,Mn)As-based semiconductor heterostructures is of primary importance. In the design of spintronic devices, the *p*-type character of (Ga,Mn)As introduces a disadvantage due the low hole spin lifetimes in GaAs. In order to obtain a spin polarized electron current using the *n*-type (Ga,Mn)As an inter-band tunneling is needed [41, 30]. Recently, a very high spin injection, about 80%, has been observed in especially tuned and fabricated Zener-Esaki diode [18]. The details of the structure is shown in Table 1.1. The stacking direction is [001].

Thickness	Material	Doping
20 nm	$Ga_{0.92}Mn_{0.08}As$	p= 3.5×10^{20}cm^{-3}
9 nm	GaAs	n= 9×10^{18}cm^{-3}
90 nm	$Al_xGa_{1-x}As$	n= 1×10^{17}cm^{-3}
100 nm	GaAs	p= 2×10^{18} cm^{-3}
200 nm	$Al_{0.3}Ga_{0.7}As$	p= 2×10^{18}cm^{-3}
1 μm	GaAs	p= 1×10^{18}cm^{-3}
Substrate	GaAs	p= 1×10^{18}cm^{-3}

Table 1.1: The spin-LED structure along stacking direction [001].

The structure is composed out of two diodes, the Zener-Esaki diode serves as an injection device, whereas the second LED diode serves as an spin detector as shown on Fig. 1.2 a. In such a device the current starts flowing after the Zener voltage is reached, see Fig. 1.2 b.

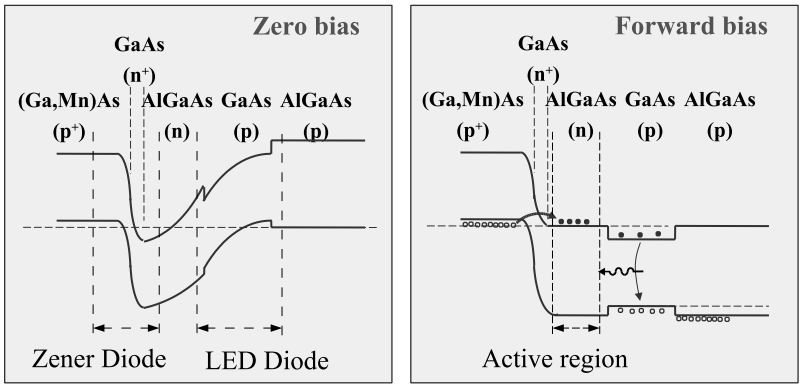

Figure 1.2: The schematic view of the band structure of the spin-LED structure for a) zero bias b) for Zener bias.

We can derive the current spin polarization out of the emitted light polarization. In this structure, the Al-concentration in the spin-drift region was engineered together with the doping concentration in order to provide an effective barrier for the holes, such that carrier generation due to impact ionization was eliminated at low bias. The observations of the spin polarization and the current versus the applied bias voltage are summarized in Fig. 1.3(a) and 1.3(b), respectively. We see that the degree of spin polarization in the injected current depends strongly on the applied bias. This effect hampers the functionality of this spintronic device as obtaining high current that would be spin polarized is difficult.

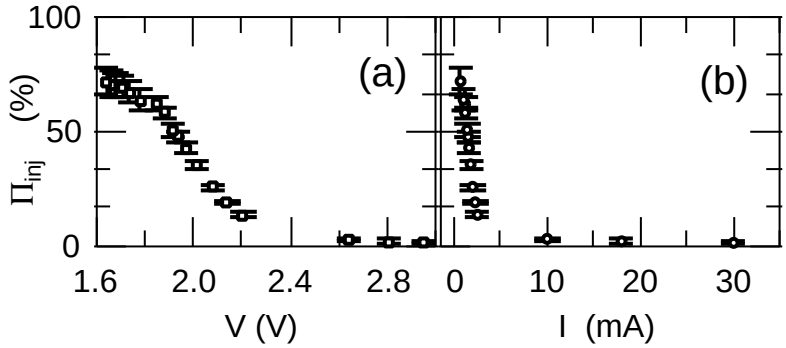

Figure 1.3: The degree of injected spin polarization measured at 4.6 K as a function of the applied bias voltage (a) and the current (b) from Ref. [18].

It should be noted that in this experiment the magnetization direction points slightly out of plane (27°), because the experiment is performed in the presence of field. The non-zero out of plane magnetic field is applied in order to force the electrons' spins to rotate by 90° in the LED diode. This is forced by the selection rules in the quantum well, because otherwise the emitted light would lose the spin information. The situation is schematically presented in the following figure.

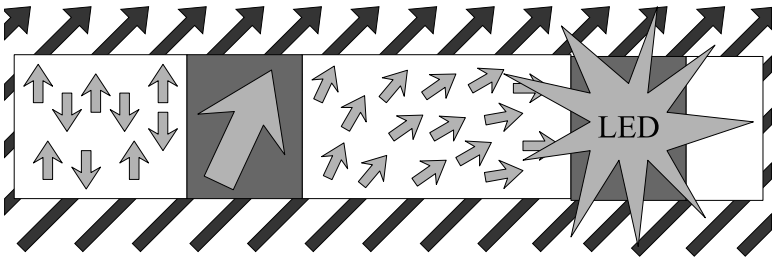

Figure 1.4: The experiment from Ref. [18] is carried out in the presence of non-zero magnetic field in order to force the electrons' spins to rotate when they reach the LED diode.

The Esaki-Zener diode besides serving as a spin injection device exhibits tunneling anisotropic magnetoresistance effects, i.e., when the magnetization direction in the spin injecting (Ga,Mn)As is changed the height of the tunneling current changes as well [18, 23]. The both effects are schematically shown on the following figure.

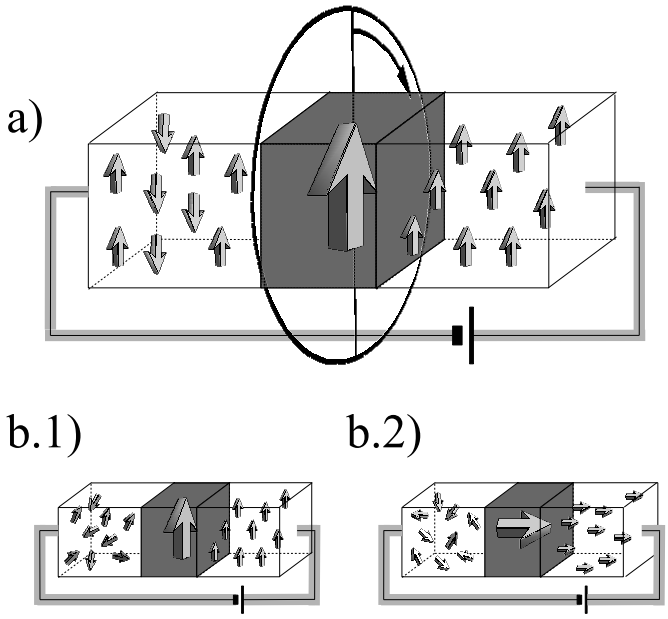

Figure 1.5: In the in-plane tunneling magnetoresistance in Esaki-Zener diode (a) the magnetization direction is rotated in the structure plane. In the perpendicular TAMR the currents in in-plane spontaneous configuration b.1) and perpendicular configuration b.2) are compared.

In the case of in-plane TAMR when rotating the magnetization direction we determine the minimum R_{min} and the maximum R_{max} resistance of the structure, which are used to determine the TAMR ratio. In contrary in perpendicular TAMR the resistance R_0 in the in-plane spontaneous configuration and the resistance $R_{H_\perp}$

in perpendicular configurations is used. The in-plane TAMR ratio is defined as:

$$TAMR_{\parallel} = \frac{R_{max} - R_{min}}{R_{min}}, \tag{1.4}$$

The perpendicular TAMR is given as:

$$TAMR_{\perp} = \frac{R(H_{\perp}) - R(0)}{R(0)}. \tag{1.5}$$

The perpendicular TAMR in Esaki-Zener diode was observed by Giraud *et al.* [23] and the seen magnitude of the effect was 20% and decreasing with applied bias. Some observation of the in-plane TAMR were pervormed by Van Dorpe *et al.* [19] and have shown a difference of several percents between the [110] and [1$\bar{1}$0] axis.

1.2.2 Tunneling Magnetoresistance

The typical tunneling magnetoresistance (TMR) devices consist of a trilayer structure with two interfaces, for instance, two magnetic p-type $Ga_xMn_{1-x}As$ contacts separated by a nonmagnetic GaAs barrier. In such structures a strong TMR effect, *i.e.*, a large difference in the resistance of the device for two configurations: parallel (ferromagnetic – FM) and the antiparallel (antiferromagnetic – AFM) alignments of magnetizations in the contacts, has been observed. The TMR device is schematically presented on Fig. 1.6.

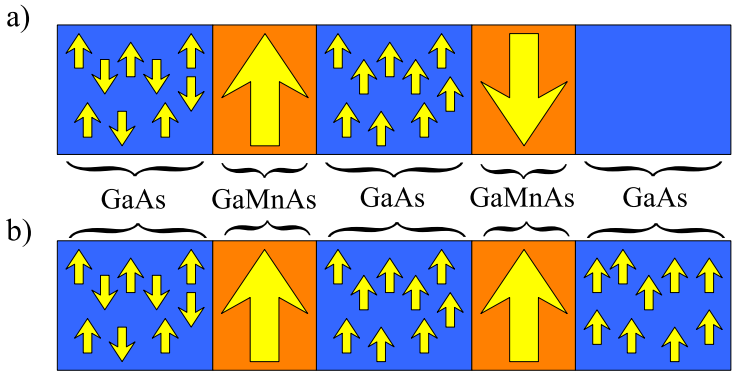

Figure 1.6: The scheme of TMR device for a) AFM configuration and b) FM configuration. Due to the mismatch of magnetization directions in AFM configuration the device exhibits higher resistance.

One should note that the GaAs spacer forms a barrier for holes originating from (Ga,Mn)As due to the materials band offsets. Hence, indeed for (Ga,Mn)As/GaAs/(Ga,Mn)As trilayers we deal with tunneling effect. This is the case for AlAs spacer as well as AlAs forms even a higher barrier. The exact band offsets are presented in details on Fig 1.7.

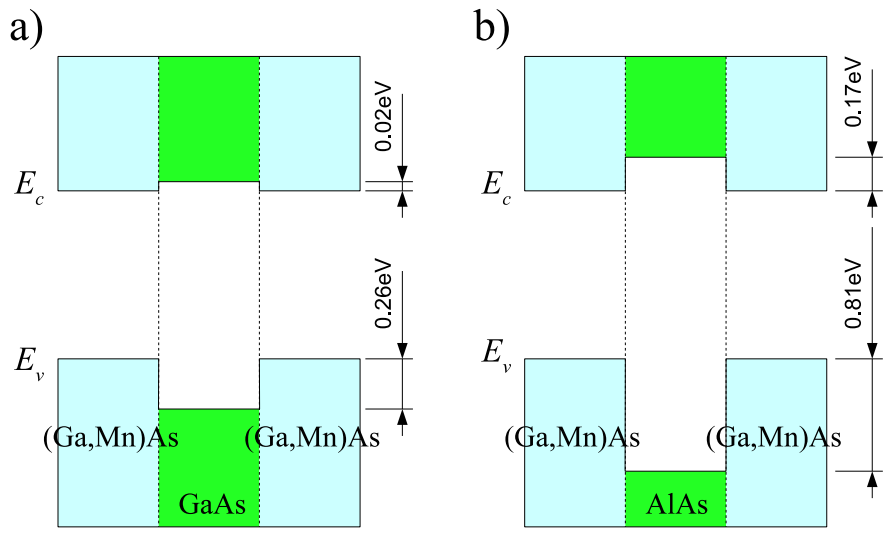

Figure 1.7: The schematic band structure of the (Ga,Mn)As/GaAs/(Ga,Mn)As (a) and (Ga,Mn)As/AlAs/(Ga,Mn)As (b) heterostructures for the hole concentration $p = 3.5 \times 10^{20}$ cm^{-3}.

The TMR value is usually described by so called TMR ratio, which is defined in the following way

$$\mathrm{TMR} = \frac{R_{\mathrm{AFM}} - R_{\mathrm{FM}}}{R_{\mathrm{FM}}}, \tag{1.6}$$

where R_{FM} and R_{AFM} are the structure resistances for the FM and AFM configuration, respectively. The ratio capture the relative change in resistance between AFM and FM configuration and similarly to the gigantic magnetoresistance effect we assume here the optimistic view.

A very large in-plane anisotropic tunneling magnetoresistance was observed in Refs. [24, 55, 22]. However, the large magnitude of the effect has been attributed to the insulator-metal transition taking place in the sample when the magnetization vector was rotated. Moreover, these observation seem to be hard to reproduce. Simultaneously a very small TAMR effect has been observed by other groups [57].

1.3 Overview

The aim of this dissertation is the development of the model capable to describe the spin effects in materials based on (Ga,Mn)As. Due to several reasons we have chosen tight-binding framework to work with. Within the tight-binding approach it is possible to take into account all the effects that play role on the interfaces, in particular the Rashba and Dresselhaus terms, which are very important for spin transport and spin tunneling [60]. Due to strong spin-orbit mixing one can expect in (Ga,Mn)As-based structures the spin diffusion length to be shorter and comparable to the phase coher-

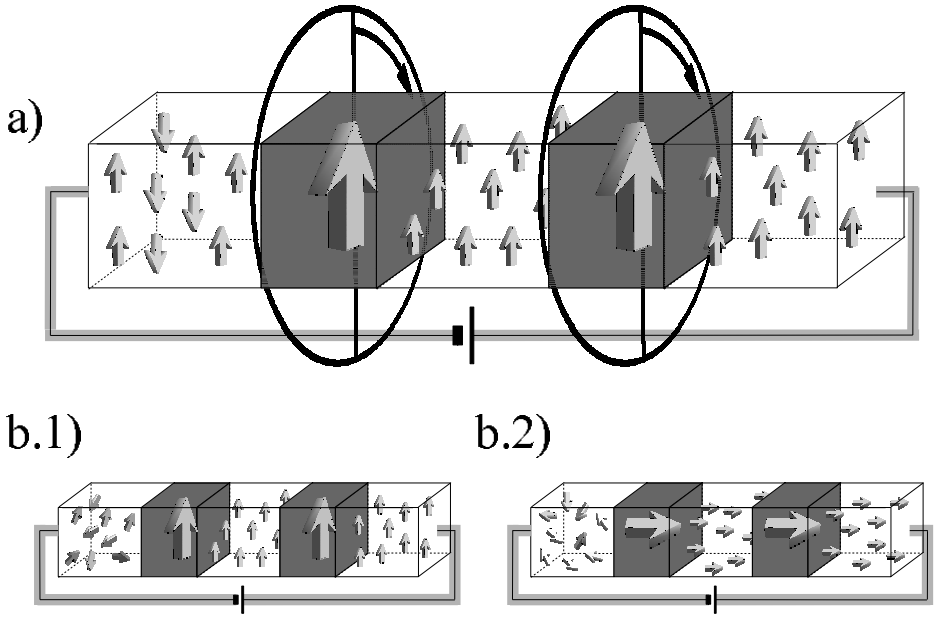

Figure 1.8: In the in-plane tunneling magnetoresistance (a) the magnetization direction is rotated in the structure plane. In the perpendicular TAMR the currents in in-plane spontaneous configuration b.1) and perpendicular configuration b.2) are compared.

ence length. This makes the models based on the diffusion equation, which describe well the spin tunneling phenomena in metallic junctions, non applicable to the structures consisting of (Ga,Mn)As layers. Thus, to describe the spin-dependent tunneling in various (Ga,Mn)As-based semiconductor heterostructures with modulated magnetization we consider vertical spin coherent transport within the Landauer-Büttiker formalism. The model disregards disorder and effects of carrier–carrier interactions, so that it is applicable to the carrier density range and length scales, where localization effects are unimportant. Additionally, in the cases when carrier relocation may play important role we enhance the model with the self-consistent procedure in order to compute band profiles in the structures.

This dissertation is structured as follows. In the next chapter we introduce our model. We start by presenting the tight-binding approach in Chapter 2. In this chapter the model is formulated using cyclic boundary condition and all details needed for (Ga,Mn)As based heterostructures are reviewed. In particulary we present our approach for modeling ferromagnetism in diluted magnetic semiconductor (Ga,Mn)As. The next chapter is devoted to the interlayer exchange coupling which is the first application of our model. The 3 chapter is devoted to the Landauer-B uticcker formalism. This time we use the formulation of the tight-binding model for open boundary condition as needed in tunneling structures with two interfaces. Moreover, we extend the model with the self-consistent procedure. The next two chapters present the results

obtained within the tunneling model. In Chapter 5 we consider Zener-Esaki tunneling diode, whereas in Chapter 6 we cope with TMR structures.

Chapter 2

Tight-Binding Method

Tight-binding model is one of the most basic approaches that allows to determine the energy band structure in solid state. This calculated dispersion relations for electron and holes can be later used to determine other material properties. The method was developed as an *ab-initio* procedure and its application shed new light on several physical phenomena. Later, new *ab-initio* methods have been created, which deliver more accurate results. Astonishingly, the tight-binding model has not been abandoned, but the development of new methods allowed to apply it to a wider spectrum of problems. This was possible due to the creation of the semi-empirical version of this method. In the *semi-empirical* method we set some values of the model to be free parameters, instead of obtaining them from calculations within the model. These parameters are determined from other *ab-initio* calculations or are taken from experiments. This approach would be useless, unless the tight-binding model had the following advantages:

- it is physically transparent;
- it is computationally efficient.

This allows us to incorporate into the model new effects and easily use the parameters coming from different calculations within it. The parameters can be taken from other more accurate models and then used in more complex calculations, which would not be possible in the original model. Additionally, the model automatically describes interaction of electrons with crystal lattice in its whole complexity, i.e.:

- describes well the interfaces and their symmetry,
- includes Rashba and Dresselhaus terms,
- takes into account the whole Brillouin zone.

In our calculations we are studying structures where the symmetry is broken along the z axis whereas along axes x and y a translational symmetry is present. Moreover, we are considering two types of boundary conditions for the z axis:

- cyclic boundary conditions,
- open boundary conditions, i.e, structures between two half infinite leads.

Dependently on the type of boundary conditions the details of the tight-binding model have to be slightly modified due to different quantum numbers needed to describe the wave functions. In the case of cyclic boundary conditions the wave functions are described by the wave vector $\mathbf{k}$ and function number n, whereas when open boundary conditions are present we need to use in-plane wave vector $\mathbf{k}_{\parallel}$ and energy E. In this chapter we describe the tight-binding description in the case of cyclic boundary conditions. This formulation is used in order to study interlayer coupling in supperlattices (Chapter 4). However, in the next chapter (Chapter 3) in order to describe tunneling we concentrate on the case of open boundary conditions. Moreover, our self-consistent tight-binding model is developed in the case of open boundary conditions, because we will be later on interested in studying the impact of charge relocation in tunneling structures.

2.1 Tight-binding Model

Let us now present ingredients forming the tight-binding method. Here, we consider the case where the studied structure has translation symmetry along all three axes. A different case in which only two symmetries are present will be considered in Chapter 3. We start by considering the Hamiltonian of electron system in presence of a static ion field:

$$\hat{H} = \hat{T} + V_{ee} + V_{ei}, \tag{2.1}$$

where $\hat{T}$ is kinetic energy operator, V_{ee} is inter-electron interaction potential, and V_{ei} is electron-ion interaction potential. The energy E and the state Φ of the system is given by the eigenvalue equation::

$$\hat{H}\Phi = E\Phi. \tag{2.2}$$

The first step in the construction is a one-election approximation, where we assume that the election interacts with ions and with effective field coming from other electrons. Now, the most important step of the tight-binding method follows. We write the above equation using linear combination of atomic orbitals (LCAO):

$$|\mathbf{k}, n\rangle = \sum_{\alpha} c_{\alpha}^{(n)} |\mathbf{k}, \Psi_{\alpha}\rangle, \tag{2.3}$$

where α is the orbital and atom index in the crystal basis. The functions $|\mathbf{k}, \Psi_{\alpha}\rangle$ are constructed from atomic orbitals Ψ_{α} and they form eigenvectors of $\hat{T}_{\mathbf{R}}$ for lattice vectors $\mathbf{R}$:

$$|\mathbf{k}, \Psi_{\alpha}\rangle = \frac{1}{\sqrt{N}} \sum_{\mathbf{R}} e^{i\mathbf{k}\mathbf{R}} \hat{T}_{\mathbf{R}+\mathbf{b}_{\alpha}} |\Psi_{\alpha}\rangle, \tag{2.4}$$

where $\mathbf{b}_{\alpha}$ is the location of basis atom, whereas N is the number of unit cells. The Schrödinger equation can be now written as:

$$(\hat{H} - E_n(\mathbf{k}))|\mathbf{k}, n\rangle = 0. \tag{2.5}$$

Multiplying this equation by $\langle \Psi_{\beta}, \mathbf{k}|$ we get:

$$\frac{1}{N} \sum_{\mathbf{R},\mathbf{R}',\alpha} c_{\alpha}^{(n)} e^{i\mathbf{k}(\mathbf{R}-\mathbf{R}')} \langle \Psi_{\beta} | \hat{T}_{-\mathbf{R}'-\mathbf{b}_{\beta}} (\hat{H} - E_n(\mathbf{k})) \hat{T}_{\mathbf{R}+\mathbf{b}_{\alpha}} |\Psi_{\alpha}\rangle = 0. \tag{2.6}$$

Using invariance of the above equation for the basis vectors:

$$\sum_{\mathbf{R},\alpha} c_{\alpha}^{(n)} e^{i\mathbf{k}\mathbf{R}} \left(\langle \Psi_{\beta} | \hat{T}_{-\mathbf{b}_{\beta}} \hat{H} \hat{T}_{\mathbf{R}+\mathbf{b}_{\alpha}} |\Psi_{\alpha}\rangle - E_n(\mathbf{k}) \langle \Psi_{\beta} | \hat{T}_{\mathbf{R}+\mathbf{b}_{\alpha}-\mathbf{b}_{\beta}} |\Psi_{\alpha}\rangle \right) = 0. \tag{2.7}$$

Loewdin [42] has shown that the atomic orbitals that are located on the vertices of the lattice can be diagonalized assuring that they maintain their characteristic properties such as magnetic moment. The resulting orbitals $|\Psi'_{\alpha}\rangle$ are not located on a single lattice vertex and are composed of orbitals located on several vertices. Using these orbitals we get (2.7):

$$\sum_{\mathbf{R},\alpha} c_{\alpha}^{(n)} e^{i\mathbf{k}\mathbf{R}} \left(\langle \Psi'_{\beta} | \hat{T}_{-\mathbf{b}_{\beta}} \hat{H} \hat{T}_{\mathbf{R}+\mathbf{b}_{\alpha}} |\Psi'_{\alpha}\rangle - E_n(\mathbf{k}) \delta_{\alpha,\beta} \delta_{\mathbf{R},0} \right) = 0. \tag{2.8}$$

The above equation allows us to write the Schrödinger equation as the matrix eigenvalue equation. The entries of the matrix $\mathcal{H}$ are indexed by α and are defined as:

$$\mathcal{H}_{\beta,\alpha} = \sum_{\mathbf{R}} e^{i\mathbf{k}\mathbf{R}} \langle \Psi'_{\beta} | \hat{T}_{-\mathbf{b}_{\beta}} \hat{H} \hat{T}_{\mathbf{R}+\mathbf{b}_{\alpha}} |\Psi'_{\alpha}\rangle,$$

now the Schrödinger equation becomes:

$$\mathcal{H}\mathbf{c}^{(n)} = E_n(\mathbf{k})\mathbf{c}^{(n)},$$

where $\mathbf{c}^{(n)}$ is the vector of the $c_{\alpha}^{(n)}$ components.

In order to simplify the above equation further we make the following assumptions:

- We include only first neighbor and next neighbor interactions, because interaction with further orbitals is usually less important.
- We include only one $|\Psi'_\alpha\rangle$ orbital for each valence electron. Due to this assumption the model becomes more physically transparent, because obtained states can be decomposed into small number of known orbitals.
- Energetically distant orbitals interact weekly, hence we include only orbitals with energy near Fermi energy. If it is needed one can include other weaker interacting orbitals within perturbation calculus.
- In the effective inter-election potential we include only two-center interactions. The multi-center interactions are neglected as less important.

After above simplifications the matrix $\mathcal{H}$ becomes block-diagonal and allows for much faster and simpler computations than general matrix.

2.2 Semi-empirical Tight-binding Model

Empirical tight-binding method was created by Slater and Koster [63]. Normally all matrix elements $\mathcal{H}_{\alpha,\beta}$ are calculated, but instead they proposed to tread them as system parameters. These parameters can be determined by fitting the tight-binding band structure to the data obtained from other calculations or from experiments. The fitting usually aims to minimize squared error between the bands in several high symmetry points of Brillouin Zone. Before the fitting we have to choose the right set of parameters. The matrix elements are not the right choice because they are not independent. Remember that we have restricted ourselves to the case of two-center interactions. Moreover, the orbitals we use have well defined symmetries and angular momentums, so we can reduce the number of free parameters by introducing interaction integrals $V_{i,j,\lambda}$ depending only on the projection of the angular momentum on the vector connecting the atoms. Using the interaction integrals we can express the matrix elements $\mathcal{H}_{\alpha,\beta}$ for $\alpha = (a, i)$ and $\beta = (b, j)$, where a, b are atom numbers and i, j are orbitals located on atoms a and b. For $i, j \in \{s, p_x, p_y, p_z, d_{xy}, d_{yz}, d_{xz}, d_{x^2-y^2}, d_{3z^2-r^2}, \ldots\}$ the values of overlapping integrals are given in Table 2.1. The numbers l, m, n denote the coordinates of the unit vector pointing the direction between interacting atoms, whereas $\lambda \in \{\sigma, \pi, \delta\}$ denotes the azimuthal quantum number.

Matrix Element	Value
$\mathcal{H}_{s,s}$	$V_{ss\sigma}$
$\mathcal{H}_{s,p_x}$	$l^2V_{pp\sigma} + (1-l^2)l^2V_{pp\pi}$
$\mathcal{H}_{p_x,p_x}$	$lm(V_{pp\sigma} - V_{pp\pi})$
$\mathcal{H}_{s,d_{xy}}$	$\sqrt{3}lmV_{sd\sigma}$
$\mathcal{H}_{s,d_{x^2-y^2}}$	$\frac{\sqrt{3}}{2}(l^2-m^2)V_{sd\sigma}$
$\mathcal{H}_{s,d_{3z^2-r^2}}$	$\left[n^2 - \frac{1}{2}(l^2+m^2)\right]V_{sd\sigma}$
$\mathcal{H}_{p_x,d_{xy}}$	$\sqrt{3}l^2mV_{pd\sigma} + m(1-2l^2)V_{pd\pi}$
$\mathcal{H}_{p_x,d_{yz}}$	$\sqrt{3}lmnV_{pd\sigma} - 2lmnV_{pd\pi}$
$\mathcal{H}_{p_x,d_{x^2-y^2}}$	$\frac{\sqrt{3}}{2}(l^2-m^2)V_{pd\sigma} + l(1-l^2+m^2)V_{pd\pi}$
$\mathcal{H}_{p_y,d_{x^2-y^2}}$	$\frac{\sqrt{3}}{2}(l^2-m^2)V_{pd\sigma} - m(1+l^2-m^2)V_{pd\pi}$
$\mathcal{H}_{p_z,d_{x^2-y^2}}$	$\frac{\sqrt{3}}{2}(l^2-m^2)V_{pd\sigma} - n(l^2-m^2)V_{pd\pi}$
$\mathcal{H}_{p_x,d_{3z^2-r^2}}$	$l\left[n^2 - \frac{1}{2}(l^2+m^2)\right]V_{pd\sigma} - \sqrt{3}ln^2V_{pd\pi}$
$\mathcal{H}_{p_z,d_{3z^2-r^2}}$	$n\left[n^2 - \frac{1}{2}(l^2+m^2)\right]V_{pd\sigma} + \sqrt{3}n(l^2+m^2)V_{pd\pi}$

Table 2.1: The matrix element between chosen orbitals according to Slater and Koster [63], where (l, m, n) is a unit direction vector between interacting atoms (for simplicity we have omitted the atom indexes α and β). The remaining elements can be obtained by permuting l, m, n according with the occurring indexes x, y, z.

2.3 Description of the Structures

In order to construct the empirical tight-binding Hamiltonian matrix for the superlattices consisting of (Ga,Mn)As and (Ga,Al)As one has to start from the description of the constituent materials. In the following, we shorty discuss each of the four steps of the construction:

- description of the non-magnetic materials GaAs, AlAs as well as (Ga,Al)As,
- inclusion of the magnetic properties into the description of GaAs in order to obtain parametrization for (Ga,Mn)As,
- modeling the lattice deformations of the materials,
- construction of the heterostructure matrix from the bulk parameterizations.

2.3.1 Non-magnetic Materials

In order to construct the empirical tight-binding Hamiltonian matrix for the SL one has to describe first the constituent materials, to select the set of atomic orbitals for every type of involved ions and to specify the range of the ion-ion interactions.

	AlAs	GaAs		AlAs	GaAs		AlAs	GaAs
E_s^a	-5.9819	-5.9819	$V_{ss\sigma}$	-1.7292	-1.6187	$V_{s_a d_c \sigma}$	-2.5535	-2.7333
E_s^c	0.9574	0.9574	$V_{s^* s^* \sigma}$	-3.6094	-3.6761	$V_{s_c d_a \sigma}$	-2.3869	-2.4095
E_p^a	3.5826	3.5820	$V_{s_a^* s_c \sigma}$	-1.6167	-1.9927	$V_{s_a^a d_c \sigma}$	-0.8064	-0.6906
E_p^c	6.3386	6.3853	$V_{s_a s_c^* \sigma}$	-1.2688	-1.5648	$V_{s_c^* d_a \sigma}$	-0.7442	-0.6486
E_d	13.0570	13.0570	$V_{s_a p_c \sigma}$	2.5175	2.4912	$V_{p_a d_c \sigma}$	-1.7240	-1.7811
E_{s^*}	19.5133	19.4220	$V_{s_c p_a \sigma}$	2.7435	2.9382	$V_{p_c d_a \sigma}$	-1.7601	-1.8002
$\Delta_a/3$	0.1721	0.1824	$V_{s_a^* p_c \sigma}$	2.1190	2.1835	$V_{p_a d_c \sigma}$	1.7776	1.7821
$\Delta_c/3$	0.0072	0.0408	$V_{s_c^* p_a \sigma}$	2.1989	2.2086	$V_{p_c d_a \sigma}$	2.0928	2.0709
$V_{pp\sigma}$	4.2460	4.4094	$V_{dd\sigma}$	-1.2175	-1.1409	$V_{dd\delta}$	-1.7540	-1.9770
$V_{pp\pi}$	-1.3398	-1.4572	$V_{dd\pi}$	2.1693	2.2030			

Table 2.2: The tight-binding parameters used for GaAs and AlAs, after [28].

Bulk GaAs is tetrahedrally coordinated cubic material in which each cation (anion) is surrounded by four anion (cation) nearest neighbors (NN) along the [1, 1, 1], [1,-1,-1], [-1, 1,-1] and [-1,-1, 1] directions, at the distances $a\sqrt{3}/4$ (where $a = 5.653$ Å is the lattice constant). GaAs is a nonmagnetic, direct gap (1.42 eV) semiconductor with the valence band maximum at the center of the Brillouin zone. The top of the valence band is formed by two twofold degenerate p-bands. The third p-band is separated from the two by spin-orbit splitting, $\Delta_{so} = 0.34$ eV. The AlAs has an indirect bandgap of 2.16 eV with the valence maximum in Γ point and the conduction band minimum in L point. The top of the valence band in AlAs is similarly formed as in GaAs, with slightly smaller spin-orbit splitting, $\Delta_{so} = 0.3$ eV and higher effective hole masses.

For the band structure of bulk GaAs and AlAs the $sp^3d^5s^*$ parametrization with the spin-orbit coupling, proposed by Jancu *et al.* [28], is used. The parametrization includes only the nearest neighbor (NN) interactions. Still, it delivers a quantitatively correct description of the valence bands and the lowest two conduction bands, both in terms of energetic positions and band curvatures. It should be noted that inclusion of the d states in the parametrization is of crucial importance for the conduction bands and allows to obtain composition of the corresponding wave functions in agreement with empirically corrected pseudopotential method in the whole Brillouin zone. The band curvatures that determine the effective masses are crucial for our application of the tight-binding method to compute the tunneling current. The spin-orbit interactions were added to the model by including the contribution from the p valence states.

The band structures of the bulk GaAs and AlAs are presented on Fig. 2.1, whereas the used parameters are given in Table 2.2. For each anion and cation 20 orbitals are used - hence, an GaAs layer (0.28 nm) of the structure is represented by the tight-binding matrix of size 40.

The electric properties of $Al_xGa_{1-x}As$ depend crucially on the chemical com-

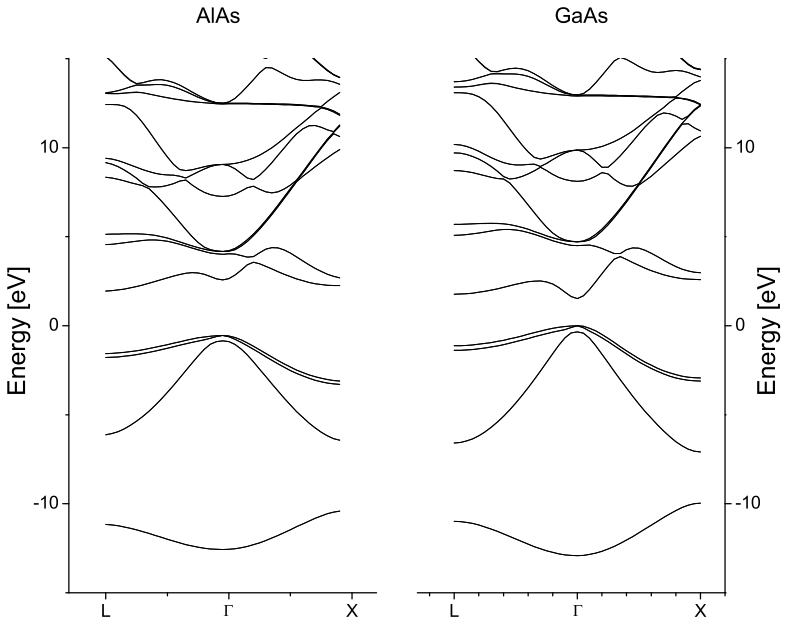

Figure 2.1: The tight-binding bulk band structure of a) GaAs and b) AlAs according to the parametrization given by Jancu *et al.* [28]

position x of the structure. For $x < 0.45$ the material has a direct band-gap, whereas for higher x the bandgap is indirect as in AlAs. Within reasonable limits most of the properties of $Al_xGa_{1-x}As$ depend linearly on x [27]. Hence, we decided to determine the parameters for (Ga,Al)As tri-component crystal within the virtual crystal approximation. In order to obtain the parameters for the cation we take the linear combination of the parameters of Ga in GaAs and Al in AlAs, whereas in order to obtain the parameters of As anion, we mix the parameters for As in GaAs and As in AlAs.

2.3.2 Magnetic Materials

The presence of Mn ions in (Ga,Mn)As is taken into account only by including the *sp-d* exchange interactions within the virtual crystal and mean-field approximations. The values of the exchange constants are determined by the experimentally obtained spin splittings: $N_0\alpha = 0.2$ eV of the conduction band and $N_0\beta = -1.2$ eV of the valence band [50]. As the valence-band structure of (Ga,Mn)As with small fraction of Mn has been shown to be quite similar to that of GaAs [50]. The other parameters of the model for the (Ga,Mn)As material are taken to be the same as for GaAs. The obtained band structure around the Gamma point is presented on Fig. 2.2.

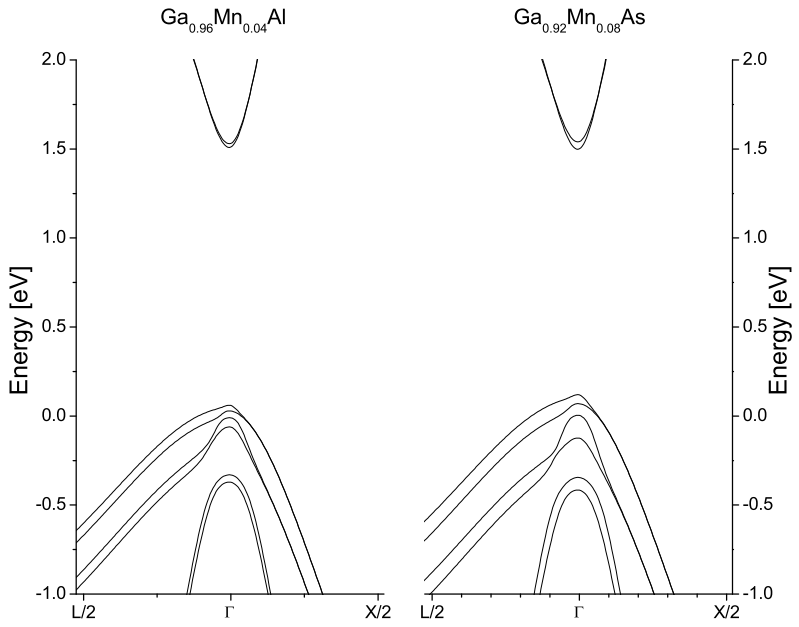

Figure 2.2: The tight-binding bulk band structure of a) $Ga_{0.96}Mn_{0.04}As$ and b) $Ga_{0.92}Mn_{0.08}As$ obtained within mean field and virtual crystal approximation. Magnetization is taken along the [001] direction.

2.3.3 Deformations of the Structures

The above description of the band structure can be easily modified to include deformation. The relations introduced by Harrison [26] allow to determine the tight-binding parameters when the distance between interacting atoms is slightly changed. The parameters scale with k'th power of the distance, where k depends on the angular quantum number of the interacting orbitals. The Harrison formula gives the matrix elements as the function of the distance d between the atoms in the following way:

$$V_{ll'm} = \eta_{ll'm} \frac{\sqrt{r_l^{2l-1} r_{l'}^{2l'-1}}}{m_e d^{l+l'+1}}, \tag{2.9}$$

where $\eta_{ll'm}$ are the universal constants and r_l is the radius of the atomic orbital, which can be determined from the *ab-initio* calculations. This equation allows as to model how the interlayer coupling and tunneling current depend on the lattice deformations and on the applied strain. In order to do this we first determine the orbitals' radii r_l, which can be than used to compute the interaction constant when the interatomic distance has changed. When describing a lattice deformation within the model we assume that the cell volume is constant. Whereas when simulating the impact of external pressure we change the lattice size in all dimensions simultaneously.

2.3.4 Modulated Structures

In the previous section we have shown how the parameters for bulk materials are obtained. However, in the case of modulated structures we have to know the interactions between different materials that constitute the structure. These parameters have to be determined in another way. Moreover, we need to know the relative positions of energy levels in the different materials, i.e., so called band offsets. The usual way of obtaining the inter-material parameters is with use of the Harrison formula (2.9). Note that in order to determine the missing inter-material parameters we only need to get the orbitals' radii r_l. In the case of GaAs/AlAs heterostructures we do not need to use this approach because both materials have a common anion – As and we include only nearest neighbor interactions.

However, this does not solve all of our problems. We still need to determine the relative potential heights in both materials. The band structure due to its nature gives only the information about the energy differences between the bands in the single material. Hence, we need more information from some other source. The general way to solve this problem is to find band structure calculations for a material that has common atoms with both materials in questions. Here, in order to determine the parametrization for GaAs/AlAs heterostructures we use different approach. We modify the parametrization in order to reproduce the experimentally observed [] and theoretically predicted [] band offset. Whereas, for (Ga,Mn)As/GaAs interfaces we

Hole Concentration	e_F
0 cm^{-3}	0 eV
1×10^{19} cm^{-3}	0.071 eV
5×10^{19} cm^{-3}	0.123 eV
1×10^{20} cm^{-3}	0.161 eV
2×10^{20} cm^{-3}	0.200 eV
3.5×10^{20} cm^{-3}	0.260 eV
5×10^{20} cm^{-3}	0.320 eV
8×10^{20} cm^{-3}	0.380 eV
1×10^{21} cm^{-3}	0.430 eV

Table 2.3: The Fermi energy level e_F in p-type $Ga_{0.92}Mn_{0.08}As$. The energy is measured from the top of the valence bands.

assume that the band offsets at the (Ga,Mn)As and GaAs interfaces are induced solely by the spin splittings in the (Ga,Mn)As bands. Again the band offset for structures containing (Al,Ga)As is determined within the virtual crystal approximation.

2.3.5 Fermi Energy in the Materials

The Fermi energy in the constituent materials is determined by summing up the occupied states over the entire Brillouin zone. The number of occupied states is determined by the assumed carrier concentration in the material. Our calculations of the Fermi energy for various hole concentrations are consistent with the corresponding results presented in Ref. [16]. Table 2.3 contains the obtained in this way Fermi energy levels for $Ga_{0.92}Mn_{0.08}As$.

Chapter 3

Landauer-Büttiker Formalism

To study the spin-dependent tunneling in the (Ga,Mn)As-based magnetic tunnel junctions, we consider a model heterostructure, which is uniform and infinite in the x and y directions and has modulated magnetization along the z direction. The heterostructure is connected to two semi-infinite bulk contacts denoted by L and R. The length of the simulated structure is comparable to the phase coherence length. In the presence of spin-orbit coupling the spin is not a good quantum number. The only preserved quantities in tunneling are the energy E and, due to spatial in plane symmetry of our structures, the in-plane wave vector $k_{\parallel}$. Our goal is to calculate the spin-dependent current, which is determined by the transmission probabilities from the ingoing Bloch states at the left contact to the outgoing Bloch states at the right contact. The transmission probabilities can be determined when the election states in the system are known. In order to compute all one electron states in the device for given $k_{\parallel}$ and E the above described tight-binding matrix is used.

3.1 Scattering Formalism and Transfer Coefficients

The Bloch states in the two contacts L and R are characterized by the perpendicular to the layers wave vector component $k_{\perp}$ and are denoted by $|L, k_{L,\perp,i}\rangle$ and $|R, k_{R,\perp,i}\rangle$, respectively. The transmission probability $T_{L,k_{L,\perp,i}\rightarrow R,k_{R,\perp,j}}$ is a function of the transmission amplitude $t_{L,k_{L,\perp,i}\rightarrow R,k_{R,\perp,j}}(E,\mathbf{k}_{\parallel})$ and group velocities in the left and right lead, $v_{L,\perp,i}$ and $v_{R,\perp,j}$:

$$T_{L,k_{L,\perp,i}\rightarrow R,k_{R,\perp,j}}(E,\mathbf{k}_{\parallel}) = \left|t_{L,k_{L,\perp,i}\rightarrow R,k_{R,\perp,j}}(E,\mathbf{k}_{\parallel})\right|^2 \frac{v_{R,\perp,j}}{v_{L,\perp,i}}. \tag{3.1}$$

The current flowing in the right direction can now be written as [15]:

$$j_{L\to R} = \frac{-e}{(2\pi)^3\hbar}\int_{BZ} d^2k_\parallel dE f_L(E) \sum_{\substack{k_{L,\perp,i},k_{R,\perp,j}\\ v_{L,\perp,i},v_{R,\perp,j}>0}} T_{L,k_{L,\perp,i}\to R,k_{R,\perp,j}}(E,\mathbf{k}_\parallel), \tag{3.2}$$

where f_L or respectively f_R are the electron Fermi distributions in the left and right interface and i,j number the corresponding Bloch states. Plugging in the expression given in Eq. 1 and using the time reversal symmetry:

$$T_{L,k_{L,\perp,i}\to R,k_{R,\perp,j}}(E,\mathbf{k}_\parallel) = T_{L,-k_{R,\perp,j}\to R,-k_{L,\perp,i}}(E,\mathbf{k}_\parallel) \tag{3.3}$$

we get:

$$j = \frac{-e}{(2\pi)^3\hbar}\int_{BZ} d^2k_\parallel dE\,[f_L(E)-f_R(E)] \sum_{\substack{k_{L,\perp,i},k_{R,\perp,j}\\ v_{L,\perp,i},v_{R,\perp,j}>0}} \left|t_{L,k_{L,\perp,i}\to R,k_{R,\perp,j}}(E,\mathbf{k}_\parallel)\right|^2 \frac{v_{R,\perp,j}}{v_{L,\perp,i}}. \tag{3.4}$$

To calculate the current one has to determine the transmission probability, thus the transmission amplitude $t_{L,k_{L,\perp,i}\to k_{R,R,\perp,j}}(E,\mathbf{k}_\parallel)$ and the group velocities $v_{L,\perp,j}$ of the ingoing and $v_{R,\perp,j}$ of outgoing states.

3.2 Scattering within Tight-binding Model

The group velocities and transmission amplitude can be obtained by solving the Schrödinger equation for the structure with the appropriate scattering boundary conditions, i.e., open boundary conditions. In the following we introduce the method presented in Ref. [10]. We start with dividing the heterostructure into layers consisting of several atomic monolayers in such a way that the tight-binding elements are nonzero only between neighboring layers. The layers in the left lead are numbered $s \leqslant 0$, the internal layers are numbered $s = 1,\ldots,N$ and the layers in the right lead are numbered $s > N$. As mentioned above, the tight-binding matrix is used to compute all one electron states in the device for given $\mathbf{k}_\parallel$ and E. Let $\mathbf{C}_s(E,\mathbf{k}_\parallel)$ denote the coefficients of a given state $|E,\mathbf{k}_\parallel\rangle$ expanded into the basis orbitals in the layer s, i.e.:

$$|E,\mathbf{k}_\parallel\rangle = \sum_{s,\alpha} c_{s,\alpha}(E,\mathbf{k}_\parallel)|\mathbf{k}_\parallel,s,\alpha\rangle, \tag{3.5}$$

where α is the atom index in the crystal basis. The functions $|\mathbf{k}_\parallel,s,\alpha\rangle$ are constructed from atomic orbitals $\Psi_{s,\alpha}$ and they form eigenvectors of $\hat{T}_{\mathbf{R}_\parallel}$ for lattice vectors $\mathbf{R}_\parallel$ along x and z axis:

$$|\mathbf{k}_\parallel,s,\alpha\rangle = \frac{1}{\sqrt{N}}\sum_{\mathbf{R}_\parallel} e^{i\mathbf{k}_\parallel\mathbf{R}_\parallel}\hat{T}_{\mathbf{R}_\parallel+\mathbf{b}_\alpha}|\Psi_{s,\alpha}\rangle, \tag{3.6}$$

Thus, the Schrödinger equation $\hat{H}|E,\mathbf{k}_\parallel\rangle = E|E,\mathbf{k}_\parallel\rangle$ implies the following conditions for the states in the s-th layer:

$$(\mathcal{H}_{s,s} - E)\,\mathbf{C}_s + \mathcal{H}_{s-1,s}\mathbf{C}_{s-1} + \mathcal{H}^\dagger_{s,s+1}\mathbf{C}_{s+1} = 0, \tag{3.7}$$

where $\mathcal{H}_{s,s}$ and $\mathcal{H}_{s,s+1}$ are the intra- and interlayer tight-binding matrices. Moreover, for the leads we need to impose the Bloch condition on the incoming wave:

$$\mathbf{C}_s = e^{ik_\perp d_\perp}\mathbf{C}_{s-1}, \tag{3.8}$$

where $d_\perp$ is the width of the layer along the z direction. Similar equation can be constructed for the right lead. From these two boundary conditions we get a general eigenvalue equation for $k_\perp$ and the corresponding eigenvectors. Let us denote by $D_{L,l}$ the eigenvectors in left lead that propagate to the left, and by $D_{L,r}$ the eigenvectors propagating to the right. Similarly, we define $D_{R,l}$ and $D_{R,r}$. Now the boundary conditions are given by:

$$\begin{pmatrix} \mathbf{C}_{-1} \\ \mathbf{C}_0 \end{pmatrix} = \begin{pmatrix} D_{L,r} & D_{L,l} \end{pmatrix} \begin{pmatrix} \mathbf{I} \\ \mathbf{r} \end{pmatrix}, \tag{3.9}$$

$$\begin{pmatrix} \mathbf{C}_{N+1} \\ \mathbf{C}_{N+2} \end{pmatrix} = \begin{pmatrix} D_{R,r} & D_{R,l} \end{pmatrix} \begin{pmatrix} \mathbf{t} \\ \mathbf{0} \end{pmatrix}, \tag{3.10}$$

where r and t are the unknown coefficient of the scattered to the left and to the right wave. We compute the inverses D_R^{-1} and D_L^{-1} and divide them into blocks:

$$D^{-1} = \begin{bmatrix} (D^{-1})_{1,1} & (D^{-1})_{1,2} \\ (D^{-1})_{2,1} & (D^{-1})_{2,2} \end{bmatrix}. \tag{3.11}$$

The width and the height of the block $(D^{-1})_{1,1}$ is given by the number of states propagating to right. One can now rewrite the parts of (3.9) and (3.10) as:

$$\begin{bmatrix} (D_L^{-1})_{1,1} & (D_L^{-1})_{1,2} \end{bmatrix} \begin{pmatrix} \mathbf{C}_{-1} \\ \mathbf{C}_0 \end{pmatrix} = \mathbf{I}, \tag{3.12}$$

$$\begin{bmatrix} (D_R^{-1})_{2,1} & (D_R^{-1})_{2,2} \end{bmatrix} \begin{pmatrix} \mathbf{C}_{N+1} \\ \mathbf{C}_{N+2} \end{pmatrix} = \mathbf{0}. \tag{3.13}$$

The equations (3.7), (3.12) and (3.13) build a full system of linear equation for $\mathbf{C}_\sigma$. After solving it we determine the coefficients t and r with:

$$\mathbf{t} = \begin{bmatrix} (D_R^{-1})_{1,1} & (D_R^{-1})_{1,2} \end{bmatrix} \begin{pmatrix} \mathbf{C}_{N+1} \\ \mathbf{C}_{N+2} \end{pmatrix}, \tag{3.14}$$

$$\mathbf{r} = \begin{bmatrix} (D_L^{-1})_{2,1} & (D_L^{-1})_{2,2} \end{bmatrix} \begin{pmatrix} \mathbf{C}_{-1} \\ \mathbf{C}_0 \end{pmatrix}. \tag{3.15}$$

The procedure allows also to determine the needed group velocity, which is given by:

$$v_\perp = \frac{1}{\hbar}\langle\Psi|[\hat{H}, z]|\Psi\rangle = \tag{3.16}$$

$$= -\frac{2d}{\hbar|\mathbf{C}_s|^2}\Im\left(\mathbf{C}_s^\dagger\mathcal{H}_{s,s+1}\mathbf{C}_s e^{ik_\perp d}\right). \tag{3.17}$$

3.3 Computing the Current Spin Polarization

The above derivations follow closely the procedure detailed in Refs. [66] and [10]. However, in those papers the calculations were carried out assuming the spin degeneracy and as the result the spin-orbit coupling was not included. The tight-binding model introduced in the previous chapter describes spin split Bloch bands, which are additionally spin mixed due the spin-orbit interaction. Thus, the number of considered scattering states doubles in comparison to the case with spin degeneracy. This considerably increases computational burden, nevertheless the transmission amplitudes between spin mixed states and the group velocities can be determined using exactly the same procedures as for the spin degenerated case.

The introduced above equations form the theoretical basis for our calculations of coherent transport in modulated structures of ferromagnetic semiconductors, in particular in the TMR and TAMR structures. However, in order to study spin injection in Zener tunneling structures we need to introduce a measure for the degree of the spin polarization of carriers injected from the ferromagnetic source into the paramagnetic drain. Our definition of the spin polarization of the transmitted current follows the scheme proposed in Ref. [7]. First of all, we need to define the spin polarization of the Bloch state:

$$P_{R,k_{R,\perp,i}}(E,\mathbf{k}_{\parallel}) = \langle R, k_{R,\perp,i}|\vec{\Omega}\cdot\vec{s}|R, k_{R,\perp,i}\rangle, \tag{3.18}$$

where $\vec{\Omega}$ is the direction vector of the spontaneous magnetization in ferromagnetic material and $\vec{s}$ is the spin operator. This quantity measures to which extent an electron in the outgoing state $|R, k_{R,\perp,i}\rangle$ conserves its original spin direction. For a given Bloch state this quantity can be easily computed using the tight-binding model. Now, we can define the spin polarized current:

$$j_s = \frac{-e}{(2\pi)^3\hbar}\int_{BZ} d^2k_{\parallel}dE\,[f_L(E) - f_R(E)] \sum_{\substack{k_{L,\perp,i},k_{R,\perp,j} \\ v_{L,\perp,i},v_{R,\perp,j}>0}} T_{L,k_{L,\perp,i}\rightarrow R,k_{R,\perp,j}}(E,\mathbf{k}_{\parallel})P_{R,k_{R,\perp,i}}. \tag{3.19}$$

The spin polarization of the coherently transmitted current is now equal to:

$$P_s = \frac{j_s}{j}. \tag{3.20}$$

3.4 Self-consistent Procedure

In this section we discuss the self-consistent tight-binding model for the structures where the translational symmetry holds for two axes, and is broken along one axis. This is exactly the case in the structures that we aim to study in this paper. The self-consistent procedure presented here is based on Ref. [43], where it was introduced for

the first time, however without taking into account spin effects. Recall the following two equation that are used to describe wave functions in the tight-binding model:

$$|E, \mathbf{k}_\parallel\rangle = \sum_{s,\alpha} c_{s,\alpha}(E, \mathbf{k}_\parallel)|\mathbf{k}_\parallel, s, \alpha\rangle,$$

$$|\mathbf{k}_\parallel, s, \alpha\rangle = \frac{1}{\sqrt{N}} \sum_{\mathbf{R}_\parallel} e^{i\mathbf{k}_\parallel \mathbf{R}_\parallel} \hat{T}_{\mathbf{R}_\parallel + \mathbf{b}_\alpha} |\Psi_{s,\alpha}\rangle,$$

where α is the atom index in the crystal basis and s numbers the layers of the structure. For given $\mathbf{k}_\parallel$ and E the eigenstates of the system are given by the following equation:

$$(\hat{H} + V_H)|E, \mathbf{k}_\parallel\rangle = E|E, \mathbf{k}_\parallel\rangle, \tag{3.21}$$

in which we have included the Hartree potential V_H. The potential V_H that describes the influence of the electronic charge rearrangement is determined the Poisson equation:

$$\frac{\mathrm{d}^2 V_H}{\mathrm{d}\, z^2} = -\frac{\rho(z)}{\epsilon}, \tag{3.22}$$

where ϵ is the static dielectric constant. The charge density $\rho(z)$ is given by the density of elections $n(z)$ and positive ions $p(z)$:

$$\rho(z) = e(p(z) - n(z)).$$

The needed charge density $p(s)$ is determined by ionization of atoms in the layer s, whereas $n(s)$ is defined as the number of electrons in layers s and equals:

$$n(m) = \frac{1}{(2\pi)^2} \int_{BZ_\parallel} \mathrm{d}\, \mathbf{k}_\parallel \sum_{\alpha,n} \left| c_{s,\alpha}(E_n, \mathbf{k}_\parallel) \right|^2 f(E_n),$$

where n labels the energy levels for a given $\mathbf{k}_\parallel$ and f is Fermi distribution function in the device. In order order to evaluate the above electron density we need to perform a full $\mathbf{k}_\parallel$ integration is performed over the 2D Brillouin Zone. Here, due to the presence of magnetization degree of freedom we cannot simplify the procedure by integrating only over the irreducible wedge what is possible only for special directions of magnetization. Nevertheless, a significant speedup is necessary, due to very high computational burden of the procedure. In the integration we take into account only points close to the Gamma point, because in all of the considered materials the states on Fermi energy are close to Gamma point. Hence the states that paly role in charge redistribution, have small $\mathbf{k}$ vectors and this simplification is justified.

Later, the Poisson (3.22) and Schrödinger (3.21) equations are solved within the TB model until the convergence. In the Schrödinger equation we use the open-chain boundary conditions presented in the previous section.

Chapter 4

Interlayer Coupling

In this chapter we use the tight-binding model to study the interlayer exchange coupling (IEC) between (Ga,Mn)As ferromagnetic layers in all-semiconductor superlattices. The advantage of this approach is that it takes into account the crystal, band and magnetic structure of the constituent superlattice components. We show that the mechanism originally introduced to describe the spin correlations in antiferromagnetic EuTe/PbTe superlattices [4], explains the experimental results observed in ferromagnetic semiconductor structures, i.e., both the antiferromagnetic coupling between ferromagnetic layers in IV-VI (EuS/PbS and EuS/YbSe) superlattices as well as the ferromagnetic interlayer coupling in III-V ((Ga,Mn)As/GaAs) multilayer structures. The model allows also to predict (Ga,Mn)As-based structures, in which an antiferromagnetic interlayer coupling could be expected.

4.1 IEC in Magnetic Semiconductor Systems

All the experimentally analyzed (Ga,Mn)As-based SL were produced on GaAs substrate along [001] crystallographic axis. In this case the primitive lattice vectors, which describe the SL elementary cell are following: $\mathbf{a_1} = a\sqrt{3}/2[1,1,0]$; $\mathbf{a_2} = a\sqrt{3}/2[1,0,m+n]$; $\mathbf{a_3} = a\sqrt{3}/2[0,1,m+n]$. The spins in the magnetic layers are placed along the [100] direction [36]. The SL elementary magnetic cell, which is taken under consideration, must consist of at least two magnetic layers, i.e., it should contain $2(n+m)$ monolayers. Altogether with the used specification of the constituent materials this generates $80(m+n) \times 80(m+n)$ matrix for the SL tight-binding Hamiltonian. By numerical diagonalization of the Hamiltonian matrices, band structure for the two SL with various relative spin configurations of the (Ga,Mn)As FM layers is obtained. The position of the Fermi level in the SL valence band is supposed to be defined by the average number of holes present in the structure – for (Ga,Mn)As/GaAs it is given by $\frac{a^3}{4}(p_m m)$, whereas for (Ga,Mn)As/GaAs:Be by $\frac{a^3}{4}(p_m m + p_n n)$. In (Ga,Mn)As/(Al,Ga)As with high Al content the holes are confined in the (Ga,Mn)As layers, due to the high po-

tential barriers presented in the valence band by the spacer layer. As all the studied structures have (Ga,Mn)As layers which were not annealed, we assume the hole density in (Ga,Mn)As to be equal to $p_m = 2 \times 10^{20}$ cm^{-3} for the sample with 4% of Mn and $p_m = 3 \times 10^{20}$ cm^{-3} for the sample 6% of Mn [51]. The density of holes introduced by Be in the spacer is assumed to be $p_n = 1.21 \times 10^{20}$ cm^{-3} [14]. In order to calculate the IEC in the spirit of Ref. [4] one compares the total energy of the valence electrons for two different SL, that is one with parallel and the other with antiparallel spin alignment in consecutive magnetic layers. These total energies are calculated by summing up all the occupied states' energies and integrating over the entire Brillouin zone. It should be stressed that in this calculation the hole charge redistribution at the interfaces is not taken into account, i.e., the calculations are not self-consistent.

We define the strength of the interlayer coupling as the difference ΔE between the energies of valence electrons in SL calculated for the two spin configurations, per unit surface of the layer. The preferred spin configuration in consecutive magnetic layers is given by the sign of ΔE – the negative value corresponds to FM IEC whereas the positive sign indicates a AFM correlation.

4.2 Calculation Results

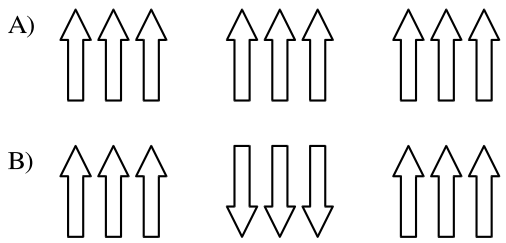

Figure 4.1: Ferromagnetic superlattice where the spins in consecutive layers are ordered A) parallel and B) antiparallel.

The results of the calculations are summarized in the Figs. 4.1, Fig. 4.2 and Fig. 4.3. Like for the EuS-based structures, once again there is no dependence of J on the thickness of the magnetic layer – all the presented results are calculated for $m = 4$.

In Fig. 4.2 the calculated dependence of the interlayer coupling constant $J = \Delta E/4$ on the spacer thickness n for $Ga_{0.94}Mn_{0.06}As/GaAs$ SL is presented together with the results obtained for $Ga_{0.96}Mn_{0.04}As/GaAs$, without and with Be-doping (the latter introducing p_n holes in the spacer layer) and $Ga_{0.96}Mn_{0.04}As/Ga_{0.7}Al_{0.3}As$, i.e., for the other experimentally studied (Ga,Mn)As-based structures. In qualitative agreement with the experiment, the obtained IEC for all these structures is, in principle, FM and declines with the thickness of nonmagnetic layers. The higher the

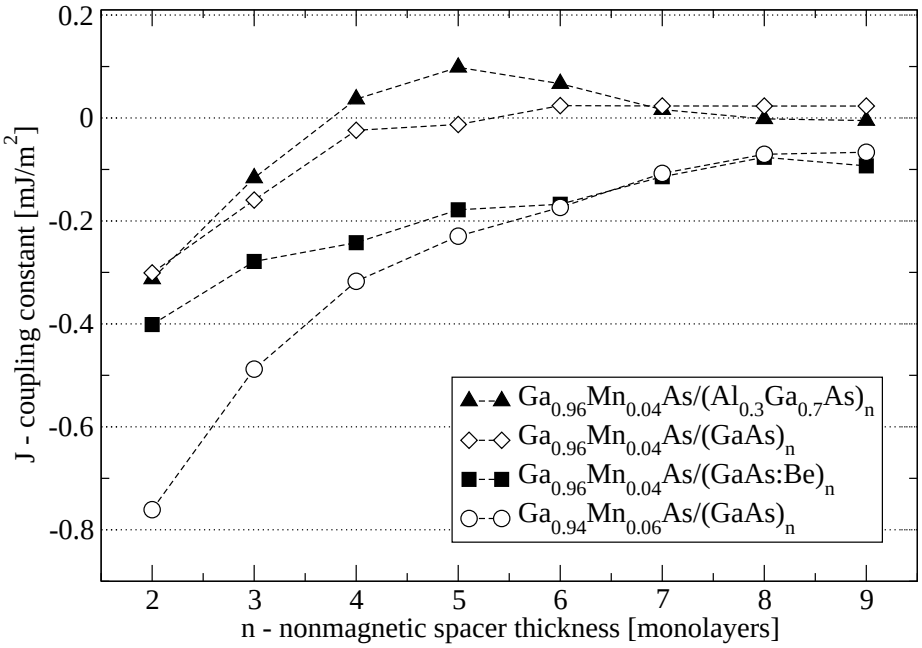

Figure 4.2: The interlayer exchange coupling calculated for (Ga,Mn)As-based structures, which were studied experimentally in Refs [1], [36] and [14].

hole concentration in the SL the stronger is the IEC. For the (Ga,Mn)As/(Al,Ga)As sample, where the holes are confined in the deep wells formed by the barriers of spacer layers, the IEC is significantly suppressed and vanishes for $n > 7$, as measured in Ref. [1] for the structure with $n = 10$. This result does not prove, however, that there is no IEC where there are no holes in the spacer layer. For very thin spacers, 2-3 monolayers, a strong FM coupling, and for $n = 5$ an AFM coupling was obtained (see Fig. 4.2).

In order to clarify these results and the role played by holes, the dependence of the calculated interlayer coupling constant J on the position of the Fermi level, i.e., on the average concentration of holes in the SL valence band, was analyzed. As presented in Fig. 4.3, J has an oscillatory RKKY-like character (for comparison IEC mediated by RKKY interaction, i.e., $J_{RKKY} \sim k_F^2 F(2k_F r)$, where k_F is the Fermi wave vector and $F(x) = (x\cos x - \sin x)/x^2$ [72], is presented in the figure by the dashed line). In contrast to J_{RKKY}, at the zero hole concentration limit J tends not to zero, but to a finite positive value, which corresponds to IEC mediated by valence band electrons in a hypothetical (Ga,Mn)As/GaAs SL with completely filled valence bands. In (Ga,Mn)As/(Al,Ga)As SL, for the concentrations up to about 4×10^{20} cm^{-3} the holes are confined in the wells – when the Fermi level reaches the value of the band offset between (Ga,Mn)As and (Al,Ga)As, the distribution of holes in the SL alters and the obtained J values for higher concentrations do not follow the previous trends. Notably, the results showed in Fig. 4.3 point out that in

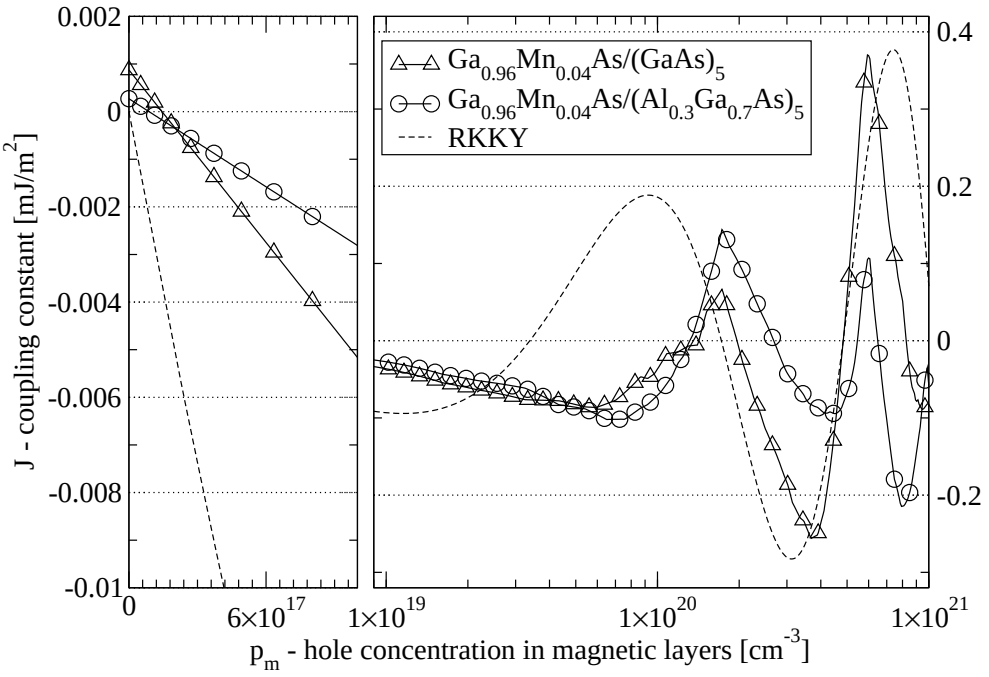

Figure 4.3: The calculated dependence of interlayer coupling constant J on the hole concentration in SL consisting of alternating $m = 4$ $Ga_{0.96}Mn_{0.04}As$ monolayers and $n = 5$ monolayers of GaAs or $Ga_{0.7}Al_{0.3}As$. J_{RKKY} is presented for comparison.

(Ga,Mn)As-based heterostructures also the AFM coupling between FM layers could be reached by an appropriate engineering of the SL and a proper choice of constituent materials. The change of the IEC sign was as well obtained within a *kp*-theory with a single parabolic valence band [32]. Nevertheless, on the grounds of the present results structures particularly suitable for the observation of AFM correlations are implied. These seem to be SLs in which the hole concentration is either increased (e.g., by appropriate annealing during the MBE growth of the SL) to about 6×10^{20} cm^{-3} or kept as low as $1.5 - 2.5 \times 10^{20}$ cm^{-3}. It should be mentioned that in the former one high Curie temperature can be expected. The (Ga,Mn)As/(Al,Ga)As system is furthermore interesting, due to high potential barriers in the nonmagnetic spacers, the carriers are confined in the DMS layers, what can result in strongly spin-polarized charge density. In the latter heterostructures the hight of the barrier, i.e., the Al content, is of high significance – the results for (Ga,Mn)As/AlAs SL (for clarity not included in the figure) demonstrates that very high barriers reduce extremely the IEC in both FM and AFM regions.

Finally, in Fig. 4.4 we illustrate the dependencies of J on the thickness of the spacer layer n for the $Ga_{0.92}Mn_{0.08}As$/GaAs and $Ga_{0.96}Mn_{0.04}As/Al_{0.3}Ga_{0.7}As$ SLs with appropriate for AFM IEC hole concentrations. The coupling is stronger for the higher concentration in both structures, however, it decreases more rapidly with the spacer thickness. Worthy to remark is fact that SL with the spacers as

thin as 3 monolayers, for which the strongest coupling has been predicted, would be hard obtainable, due to the strong interdiffusion in the LT MBE grown (Ga,Mn)As structures [46]. Still, for $n = 5 - 6$, the predicted AFM IEC is of the same order of magnitude as the FM coupling spoted in the (Ga,Mn)As-based SL.

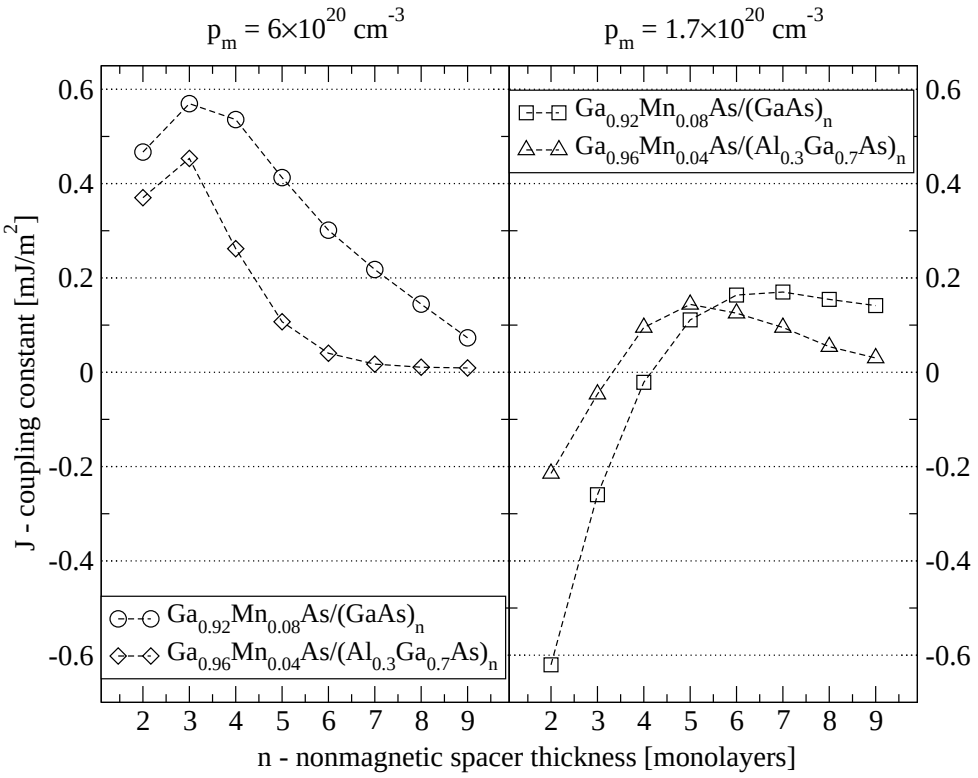

Figure 4.4: The coupling constant vs. spacer thickness for (Ga,Mn)As-based SL in the two regions of hole concentration, in which the model predicts an antiferromagnetic interlayer coupling.

In this chapter, our study concentrated on the sensitivity of the band structure of (Ga,Mn)As-based SLs and the spin configuration in successive DMS layers within a tight binding model. Such effects describe correctly the AFM IEC between the FM layers in EuS/PbS and EuS/YbSe. Additionally, they seem to provide, up to now, the only effective mechanism capable to deliver explanation to the origin of interlayer correlations in AFM EuTe/PbTe SL. We have demonstrated that by this mechanism also the FM interlayer coupling in (Ga,Mn)As/GaAs SL can be described. Furthermore, the model shows a possibility of engineering (Ga,Mn)As-based multilayers for obtaining an AFM interlayer coupling.

Chapter 5

Interband Zener Tunneling

In this chapter we aim to study a Zener-Esaki light emitting diode in which the p-type lead is fabricated out of (Ga,Mn)As ferromagnetic semiconductor. Engineering this structure allowed to observe a very high $\approx 80\%$ spin polarization of election current obtained via inter-band tunneling in 4.6 K [18]. In this chapter we first give the details of the tight-binding description of the Zener-Esaki diode. Next, we present the results of the calculations with focus on the bias dependence of the tunneling, as well as, on the dependence of tunneling on magnetization direction. The presentation of the calculation results is accompanied by a careful comparison with available experimental findings.

As we have mentioned before, the model takes into account all the effects resulting from the electric field in the depletion zone of the diode, i.e., the Rashba and Dresselhaus terms. The cost of these advantages comes with the reduction of the possible size of the simulated device. Hence, the whole LED structure from Ref. [18] cannot be considered by this approach. Thus, in the calculation of the current spin polarization we concentrate only on the description of the (Ga,Mn)As/GaAs interface.

First of all we analyze the current spin polarization as a function of the applied bias and show that our model correctly describes the experimentally observed dependence. It has to be mentioned that in order to get correct results the (Ga,Mn)As/GaAs interface needs to be considered using self-consistent calculations. Next, the calculated dependencies of spin polarization of the current in the Zener-Esaki diode on carrier density and Mn content in magnetic layer are presented. It is predicted that the higher the Mn content the higher is the injected spin polarization, whereas the increase of the hole concentration has opposite impact on the spin polarization.

Next, we use our model to consider the Esaki-Zener tunneling junction for different in-plane directions of the magnetization vector, in the weak bias limit. Surprisingly, the model predicts that, even without any extrinsic strain, the Zener current spin polarization differs for magnetization along [110] and along $[\bar{1}10]$ crystallographic axis. This character of anisotropy reflects the C_{2v} symmetry of a single zinc-blende

interface. The obtained theoretically 6% difference in spin polarization of the Zener tunneling current has been also observed experimentally [19]. Typically, (Ga,Mn)As films exhibit uniaxial in-plane magnetic anisotropy, which was explained assuming a small, of the order of 0.05%, trigonal distortion along the [110] axis [62]. Such strain enhances the in-plane anisotropy of the Zener currant and its spin polarization. However, within our model a relatively strong extrinsic deformation (0.3%) is needed to obtain a significant dependence of the current and its spin polarization on the direction of the magnetization vector.

The spin dependent tunneling is sensitive not only to the in-plane rotation of the magnetization vector but changes also when magnetization assumes the out-of-plane direction [23]. Our theory describes correctly the experimental magnitude of perpendicular tunneling anisotropic magnetoresistance ($\mathrm{TAMR}_\perp$) for small forward and reversed bias. For larger applied voltages, other phenomena, not related to tunneling, *e.g.*, standard AMR, affect the experimental results.

Here, our aim is to understand this effect and be able to predict structures and conditions that would weaken this dependence. In this dissertation we analyze theoretically the transport in the spin-LED structures in which the very high spin polarization of the injected current was observed.

5.1 Bias Dependence

Because of computational constraints in approaches involving the transfer matrix formalism carrier transport along the whole device cannot be simulated. Hence, we need to concentrate ourselves on the interface between magnetic p-type (Ga,Mn)As and nonmagnetic n-type GaAs. The interband tunneling taking place on this interface is the only factor that determines the spin polarization of the obtained current and the rest of the device serves only for measurement purposes. Moreover, in the first calculation we consider the simplest flat-band p-$\mathrm{Ga}_{1-x}\mathrm{Mn}_x\mathrm{As}$/$n$-GaAs tunneling structure shown in Fig. 5.1, where we take the hole concentration that corresponds to the Mn content $x = 0.08$ in (Ga,Mn)As equal to $p = 3.5 \times 10^{20}$ cm^{-3} [20], and the electron concentration in the GaAs $n = 1 \times 10^{19}$ cm^{-3}. We perform these oversimplified calculations first, in order to understand the interplay between the band structures in both leads. Inclusion of the intermediate region would obscure the situation. However, latter we present self-consistent calculations where the interface is more completely described (see Section 5.1.1). Additionally, we assume that the magnetization vector is at 27° out of plane, as implied by experimental conditions [18]. While in such a model the bias voltage is only applied over the Zener diode, in contrast to the actual device, it should provide correct information on the spin polarization. Despite that such a model certainly overestimates the tunneling current, it can provide quantitative information on current spin polarization that is determined by inter-band tunneling

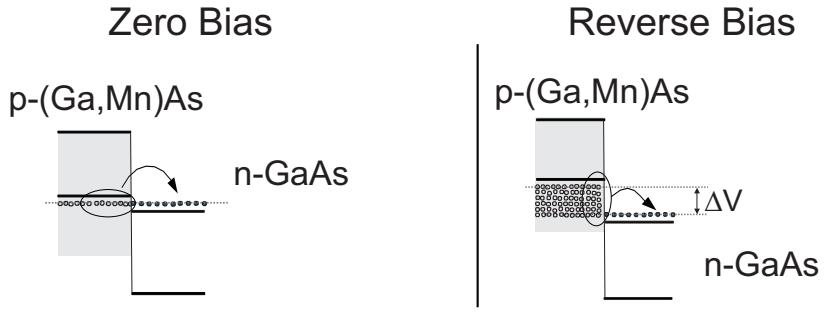

Figure 5.1: Scheme of the (abrupt) (Ga,Mn)As/GaAs p-n-diode structure used in the simplified tight-binding calculations at zero and reverse bias.

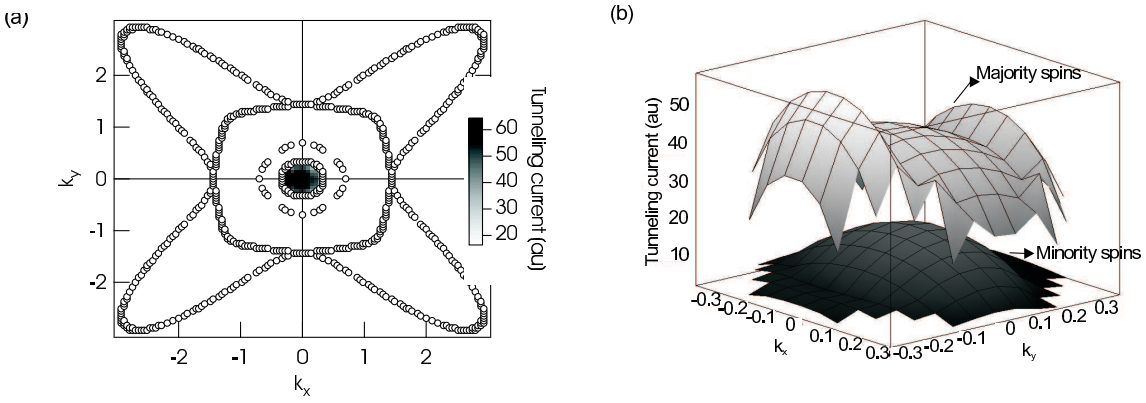

Figure 5.2: a) The calculated valence band intersection of (Ga,Mn)As for a hole concentration of $3.5 \times 10^{20}\text{cm}^{-3}$ and the tunneling current as function of k_x and k_y. b) The magnitude of the tunneling currents for both the majority spins as the minority spins for different $k_{||}$-vectors in the structure presented in Fig.5.1 for zero bias.

matrix elements and degree of spin polarization in the ferromagnetic electrode.

In Fig. 5.2 the contributions to the tunneling current and its spin polarization from carriers with different k-vectors in (Ga,Mn)As valence sub-bands is presented. These results show that in the tunnelling process practically only the light holes take part. A first reason for this is that their transverse k vectors match well the transverse k vectors of the conduction band states in the n-GaAs. Secondly, in the interband tunneling process, the tunneling electrons travel on an imaginary band while traversing the forbidden energy zone. As can be seen in Fig.5.3, in GaAs only the light hole band connects to the first conduction band while the heavy hole band connects to a higher energy conduction band [10]. This is, however, only true for tunneling from states at the Γ-point. Due to the large Fermi energy, the tunneling electrons all possess a significant $k_{||}$, which allows also the tunneling of electrons from the heavy-hole bands. One may also note that at the Fermi level for the considered hole concentration, the contribution to the tunneling from majority states increases with k. Hence, also the spin polarization increases with k.

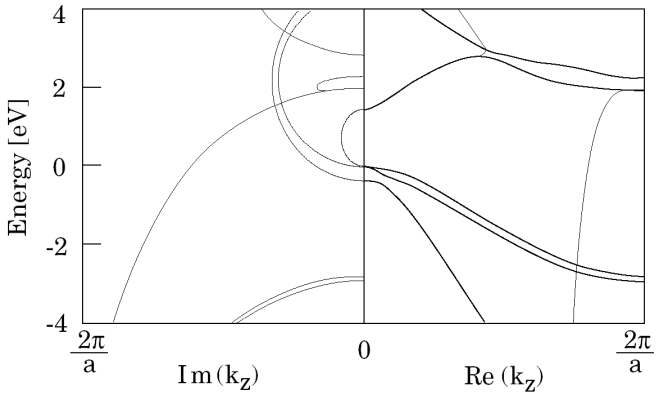

Figure 5.3: The complex band structure of GaAs, adopted from Ref. [10]. The light hole band connects to the lower conduction band, while the heavy-hole band connects to a higher energy conduction band

We have investigated also the dependence of the spin polarization of the tunneling electrons on the bias voltage, in the configuration of Fig.5.1. In Fig.5.4 we notice that the polarization indeed decreases with bias, but that the effect is not as strong as in the experiment.

We show in the next section that in order to rapid decrease of the bias dependence the inclusion of the intermediate region with use of the self-consistent calculation is necessary.

5.1.1 Self-consistent Model

In an attempt to adjust our model to fit better with the experimental conditions, we consider the whole Zener diode in the spin-LED device, i.e., the p-$Ga_{1-x}Mn_xAs$/n-GaAs heterojunction and use the self-consistent tight-binding model from Section 3.4 in order to compute the band deformation in this region. The obtained self-consistent band profile is presented on Figure 5.5.

According to the self-consistent calculations, the scattering region consists of approximately 100 monolayers of (Ga,Mn)As and GaAs, and corresponds roughly to the depletion zone of the diode. We make use of these results to describe the potential profile in the tight-binding calculations, as shown in Fig. 5.6. In particular, the self-consistently calculated electrostatic potential which describes the band bending for $V_0 = 1.81$ V, i.e., for the voltage when the interband tunneling process starts, is the basis for the potential profile that is incorporated into the tight-binding matrix. An additional component of the potential profile is the bias ΔV that corresponds to the potential drop across the Zener diode when the bias on the whole spin-LED is changed. We assume a linear potential drop which fairly well renders the real band bending across the p-n-junction.

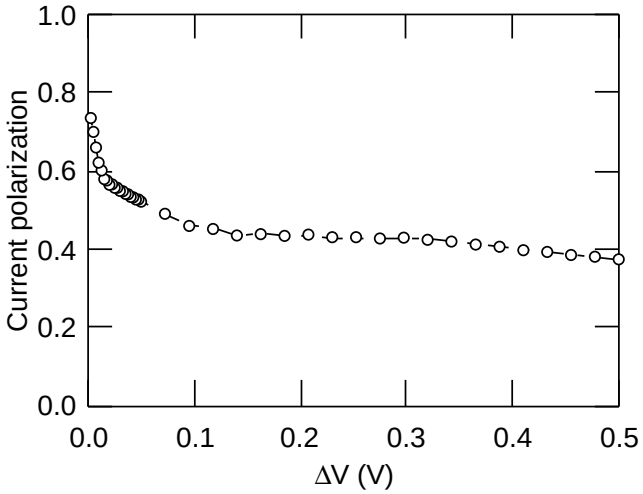

Figure 5.4: The calculated bias dependence of the current spin polarization in the p-$Ga_{1-x}Mn_xAs$/n-GaAs structure in the configuration of Fig. 5.1 for a hole concentration of $p = 3.5 \times 10^{20}$ cm^{-3} (dashed-dotted line) in the p-$Ga_{1-x}Mn_xAs$-layer. ΔV is the bias voltage applied solely to the Zener diode, as depicted in Fig. 5.1.

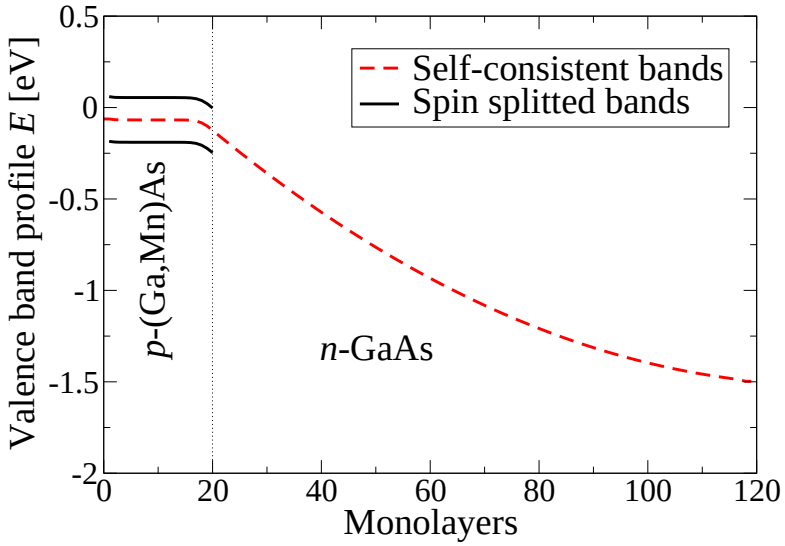

Figure 5.5: The calculated valence bands profile in $[p$-(Ga,Mn)As$]_{20}/[n$-GaAs$]_{100}$ diode.

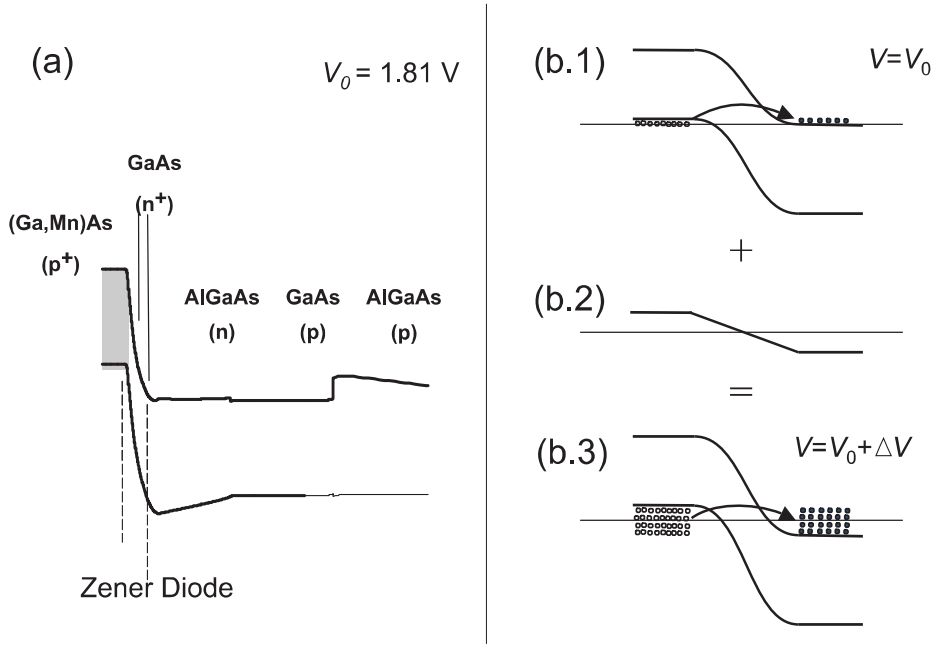

Figure 5.6: Scheme of the structure description used in the calculations: (a) the calculated with $k \cdot p$ method band profiles of the whole device for $V_0 = 1.81V$; (b.1) in the tight-binding calculations only the Zener diode region is considered; (b.2) a linear band bending given by applied bias ΔV is added; (b.3) the band profile used in tight-binding calculations is a sum of (b.1) and (b.2).

Figure 5.7 shows P_j as a function of the bias ΔV in the Zener tunneling diode. We see that at low bias, P_j is of the order of 0.6, in good agreement with the experimental results (0.8). Interestingly, P_j decreases rapidly with ΔV. The strong dependence of P_j on bias is again in agreement with the experimental findings, though a direct comparison is hampered by the fact that the exact relation between ΔV and the total bias V applied to the device is known only from simulations. However, recent experiments of Kohda *et al.* [38] performed in a three contact configuration, which allows to determine the potential drop on the tunnel junction alone, fully confirm the presented in the Figure 5.7 results.

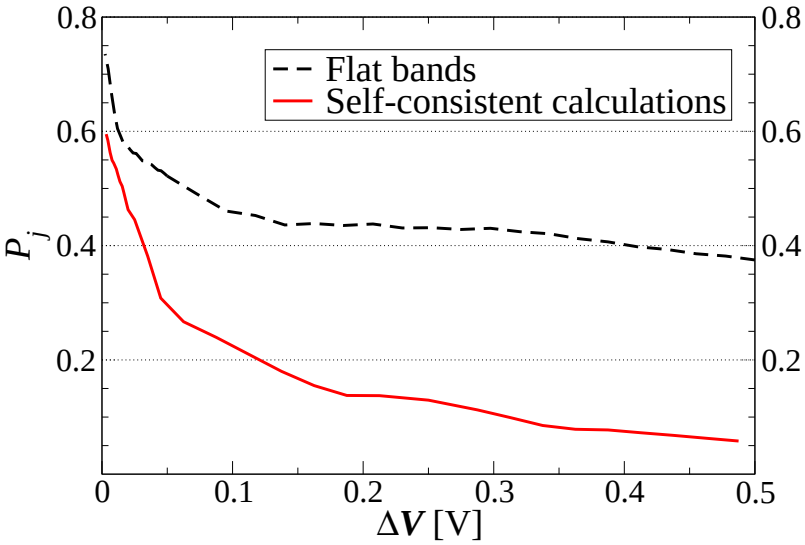

Figure 5.7: The calculated bias dependence of the current polarization for the structure in Fig. 5.6(b).

Although the spin-polarized tunneling has been intensively studied since Jullière discovered the tunnel magnetoresistance (TMR) effect 30 years ago [31], it is still far from being completely understood. In particular, the rapid decrease of TMR with increasing bias voltage observed by many authors in the planar metal-insulator-metal tunnel junctions still calls for explanation. This behavior is not implied by the simple Jullière model and many different phenomena, like emission of magnons or scattering at impurities or defects, were invoked to account for this effect, however, none of these attempts was conclusive [47, 17]. Surprisingly, the results of our simple tight-binding model of coherent tunneling, which does not account for any of these phenomena (but instead describes carefully the band structure of the heterostructure, especially the interface region) agree well with the experimental data, both regarding the maximum injected spin polarization and the bias dependence of injected spin polarization. This fact suggests that here the decrease of the spin-polarization of tunneling current with the applied dc bias has a more fundamental origin, related to band structure effects.

For the hole densities in the (Ga,Mn)As layer, we do not deal with the half-

metallic situation ($E_F = 0.26$ V, $E_{exchange} = 0.1$ V, and a contribution of the tunneling from the minority spin subband is expected for any bias. This makes the current spin polarization to be smaller than one even for $\Delta V = 0$. Furthermore, due to the presence of spin-orbit interactions the wave function in the majority spin subband contain spin up and spin down components, so that electrons with the minority spin orientation would contribute to the tunneling current even in the half-metallic situation.

We relate the strong dependence of P_j on ΔV to the fact that the current polarization is determined not only by the electron spin polarization at the Fermi energy, but also by the transmission coefficients through the structure for electrons below the Fermi energy in (Ga,Mn)As and to higher states in the conduction band of GaAs, as shown schematically in Fig. 5.6. When we increase the bias we start to have an increased contribution to the tunneling current from the minority spin subbands. An important aspect of the coherent transport through a structure is the "group velocity mismatch". Namely, due to the conservation of the transverse quasi-momentum and of the energy, the transmission coefficient through an interface decreases with the difference between the group velocities in the two materials at the energy in question, i.e., (Ga,Mn)As and undoped GaAs spacer. The "velocity mismatch" can result in a smaller transmission coefficient through the GaAs spacer for the majority spin electrons as compared to the minority spin electrons. The minority spin electrons have a smaller quasi-momentum and hence their velocities match better. Thus, one can argue that the bias, by increasing the concentration of the minority spin electrons and by increasing the importance of the region with a small group velocity, enhances the tunneling of minority spin electrons, which reduces the current spin polarization with bias seen in Fig. 5.7. To test this expectation we have computed separately the currents of the majority and minority spin electrons for different undoped spacer widths, i.e., we have considered within the flat band model the structure p-(Ga,Mn)As/p-GaAs/n-GaAs consisting of three regions.

In Zener diodes with a larger undoped spacer width, electrons with a small group velocity are favored due to the large amount of empty small group velocity conduction states in the spacer. We indeed found that relative contribution of the minority spin carriers increases with the undoped spacer width Fig. 5.8 (b), whereas the contribution of the majority spin carriers remains on the same level Fig. 5.8 (a).

Even though we can significantly speedup the self-consistent procedure by considering only the vicinity of the Gamma point in the integration the calculations are highly time consuming. The self-consistent band profile can be determined once and later reused in different calculations. However, in such a case we need to consider the structure consisting of 120 monolayer. For example the crude calculations of the dependence presented in Fig. 5.7 took nearly three months of processor time. Hence, in order to keep the computation time on reasonable level all subsequent calculations were performed using a simplified band profiles. In the case when bias dependence was not important we have used the flat band calculations presented in the beginning

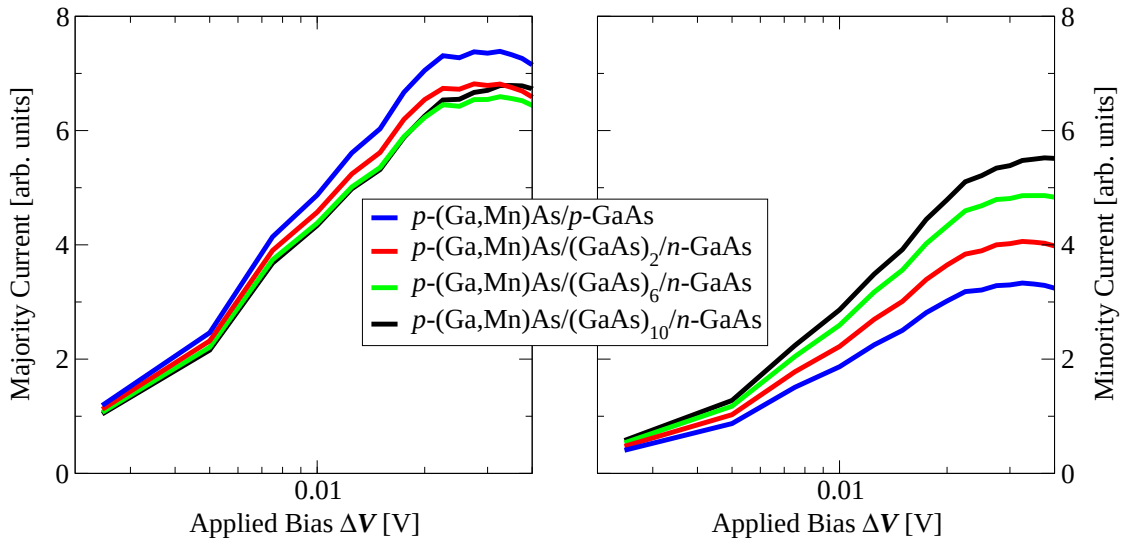

Figure 5.8: The calculated bias dependence of majority current (a) and minority current (b) in three layer heterostructure p-(Ga,Mn)As/p-GaAs/n-GaAs.

of the section, whereas when calculating bias dependence we have used a structure consisting of 24 monolayer. In this structure the band bending was assumed to be linear, but as our calculations have shown this intermediate region is wide enough to reproduce bias dependence correctly.

5.2 Effect of Material Properties

As we have seen in the previous sections the degree of current spin polarization decreases sharply with the bias what prevents obtaining high spin polarized current. Our model describes quantitatively this dependence, so it can be used to investigate how one can influence the bias dependence. It is well known that magnetic characteristics of (Ga,Mn)As depend strongly on both hole and manganese concentrations. It is thus obvious that the degree of spin polarization of the tunneling current may depend on these intrinsic features of (Ga,Mn)As layers. Using our model we can show that a higher content of magnetic ions x in $Ga_{1-x}Mn_xAs$ results in an increase of the spin polarization of the tunneling current. In contrast, an opposite change was obtained when the hole concentration was increased. This agrees with the result obtained in Ref. [16] that in $Ga_{1-x}Mn_xAs$ higher hole concentrations lead to smaller spin polarization of the hole liquid. This is naturally caused by the fact that in the relevant range of p and x, $Ga_{1-x}Mn_xAs$ is not half-metallic, so that the Fermi energy is greater than the spin-splitting. A increasing Fermi energy (higher hole concentration), combined with a constant exchange splitting, obviously leads to a smaller spin polarization. The dependencies of P_j on the hole concentration p and Mn content x are depicted in Fig. 5.9.

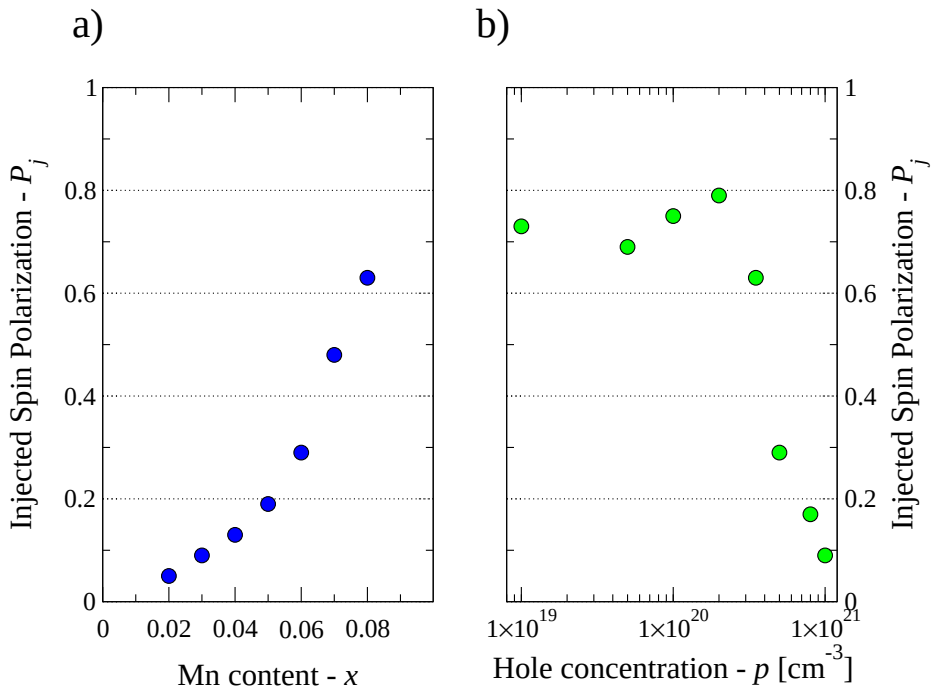

Figure 5.9: Spin current polarization P_j in p-$Ga_{1-x}Mn_xAs$/n-GaAs as a function of: (a) hole concentration p (for $x = 0.08$); (b) Mn content (for $p = 3.5 \times 10^{20}$ cm^{-3}). The bias applied to the structure is $V = 0.01$ V, whereas We assume that the $n = 10^{19}$ cm^{-3} as indicated by the experiment [18].

We might expect to see that P_j increases to 100% for small hole concentrations, because the spin polarization of states at Fermi level does. However, the results show that P_j saturates at around 80%. This indicates that degree of the injected spin polarization is determined not only by magnetic material properties but there are some other parameters playing important role as well.

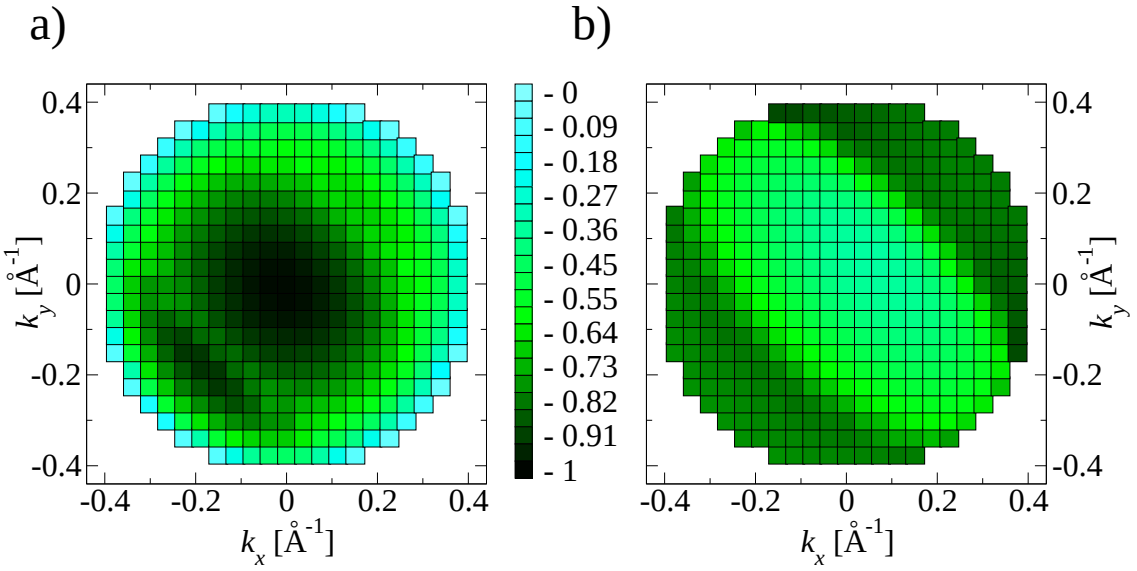

Figure 5.10: Dependence of tunneling current in arbitrary units (a) and its spin polarization (color scale)(b) on the in-plane wave vector in p-$Ga_{1-x}Mn_xAs$/n-GaAs Zener-Esaki diode in the limit of low bias (0.01 V). The calculation was performed for the hole concentration $p = 3.5 \times 10^{20}$ cm^{-3}, electron concentration $n = 10^{19}$ cm^{-3}, and the saturated magnetization (along the [110] crystallographic axis) corresponding to the Mn content $x = 0.08$.

In order to get a better insight into processes controlling spin polarization of the current, we have examined the dependence of tunneling on the in-plane wave vector in the low bias limit (the bias applied to the structure is 0.01 V). As shown in Fig. 5.10(a), the total current is dominated by the tunneling from states close to the Γ point. This is because in the tunneling process the in-plane components of $\mathbf{k}_\parallel$ wave vectors are conserved, *i.e.*, they have to match to the small $\mathbf{k}_\parallel$ vectors at the Fermi level in the conduction band of n-type GaAs ($n = 10^{19}$ cm^{-3}). Thus, only a small part of the states at the Fermi energy in the valence band of p-(Ga,Mn)As takes part in the tunneling,as shown schematically in Fig. 5.11.

At the same time we find that for this hole concentration larger $\mathbf{k}_\parallel$ vectors are responsible for the spin polarization of the current, as depicted in Fig. 5.10(b). This is due to the fact that for the hole concentration in (Ga,Mn)As layer $p = 3.5 \times 10^{20}$ cm^{-3} the spin polarization of the states at the Fermi level is small in the vicinity of the center of the Brillouin zone (compare Fig. 5.12). Furthermore, in Fig. 5.10(b) it is seen that the spin polarization is larger for $\mathbf{k}_\parallel$ vectors parallel to the magnetization,

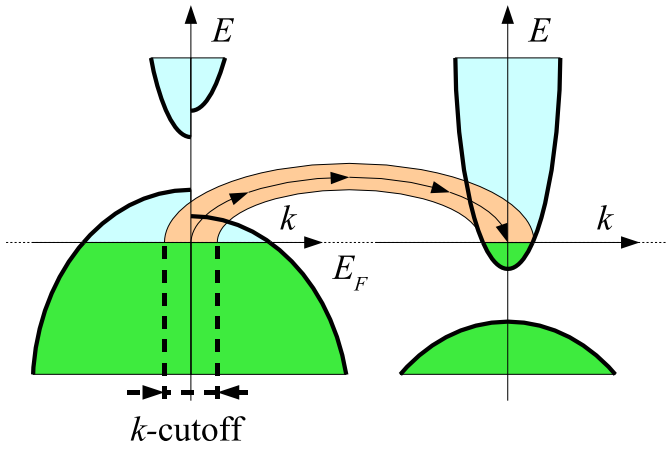

Figure 5.11: Schematic of the tunneling process from the valence band of p-type (Ga,Mn)As to the conduction band of n-type GaAs.

whereas smaller in the perpendicular to magnetization directions. This is because the spin splittings in the heavy hole bands vanish for magnetization vector perpendicular to $\mathbf{k}$ [16]. It is also worth noting that in the tunneling $\mathbf{k}_{\|}$ vectors in $[\overline{1}10]$ direction are favored (compare Fig. 5.10(a)). We assign this effect to the lifting of Kramers' degeneracy in the presence of both, the spin splittings and linear in k spin-orbit terms.

In Fig. 5.12 where the cross sections of the Fermi sphere for different hole concentrations in p-$Ga_{0.92}Mn_{0.08}As$ with the saturated value of magnetization are presented, one can notice that the higher p the smaller is the spin polarization at the Fermi level around the center of the Brillouin zone. This explains why the spin polarization of tunneling current decreases with the hole concentration. The results presented in the above figures suggest, however, that a higher concentration of electrons in n-GaAs layer should result in matching of the larger k vectors and thus in higher spin polarization of the current. Indeed, when the electron concentration is increased from $n = 10^{19}$ cm^{-3} to $n = 10^{20}$ cm^{-3}, the calculated current spin polarization becomes higher by about 8% as shown on Fig. 5.13.

5.3 Anisotropic Zener tunneling

The (Ga,Mn)As films exhibit a variety of anisotropic properties [16, 61, 62] and we will check in this section how these properties influence Esaki-Zener tunneling. The effect assessed here is called tunneling anisotropic magnetoresistance (TAMR). This effect consists of a change in the tunnel resistance upon the rotation of magnetization. The phenomenon, recently discovered in structures with a single (Ga,Mn)As ferromagnetic layer [24, 23], results from the fact that tunneling resistance depends on the relative orientation of magnetization in respect to the direction of current and crystallographic

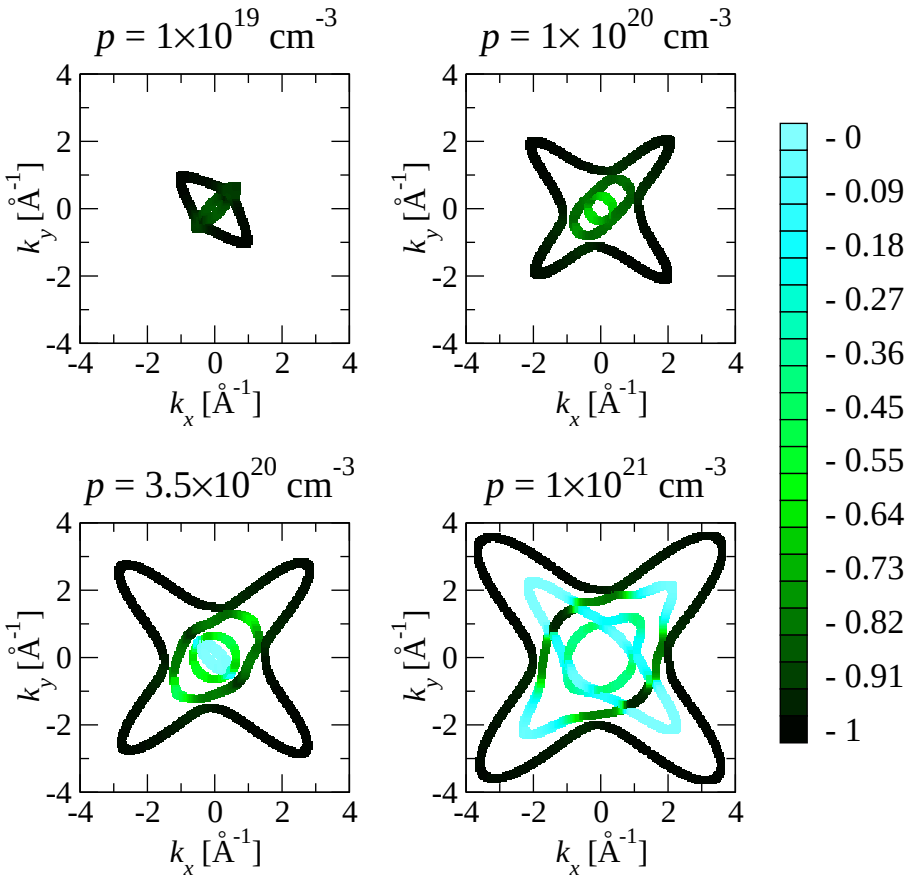

Figure 5.12: Cross section of the valence bands at the Fermi energy for various hole concentrations p in p-$Ga_{0.92}Mn_{0.08}As$. Color scale denotes spin polarization. Magnetization is taken along the [110] direction.

axes. This is due to the strong spin-orbit coupling and the highly anisotropic Fermi surface in (Ga,Mn)As (compare Fig. 5.12) – it is why TAMR was not reported for structures based on ferromagnetic metals, where typically spin-orbit characteristic energies are smaller than the Fermi energy.

5.3.1 In-plane Magnetization

We consider a simple junction consisting of several layers of p-type $Ga_{1-x}Mn_xAs$, $x = 0.08$, $p = 3.5 \times 10^{20}$ cm^{-3}, followed by several layers of n-type GaAs, $n = 10^{19}$ cm^{-3} in the weak bias limit, *i.e.* the same structure as considered in the previous subsection. Interestingly, as shown in Fig. 5.14 the model reveals that the current magnitude and its spin polarization differ for magnetization along [110] and along $[\bar{1}10]$ crystallographic axis, even in the absence of any extrinsic deformation, solely due to the relation between the anisotropy of the Fermi surface and the symmetry breaking introduced by the magnetization direction. This reflects the asymmetry of

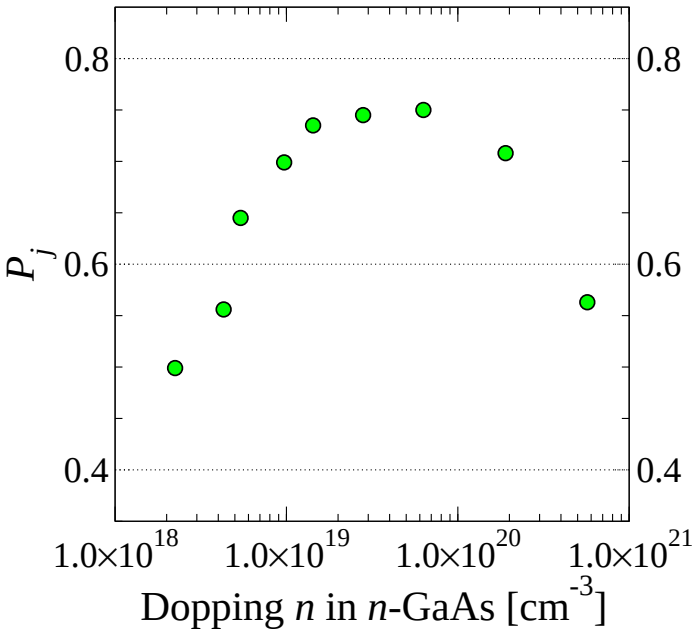

Figure 5.13: The calculated spin current polarization P_j in dependence on doping in n-GaAs layer.

the (Ga,Mn)As/GaAs interface, at which the [110] and [$\bar{1}$10] directions are not equivalent, so that the T_d symmetry of the zinc-blende crystal is reduced to C_{2v} for the heterostructure in question. Actually, a 6% difference in spin polarization of the current for the unstrained structure, which is visible in Fig. 5.14(b), agrees with that observed experimentally [19].

The intrinsic anisotropy of the Zener tunneling current depends on the hole concentration, as shown in Fig. 5.15. The change in the tunneling current upon rotation of the magnetization vector from [110] to [$\bar{1}$10] direction increases with the decrease of hole concentration, reaching 8.5% for $p = 1 \times 10^{19}$ cm^{-3}. Such a low hole concentration can, in fact, correspond to a depletion region in the p-(Ga,Mn)As/n-GaAs junction [56, 22], though hole localization may render our theory invalid in this low hole concentration range. Thus, our model predicts for (Ga,Mn)As/GaAs Zener diodes an in-plane TAMR magnitude of the order of several percents without assuming any extrinsic strain. Although the obtained TAMR value agrees with the observation reported in Ref. [24], it should be emphasized that in that experiment (Ga,Mn)As/AlO$_x$/Au tunnel junction was examined. Moreover, the symmetry of the experimental TAMR effect implies the existence of an extrinsic deformation breaking the equivalence of [100] and [010] crystallographic axes.

Typically (Ga,Mn)As films exhibit uniaxial anisotropy, whose character implies the presence of an extrinsic trigonal distortion along the [110] axis [62]. A strain as small as 0.05% was found to explain the magnitude of the corresponding uniaxial in-plane anisotropy field [62]. The effect of the trigonal strain on the Zener current

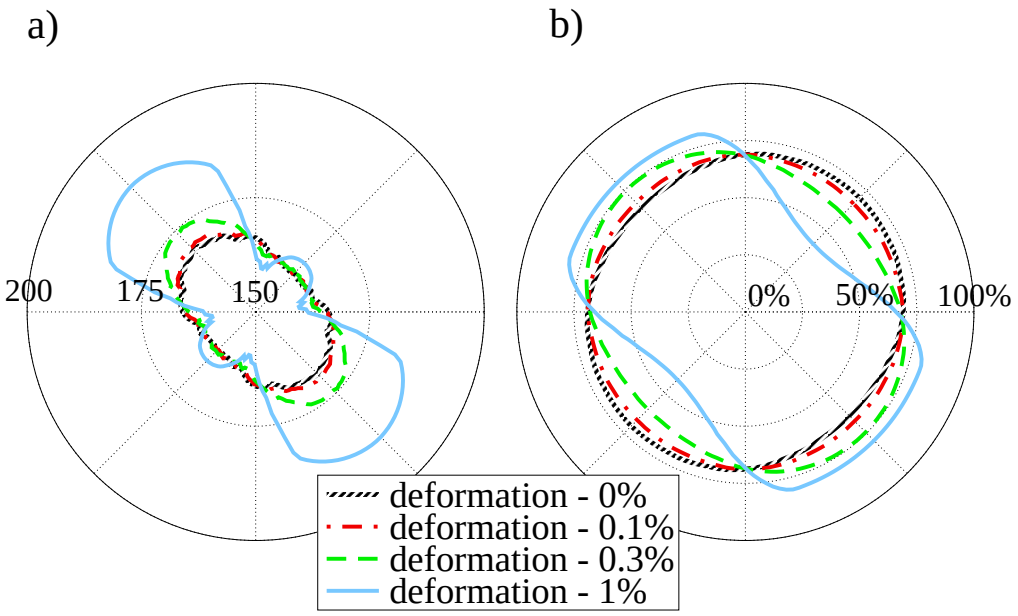

Figure 5.14: Dependence of Zener tunneling current in arbitrary units (a) and its spin polarization (b) on the direction of in-plane magnetization without strain and for deformations up to 1% applied along the [110] axis. Calculations performed for Mn content $x = 0.08$, hole concentration $p = 3.5 \times 10^{20}$ cm^{-3}, and electron concentration $n = 10^{19}$ cm^{-3} in the limit of low bias (0.01 V).

and its spin polarization is presented in Fig. 5.14 together with previously discussed results for unstrained structures. As seen, the strain causes an additional in-plane anisotropy. However, a rather strong deformation is needed to obtain a significant dependence of spin current polarization on the direction of the magnetization vector. Even for 0.1% deformation, which is two times larger than that evaluated in Ref. [62], the anisotropy of the spin polarization of the current is still very small. When a strong, 1%, deformation is assumed, the calculation predicts a 10% increase of current spin polarization for magnetization along [$\bar{1}$10] axis. At the same time, the obtained spin polarization for the magnetization along [110] direction is smaller by about 30%.

5.3.2 Out-of-plane Magnetization

The spin dependent interband tunneling is sensitive not only to the in-plane magnetization direction. It has been shown in Ref. [23] that rotation of magnetization by applying an out-of-plane magnetic field leads also to a TAMR signal in a Zener-Esaki diode. The magnitude of perpendicular tunneling anisotropic magnetoresistance is defined as

$$TAMR_{\perp} = \frac{R(H_{\perp}) - R(0)}{R(0)}, \tag{5.1}$$

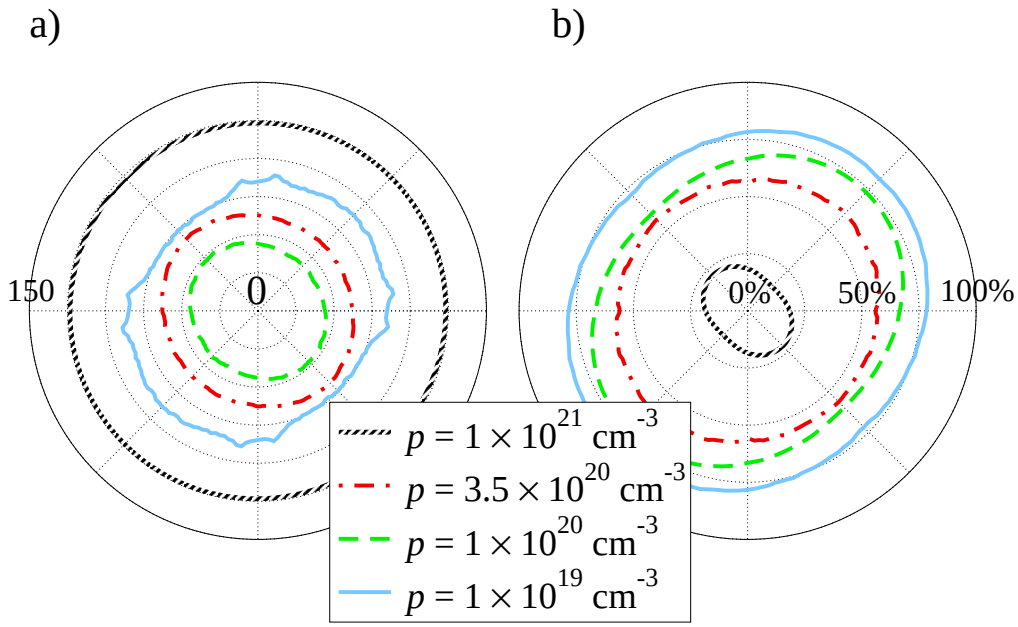

Figure 5.15: Dependence of Zener tunneling current in arbitrary units (a) and its spin polarization (b) on the direction of in-plane magnetization for various hole concentrations; Mn content $x = 0.08$ and electron concentration $n = 10^{19}$ cm^{-3} in the limit of low bias (0.01 V).

where R(H$_\perp$) and R(0) are the resistances for two mutually perpendicular, out-of-plane and in-plane configurations of saturated magnetization, *i.e.*, for magnetization along [001] and [100] crystallographic axis, respectively. It is worth noting that under the presence of spin-orbit interaction, a relatively large change in resistance is expected when the direction of magnetization alternates from perpendicular to parallel in respect to the current, even if the effect of epitaxial strain, which makes the [100] and [001] directions non-equivalent, is disregarded. In the Boltzmann conductance regime, the effect is known as anisotropic magnetoresistance (AMR), and has already been studied in (Ga,Mn)As experimentally and theoretically [3, 33].

The calculated relative changes of the structure resistance for the magnetization vector flipping between perpendicular-to-the-plane and in-plane directions are shown in Fig. 5.16 as a function of bias for various hole concentrations in $Ga_{0.94}Mn_{0.06}As$. For $p = 3.5 \times 10^{20}$ cm^{-3}, the maximum of the computed TAMR effect, exceeding 20%, is seen at small bias voltages. These results are compared with the experimental findings of Ref. [23], where the structure containing ferromagnetic $Ga_{0.94}Mn_{0.06}As$ with $T_C \approx 70$ K was studied. According to the p-d Zener model,[16] such a value of T_C corresponds to $p \approx 10^{20}$ cm^{-3}.

We see in Fig. 5.16 that the theory describes correctly the experimental magnitude of TAMR$_\perp$ for small bias at both polarizations. We see also that the computed TAMR$_\perp$ tends to vanish with the increase of the reverse bias, whereas when the for-

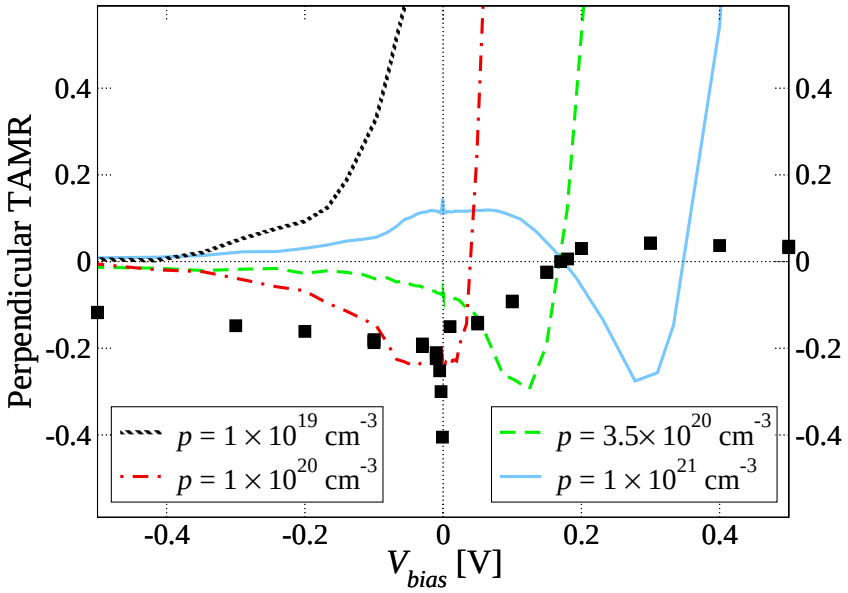

Figure 5.16: The bias dependence of the relative change in the tunneling resistance in Zener-Esaki p-$Ga_{0.94}Mn_{0.06}As$/n-GaAs diode when magnetization is rotated out-of-the-plane, for various hole concentrations; $n = 10^{19}$ cm^{-3}. The black squares are experimental points from Ref. [23].

ward bias is assumed, $TAMR_\perp$ changes sign and tends to infinity. Such change of sign for the forward bias is also revealed experimentally, but the measured $TAMR_\perp$ appears to vanish for higher values of positive bias. This inconsistency can be explained by recalling that the computed tunneling current stops to flow above the tunneling cutoff voltage, which is determined by a sum of the energy distance from the hole Fermi level E_F^v to the top of the valence band in (Ga,Mn)As and the energy difference between the bottom of the conduction band and electron Fermi level E_F^c in GaAs. In the experiment, however, some current related to band-gap states appears to dominate near the cutoff voltage. In turn, series bulk resistances, which are not taken into account in the calculations, may dominate at high reverse bias. Accordingly, standard AMR appears to contribute to the experimental value of $TAMR_\perp$ in this bias regime [23].

Figure 5.16 shows also the $TAMR_\perp$ calculated for different hole concentrations in the magnetic layer. Due to the strong *pd* exchange and large spin splitting in the (Ga,Mn)As valence band, for the low value $p = 1 \times 10^{19}$ cm^{-3} all spin subbands above the Fermi energy have the same spin polarization and thus $TAMR_\perp$ does not change the sign upon applying the positive bias. When, however, the Fermi level is very deep in the band, in the case of large $p = 1 \times 10^{21}$ cm^{-3}, different spin subbands contribute to the current for various voltages and $TAMR_\perp$ as a function of bias changes the sign twice.

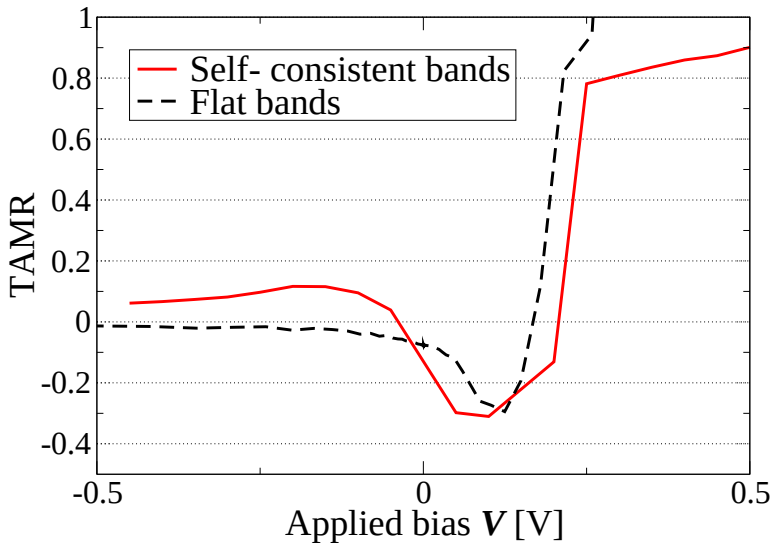

Figure 5.17: Perpendicular TAMR in Zener diode calculated using the self-consistent model after the Fig. 5.6(b).

5.3.3 Self-consistent Model

As we have seen at the beginning of the section that a good description of the band profiles is essential for proper description of the dependence of the spin current polarization on applied bias. We have argued that correct band profiles play important role in the high bias limit. Here again, we are considering such case, so in order to check the validity of the calculation we need to use the self-consistent band profiles. The obtained results are presented on Fig. 5.17. These results show that band bending does not affect significantly the TAMR effect.

Chapter 6

Tunneling Magneto-resistance

In the previous chapter we have studied devices where only one magnetic layer was present and the spin polarization of the current was measured using external devices like LED diode. In this chapter we consider the case where two magnetic layers are present and are used for both generation and detection of the spin polarized current. We study here the tunneling magnetoresistence (TMR) effect in (Ga,Mn)As based heterostructures, where the magnetic layers are separated by tunneling barrier. We start by presenting the analysis of the bias dependence of the effect, which is be followed by the study of anisotropy in the tunneling. The end of the chapter is devoted to a free hole model, that captures and explains in a simple way the bias dependence of the TMR.

In order to check the validity of our model in the case of TMR structures, we start by studying the bias dependence of the effect. The model correctly describes the observed fast decay with the bias voltage of spin polarization of the tunneling current. Importantly, this theory does not invoke inelastic processes, which were predicted to play role in this effect. These processes together with heating of Mn spin subsystem may become crucial in the highest bias regime. Nevertheless, this allows us to conclude that the bias anomaly in the (Ga,Mn)As structures has a fundamental origin, related to band structure effects. Moreover, we study the impact of the interface roughness on the TMR effect. Astonishingly our results show that imperfect interfaces should have positive impact on TMR ratio and on its bias dependence. The reason for this is that due to the spread of ions the magnetic layers become virtually closer. Additionally, the results suggest that the TMR and its decrease with the applied bias can be controlled by appropriate engineering of the band offsets in the heterostructure, in particular, by a proper choice of the nonmagnetic barrier. Moreover, the spin splittings in the magnetic layers, i.e., the content of magnetic ions in (Ga,Mn)As, seem also to affect the rate of the decrease of TMR with the bias.

Next step in our study is the anisotropy of the TMR. In the case of TMR the [100] and [110] magnetization directions are not equivalent, while TMR is identi-

cal for [110] and [$\bar{1}$10] directions. Thus, for the TMR effect, in which two interfaces contribute to the tunneling, the D_{2d} symmetry of zinc-blende is recovered. For hole concentrations exceeding 10^{20} cm^{-3} the obtained anisotropy of TMR is, however, below 10%. This suggests that the high TAMR values detected experimentally [55] result probably from effects of extrinsic deformations and/or hole depletion. Indeed, the calculated anisotropy of TMR can be considerably enhanced by lowering the hole concentration (for $p = 10^{19}$ cm^{-3} up to ca 250%). Yet, for such low concentrations, hole localization effects, disregarded in our model, can be important. A careful analysis of our results shows that the anisotropy of the TMR results solely from directional dependence of the current in the AFM configuration. For the FM configuration, in which a high in-plane TAMR was experimentally observed, only a rather small resistance difference is theoretically expected when magnetization is flipping between [110] and [010] directions. In addition, as long as magnetizations remain parallel, the computed current is virtually independent of the structure deformation. A strong 0.3% trigonal distortion introduces some visible angular dependence only in the case of the AFM configuration. As for the out-of-plane magnetization directions, the calculated tunneling current in the FM configuration changes by a few percents when the magnetization vector assumes the direction perpendicular to the plane. The effect of the same sign and of a magnitude of about 12%, was observed experimentally [22].

The results described above show that the full tight-binding description is essential for reliable modeling of TMR in modulated structures of (Ga,Mn)As. In particular, it is indispensable for studying the symmetries and angular dependencies of the tunneling. Still, we are aware that this approach, which requires the availability of a very good semi-empirical tight-binding parametrization for all constituent materials and leads always to large matrix Hamiltionians (e.g., in the case of GaAs or AlAs barriers the used by us relatively simple $sp^3d^5s^*$ tight-binding Hamiltonian, with only nearest neighbor interactions included [28], resulted in a 40×40 matrix for each double (cation+anion) layer of the structure), is not very practical for one, who wants to undertake a systematic study of different TMR structures. Therefore, to facilitate the study of the TMR structures and devices, we are looking for a simple, albeit accurate, approach that would emphasize intuitive understanding of such structures. We construct a free hole model in the spirit of Slonczewski approach [64], being, however, advised by the results of tight-binding calculations about which parameters are important for the bias anomaly and have to be included in the model. The validity of the free hole model is checked by a comparison with the results of the full tight-binding method, for structures with GaAs and AlAs barriers. The results of the model show that two parameters – spin splitting in the magnetic layers and spacer barrier height – define the two range decay of TMR with bias. This two range decay is clearly seen here in this simple model, whereas it was obscured in the tight-binding approach. Additionally, the model predicts that the TMR decay can be reduced when asymmetric polarizations in the leads are introduced. This prediction

is again verified with the tight-binding model. Finally, the case of one-dimensional tunneling is considered, which eventually can be used to predict the behavior of TMR in (Ga,Mn)As nanowires. Finally, we point out that in the limit when the height of the barrier tends to infinity, our one-dimensional approach corresponds to the Jullière model.

6.1 Bias dependence

As we have mentioned in the introduction in all experiments the observed TMR shows a rapid and hitherto unexplained decay with the increase of the applied bias. As shown in Fig. 6.1, our calculations reproduce such decay. This suggests that the dependence of TMR on the applied bias results predominantly from the band structure effects in this case.

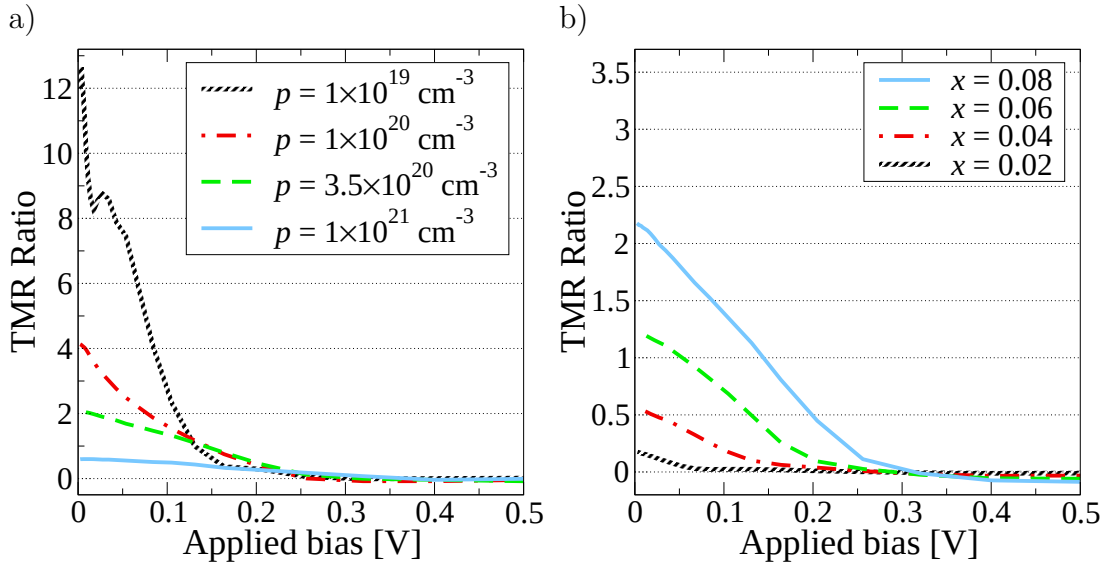

Figure 6.1: The calculated bias dependence of the TMR effect in p-$Ga_{1-x}Mn_xAs/(GaAs)_4/p$-$Ga_{1-x}Mn_xAs$ trilayer (with the GaAs barrier width $d = 4$ monolayers) for various hole concentrations p and Mn ions content $x = 0.08$ (a) and for various values of x and $p = 3.5 \times 10^{20}$ cm^{-3} (b).

In Fig. 6.1(a) one should note a strong dependence of TMR and its decay with applied voltage on the hole concentration in the magnetic contacts. However, one can also see that the hole concentration does not influence very strongly the bias where the TMR reaches zero. This voltage, ca 0.26 V, corresponds to the valence band offset between $Ga_{0.92}Mn_{0.08}As$ and GaAs, which is determined by the spin splitting in the valence band of the former. The presented in Fig. 6.1(b) TMR ratios for the magnetic contacts with various Mn content, *i.e.*, with different spin splitting, confirms this conclusion. These results suggest that the TMR and its decrease with

the applied bias can be controlled by appropriate engineering of the band offsets in the heterostructure, in particular, by a proper choice of the nonmagnetic barrier. To check this prediction theoretically, we replace in the calculations the GaAs by AlAs, which produces a higher by 0.55 V barrier for the holes (see Fig. 1.7). The results presented in Fig. 6.2 show that, indeed, for tunneling through the AlAs barrier, the TMR magnitude decreases with the bias much slower than in the case of GaAs. Moreover, for a higher tunneling barrier one can expect also higher TMR ratios.

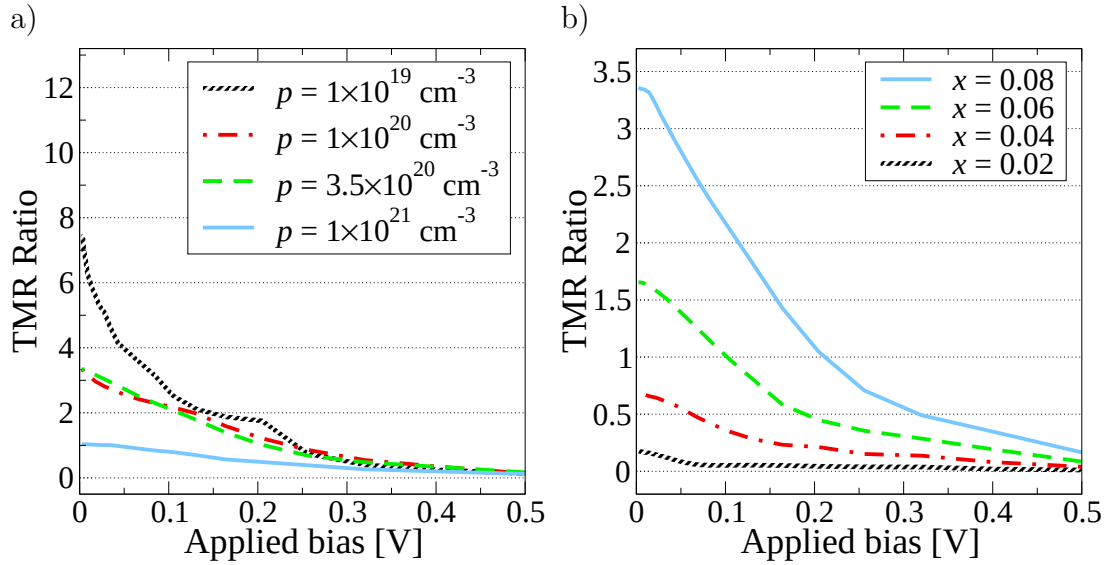

Figure 6.2: The bias dependence of the TMR ratio for p-$Ga_{1-x}Mn_xAs/(AlAs)_4/p$-$Ga_{1-x}Mn_xAs$ with $x = 0.08$ and various hole concentrations (a); for various values of x and $p = 3.5 \times 10^{20}$ cm^{-3} (b).

A related behavior can be seen in the study of the dependence of TMR effect on the width of the barrier, presented in Fig. 6.3. In agreement with experimental observations [68], the calculated TMR drops rapidly when the barrier becomes wider. However, for AlAs which forms a higher barrier, the decrease of the TMR ratio with the number of barrier monolayers is much weaker.

6.1.1 Self-consistent Model

In the case of inter-band tunneling in Zener-Esaki diode we have seen that a decent description of band profiles is essential in order to obtain correct description of the bias dependence. Hence, our extensive discussion of the bias dependence might seem to be premature. However, it should be noted that in the studied trilayers the carrier relocation has minor influence on the band profiles. In contrary to the *pn* Zener-Esaki diode we deal here only with interfaces between p-type and neutral materials with very small band offsets. Anyway we have checked the validity of this assumption by performing self-consistent calculations for the (Ga,Mn)As/GaAs/(Ga,Mn)As

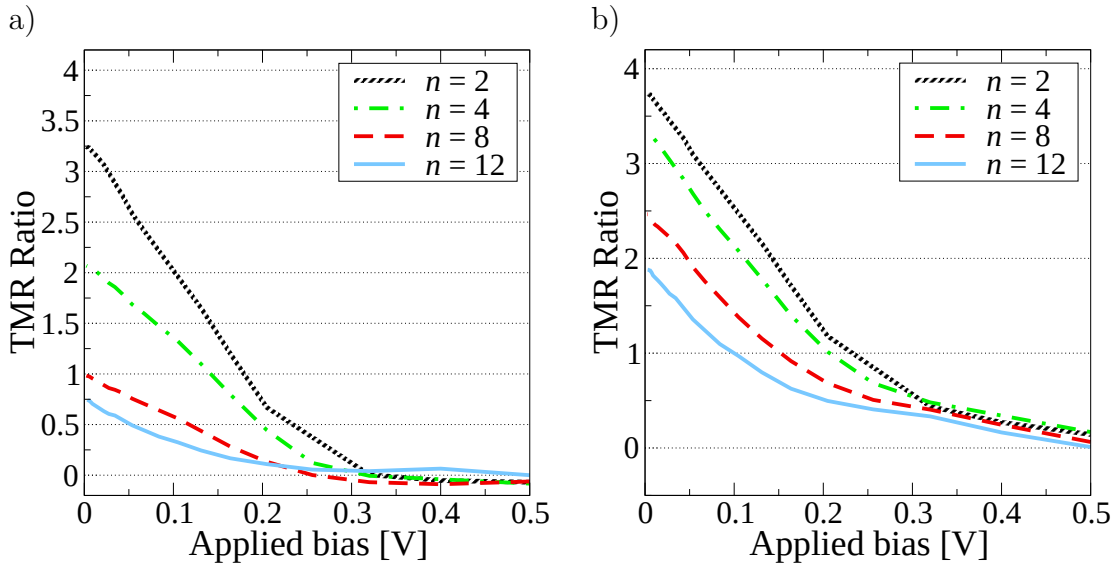

Figure 6.3: The bias dependence of the TMR ratio for various thicknesses d of the barrier layer in (a) p-$Ga_{0.92}Mn_{0.08}As/(GaAs)_d/p$-$Ga_{0.92}Mn_{0.08}As$; (b) p-$Ga_{0.92}Mn_{0.08}As/(AlAs)_d/p$-$Ga_{0.92}Mn_{0.08}As$ trilayers. The obtained band profiles are shown on Fig. 6.4.

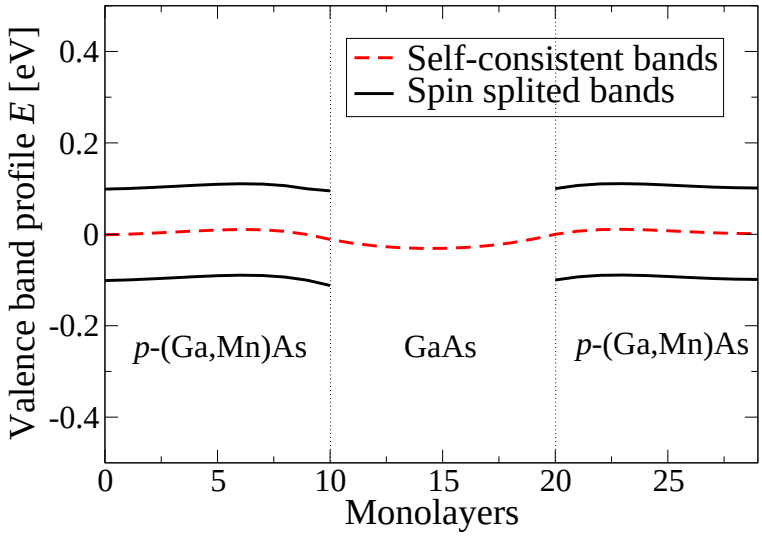

Figure 6.4: The calculated valence bands profile in p-(Ga,Mn)As/GaAs/p-(Ga,Mn)As TMR trilayers - all layers of the structure are 10 monolayers thick.

The results show that the band bending introduced by carrier relocation are relatively small and do not change drastically the situation. The next figure (Fig. 6.5) presents TMR ratio obtained for the discussed band profiles. As we have suspected the impact of the band-bending on TMR is small and does not influence the details of the bias dependence.

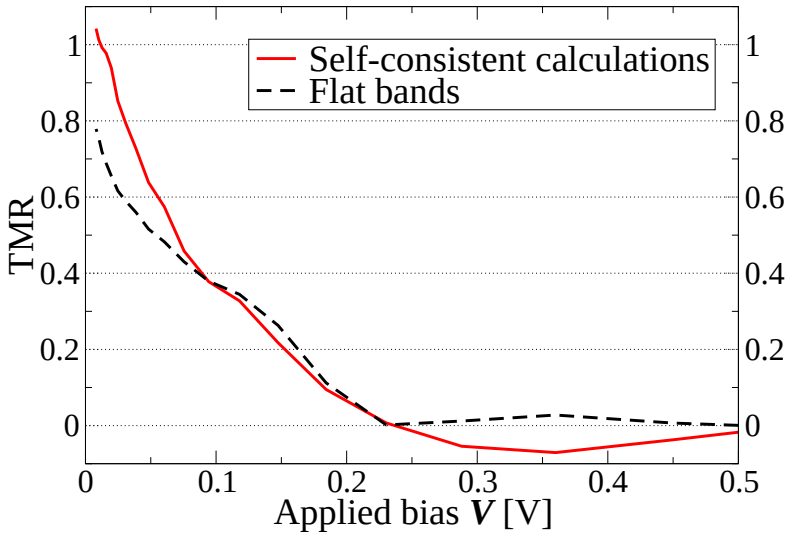

Figure 6.5: TMR ratio vs. bias in p-(Ga,Mn)As/GaAs/p-(Ga,Mn)As - all layers of the structure are 10 monolayers thick.

6.1.2 Interface Roughness

To account, at least partially, for the interface roughness, inevitable in the real structures, we introduce a Gaussian distribution of the ions within σ monolayers thick interface region. This interface spread is taken into account in the calculations within the virtual crystal approximation, *i.e.*, instead of considering a structure where the ions are randomly relocated according to a given distribution, we consider a structure where the tight-binding atom parameters are spread according to the given distribution. The results of this calculation are presented on Fig. 6.6.

Astonishingly, for larger interface roughness the TMR ratio is higher and vanishes for higher bias values – this can be explained by a better k-matching in both regions, resulting from the spread of available states in the interfaces.

6.2 Effect of Material Properties

Similarly to the spin polarization of the tunneling current in Zener-Esaki diode, TMR increases with the content of the magnetic ions and decreases with the concentration of the holes in (Ga,Mn)As layers. In Fig. 6.7 (a) the obtained TMR values, for a given (8%) Mn content are plotted as function of hole concentrations in the FM layers.

As shown, TMR depends strongly on the hole concentration. As TMR is primarily determined by spin polarization of the carriers at the Fermi level, the higher hole concentration the smaller is spin polarization at the Fermi level at given Mn spin polarization. For $p = 3.5 \times 10^{20}$ cm^{-3}, which is the typical hole concentration

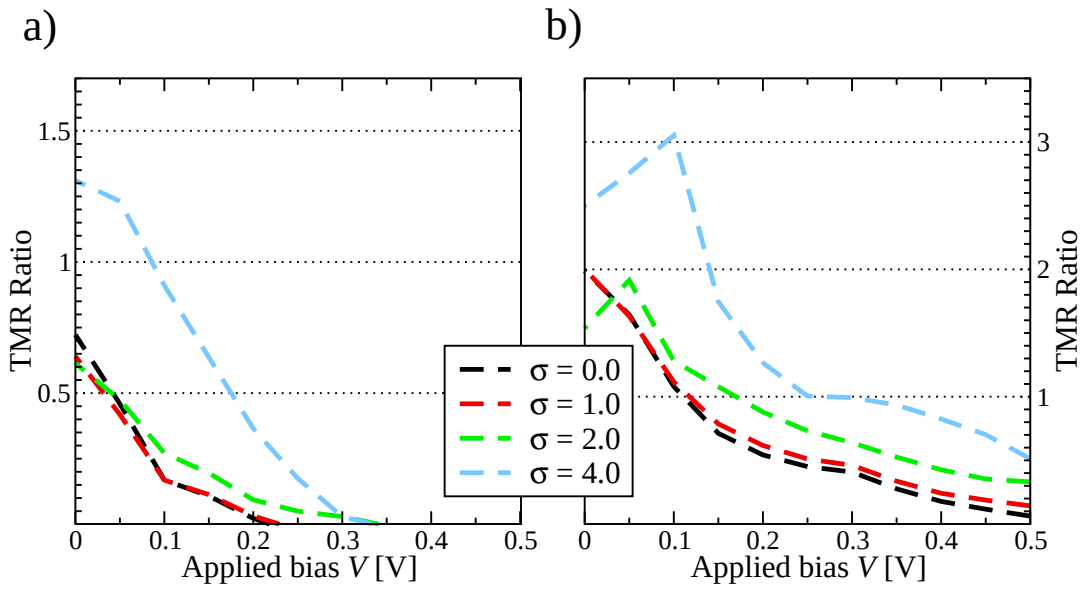

Figure 6.6: The bias dependence of the TMR ratio for a) p-$Ga_{0.92}Mn_{0.08}As/(GaAs)_{12}/p$-$Ga_{0.92}Mn_{0.08}As$ v) p-$Ga_{0.92}Mn_{0.08}As/(AlAs)_{12}/p$-$Ga_{0.92}Mn_{0.08}As$ for various interface roughnesses σ and $p = 3.5 \times 10^{20}$ cm^{-3}.

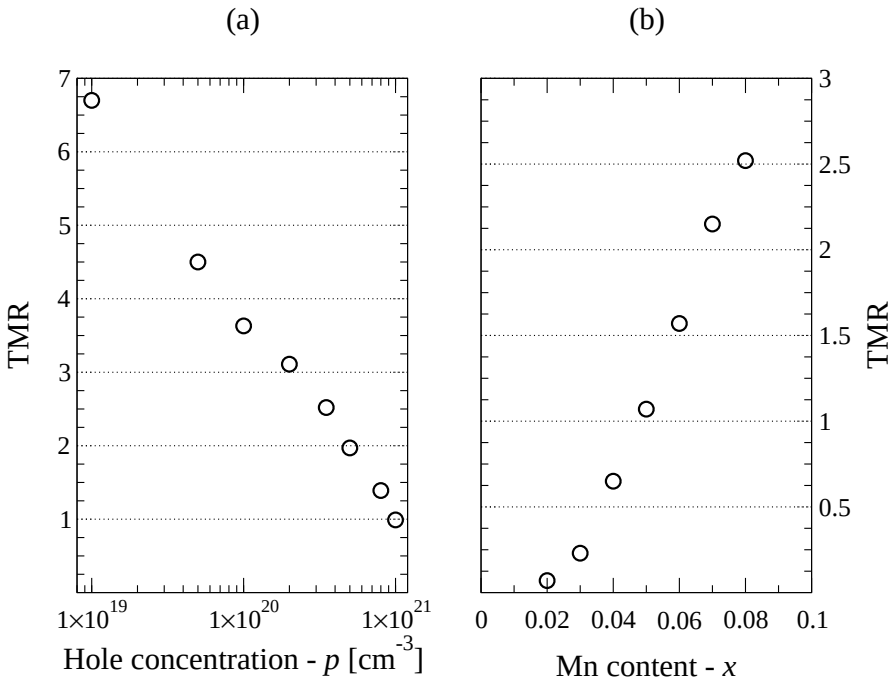

Figure 6.7: TMR in p-$Ga_{1-x}Mn_xAs$/GaAs/p-$Ga_{1-x}Mn_xAs$ as a function of: (a) hole concentration p (for $x = 0.08$); (b) Mn content (for $p = 3.5 \times 10^{20}$ cm^{-3}). The bias applied to the structure is $V = 0.01$ V.

in (Ga,Mn)As samples with a high Mn content [73], the TMR of about 250% is obtained. Because of self-compensation, the hole concentration depends rather weakly

on x – thus, we have calculated the TMR for different x in the magnetic layers, while keeping the hole concentration constant, $p = 3.5 \times 10^{20}$ cm^{-3}. The results of such computations are presented in Fig. 6.7(b).

As seen, our simple model reproduces fully the experimental data: for structures with 8% of Mn we obtain the TMR of the order of 250%, as observed recently by Chiba *et al.* [13]; for 4% of Mn the calculations lead to the TMR of the order of 60%, in perfect agreement with the observations of Tanaka and Higo [68] and Mattana *et al.* [45]. Therefore, our calculations seem to suggest that for obtaining a high TMR, large exchange splittings, *i.e.*, high content of magnetic ions is needed. Unfortunately, the presented in Fig. 6.7 dependence suggests that the attempts to increase the hole concentration in (Ga,Mn)As, in order to obtain higher Curie temperature, may result in a reduced TMR value.

6.3 Anisotropy of Tunneling Magnetoresistance

Let us now analyze the dependence of the TMR on magnetization direction, *i.e.*, the anisotropy of the effect. The calculated dependence of TMR on the in-plane direction of the magnetization vector is shown in Fig. 6.8. It is seen that in the case of TMR the [100] and [110] magnetization directions remains not equivalent, while TMR is identical for [110] and [$\bar{1}$10]. Thus, the D_{2d} symmetry is recovered if two interfaces are involved, in contrast to the case of spin current polarization in the Esaki-Zener diode, where C_{2v} symmetry of a single zinc-blende interface led to the non-equivalence of the [110] and [$\bar{1}$10] directions, as discussed in previous chapter.

As shown in Fig. 6.8, the in-plane anisotropy of TMR depends crucially on the hole concentration in the magnetic layer. For hole concentrations p in the range of 10^{20} cm^{-3} the obtained anisotropy of TMR is below 10%. However, for low concentrations, $p = 10^{19}$ cm^{-3}, it becomes as strong as 250%. The reason for this behavior becomes clear when we look at Fig. 6.9 that shows the dependence of the tunneling current in the AFM configuration on the in-plane wave vector for different directions of magnetization. In Fig. 6.9(a), *i.e.*, in the case of $p = 10^{19}$ cm^{-3} the region of the Brillouin zone that takes part in the tunneling is strongly dependent on the magnetization direction, in contrast to the results for higher hole concentrations presented in Fig. 6.9(b). It should be stressed that such behavior has been obtained only for the AFM alignment. The calculated tunneling current in the FM configuration does not virtually depend on the direction of magnetization – only a very small difference between [110] and [010] direction has been found.

A similar effect can be also noticed in the calculated dependence of the TMR ratio on strain, as shown in Fig. 6.10. Here, again we see that upon trigonal strain the tunneling current becomes anisotropic only for the AFM alignment of magnetization in the two magnetic contacts.

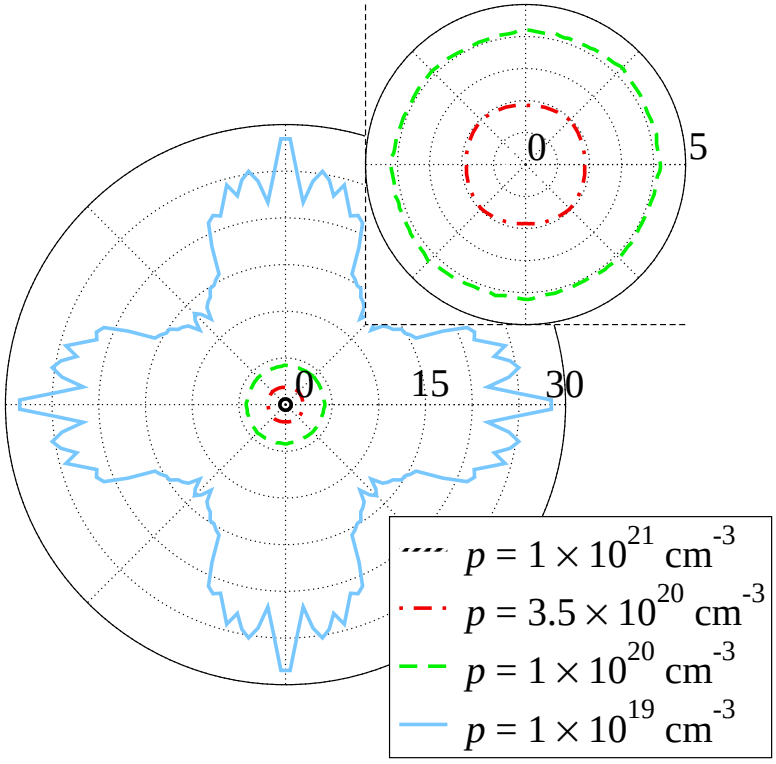

Figure 6.8: Dependence of TMR ratio on the direction of in-plane magnetization for various hole concentrations in p-$Ga_{0.92}Mn_{0.08}As$/$(GaAs)_4$/p-$Ga_{0.92}Mn_{0.08}As$ trilayer structure.

6.4 Tunneling Anisotropic Magnetoresistence

The results presented above show that the computed anisotropy of TMR results exclusively from the anisotropy of tunneling in the AFM configuration. Thus, this anisotropy cannot explain the in-plane TAMR effect observed in the trilayer structures based on (Ga,Mn)As [55, 22], *i.e.*, the difference in the resistance of the structures in FM configuration between the x and y directions. As stated before, we obtain only a very small difference in the FM tunneling current between the [110] and [010] direction. Although this anisotropy can be increased to about 15% by assuming a low hole concentration of $p = 1 \times 10^{19}$ cm^{-3} (compare Fig. 6.11), the depletion effects would not affect the anisotropy directions determined by the symmetry of the structure. In agreement with the calculations, D_{2d} symmetry of a rather small (below 10%) anisotropy of the TMR as well as in-plane TAMR has been recently observed by Saito *et al.* [57].

However, the calculated tunneling current for magnetization vector perpendicular to the plane differs from the current calculated for the in-plane magnetization vector even for the FM configuration. Using the $TAMR_\perp$ ratio defined in Eq. (5.1), we have calculated the perpendicular TAMR for the (Ga,Mn)As/GaAs/(Ga,Mn)As

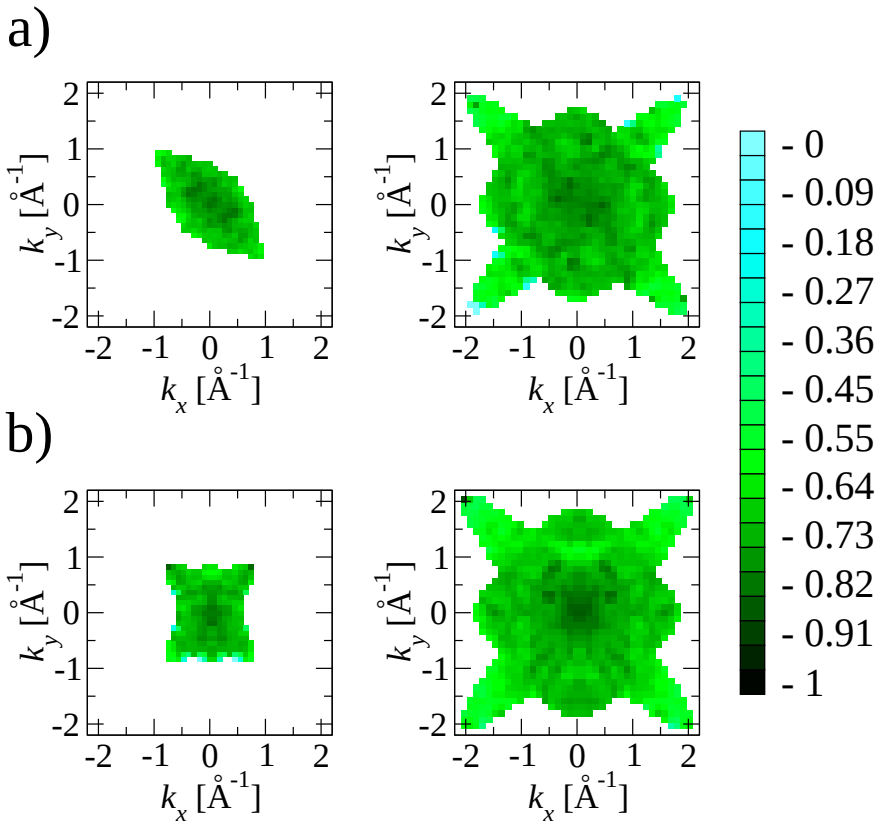

Figure 6.9: Dependence of tunneling current (in arbitrary units, in the limit of low (0.01 V) bias) on the direction of the in-plane wave vector for antiparallel configuration of magnetizations (AFM) along the [110] (a) and [010] (b) crystallographic directions. Two different values of hole concentration were assumed: 1×10^{19} cm^{-3} (left panels) and $p = 3.5 \times 10^{20}$ cm^{-3} (right panels).

and (Ga,Mn)As/AlAs/(Ga,Mn)As structures. The results are presented in Fig. 6.12. In the case of the GaAs spacer, for hole concentrations of about 1×10^{20} cm^{-3} a very small effect that weakly depends on the applied bias can be observed. Still, for small hole concentration we see a positive TAMR$_\perp$ of the order of 60%. The difference between the out-of-plane and in-plane resistances of the same sign and of about 12% was experimentally observed in Ref. [22]. As shown in Fig. 6.12, again a higher barrier, *i.e.*, the AlAs spacer, should enhance the TAMR$_\perp$ effect.

6.5 Free Hole Model

In Section 6.1 we have seen that our tight-binding model describes correctly the bias dependence of the TMR ratio. This sheds some light on the nature of this phenomena, and shows that the rapid decrease is the result of band structure effects. Of course other effect might play here some role as well. Nevertheless, good description of the

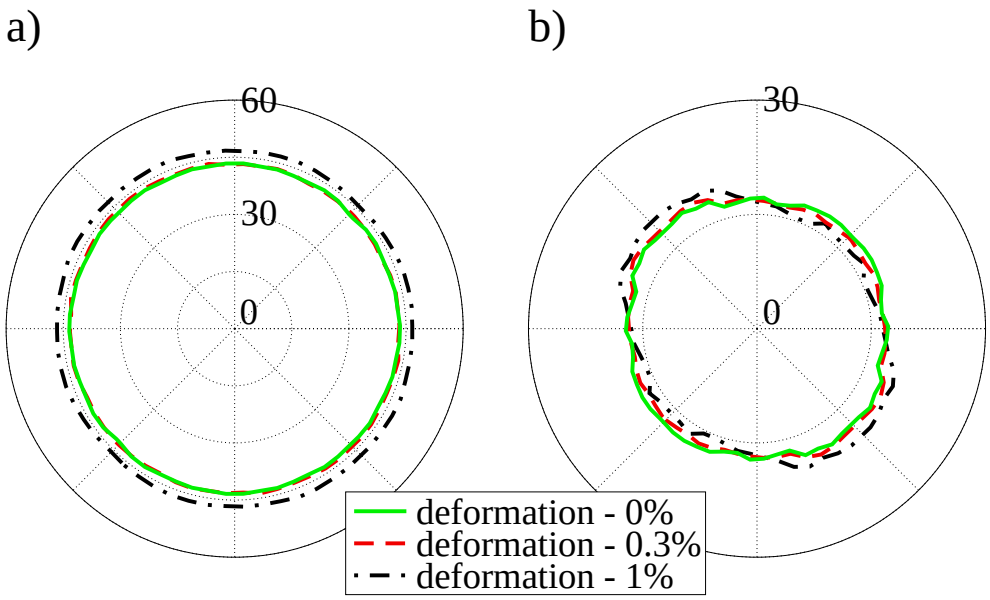

Figure 6.10: Dependence of tunneling current (in arbitrary units) on the direction of in-plane magnetization for (a) parallel (FM) and (b) antiparallel (AFM) magnetization orientations in p-$Ga_{0.92}Mn_{0.08}As/(GaAs)_4/p$-$Ga_{0.92}Mn_{0.08}As$ trilayer structures trigonally distorted along the [110] crystallographic axis; $p = 3.5 \times 10^{20}$ cm^{-3}; applied bias 0.01 V.

tunneling process is essential in order to describe this TMR decay. Here, we apply a very simple free hole model that includes only essential parameters. This simplified model allows a systematic study of the phenomena and leads to new predictions that are later on verified against the tight-binding approach.

6.6 Free Hole Model for TMR Structures

We consider a TMR device, in which two half-infinite ferromagnetic layers (L and R) are separated by a non-magnetic barrier (B). To describe such hypothetical $L/B/R$ structure we assume the dispersion relations in the three layers as given in Table 6.1. The effective masses in the three layers are denoted by m^L, m^B, m^R and are assumed to be equal to the light hole masses in the materials. For GaAs and (Ga,Mn)As, the light hole mass is $0.082m_e$ whereas for AlAs it is $0.15m_e$. We assume that the bands in the magnetic leads are split into two, minority and majority, spin bands and that in general the splitting s^L in the L ferromagnetic layer differs from the splitting s^R in R. In our calculations the magnetic material is described by two free parameters: the spin splitting s of the valence bands and the Fermi energy e_F. These parameters determine the hole concentration p or, respectively, p and s can be used to determine e_F. As shown in Fig. 6.13 for different values of the spin splitting s, the higher is the concentration of holes (the deeper in the valence band is the Fermi energy) the

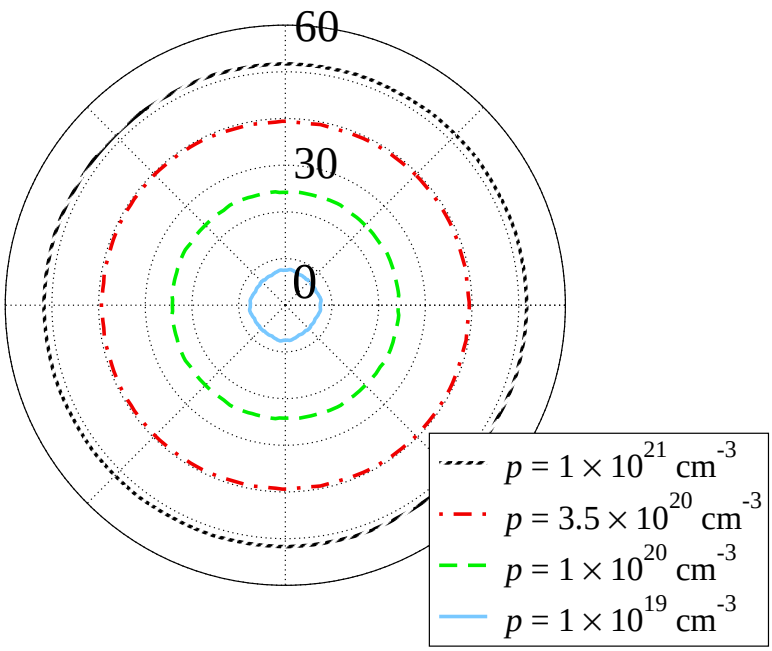

Figure 6.11: Dependence of tunneling current in arbitrary units on the direction of in-plane magnetization structures with parallel magnetization configuration (FM) for various hole concentrations in p-$Ga_{0.92}Mn_{0.08}As/(GaAs)_4$/p-$Ga_{0.92}Mn_{0.08}As$ trilayer structure; $p = 3.5 \times 10^{20}$ cm^{-3}; applied bias 0.01 V.

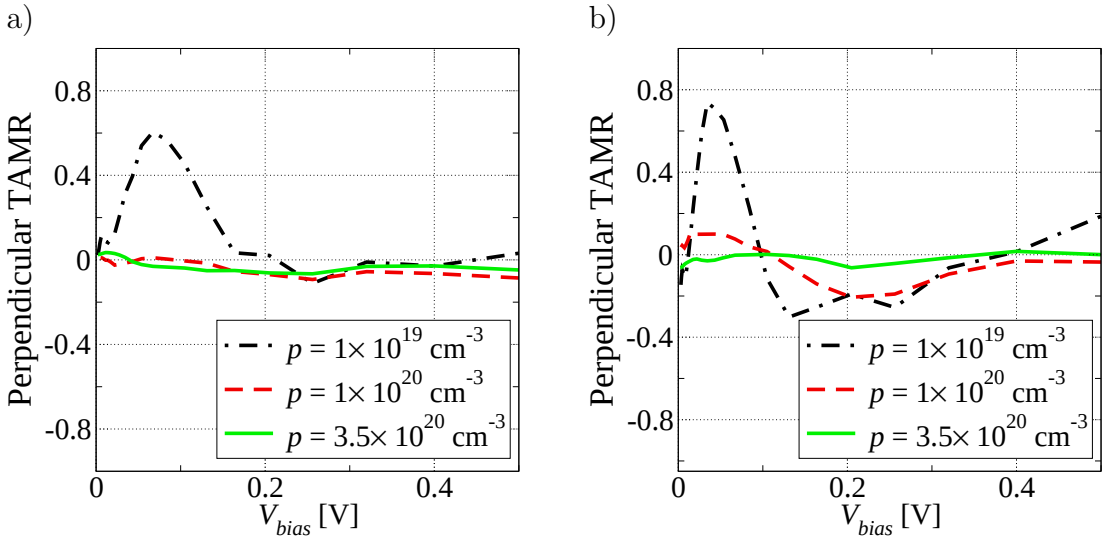

Figure 6.12: Bias dependence of the $TAMR_{\perp}$ ratio for TMR structure consisting of two magnetic p-$Ga_{0.92}Mn_{0.08}As$ layers separated by (a) GaAs and (b) AlAs barrier layer; $p = 3.5 \times 10^{20}$ cm^{-3}.

smaller is the spin polarization at the Fermi level.

For the non-magnetic spacer the free parameters are: the layer width a and Δ,

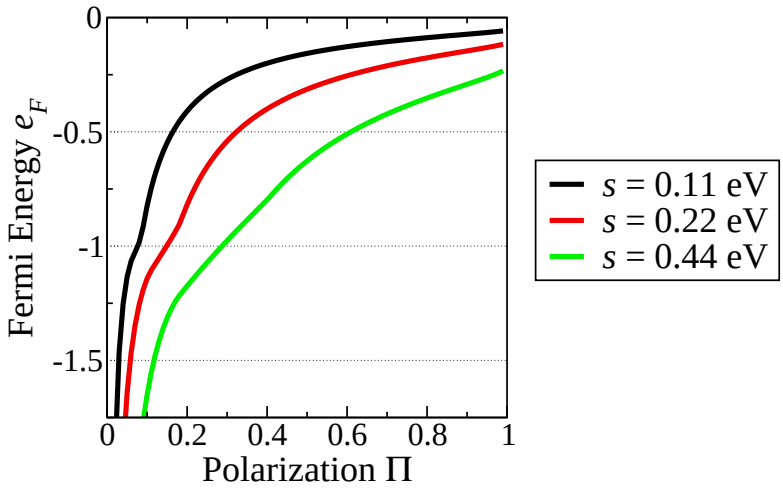

Figure 6.13: The Fermi energy e_F versus the spin polarization Π in the (Ga,Mn)As layers ($m = 0.082m_e$) for various values of the spin splitting s.

	Majority Bands	Minority Bands
Left lead	$k^L_{\Updownarrow} = \frac{\sqrt{2m^L(E-e_F^L-\frac{s^L}{2})}}{\hbar}$	$k^L_{\updownarrow} = \frac{\sqrt{2m^L(E-e_F^L+\frac{s^L}{2})}}{\hbar}$
Barrier	$k^B = \frac{\sqrt{2m^B(E-\frac{V}{2}+\Delta)}}{\hbar}$	
Right lead	$k^R_{\Updownarrow} = \frac{\sqrt{2m^R(E-e_F^R-\frac{s^R}{2}-V)}}{\hbar}$	$k^R_{\updownarrow} = \frac{\sqrt{2m^R(E-e_F^R+\frac{s^R}{2}-V)}}{\hbar}$

Table 6.1: Dispersion relations for holes in the studied structure, where m^L, m^B, m^R are the effective masses; s^L, s^R are the spin splittings; e_F^L, e_F^R are the Fermi energies; Δ is the spacer band offset and V is the bias applied to the structure.

i.e., the position of the top of the spacer valance band with regard to the Fermi level in the left contact, which is assumed to be the zero energy level (thus, the energy difference between the tops of the valence bands in the L and B layers is equal to $\Delta + e_F^L + s^L/2$). The band structure in the three regions of the simulated $L/B/R$ device is shown schematically in Fig. 6.14 (a). In the figure the tunneling of holes is depicted, because the magnetic layers considered in the paper are p-type (Ga,Mn)As.

Fig. 6.14 (b) shows the band structure when a non-zero bias V is applied. We assume the same voltage drop on each of the interfaces. Thus, due to the applied bias the bands in the barrier B are shifted by $V/2$, whereas the bands in the right magnetic lead R are shifted by V. One should note that the model is sound only when $V \leqslant \Delta$, because otherwise the current is dominated by the drift current which is not

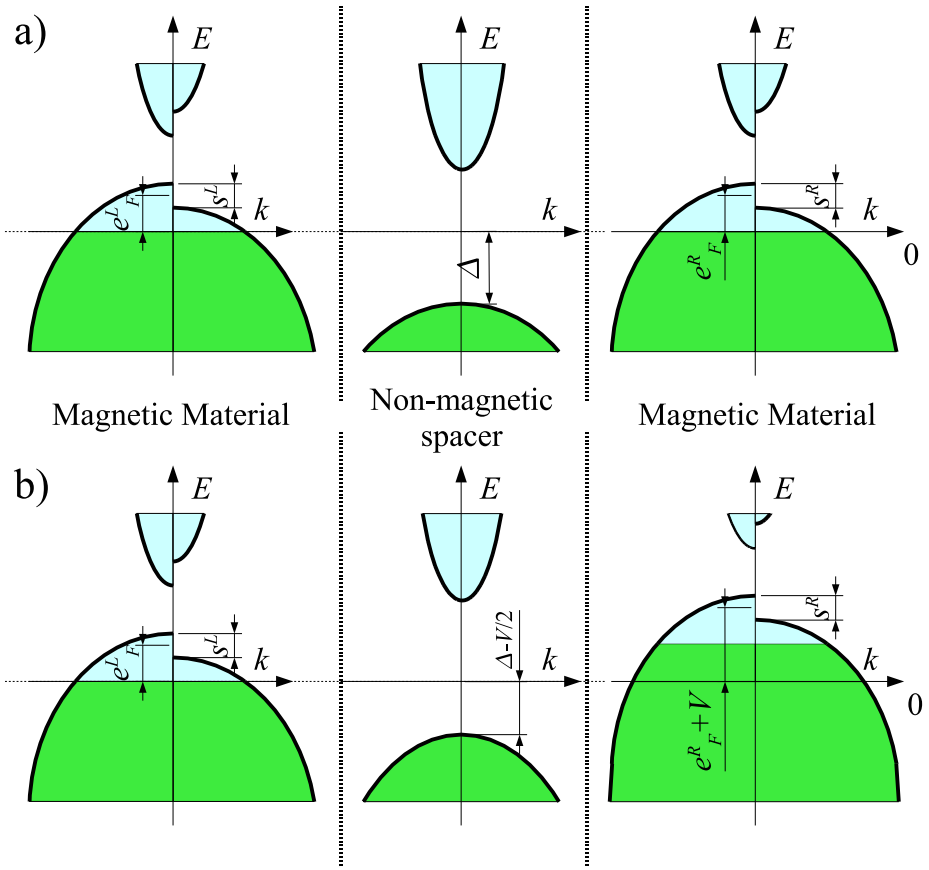

Figure 6.14: The simulated TMR device consists of three regions: ferromagnetic p-type leads and non-magnetic spacer. The device band structure for $V = 0$ (a) and for $V \neq 0$ (b).

taken into account in our model.

The number σ_α^Λ of spin-α states ($\alpha = \Updownarrow$ or $\updownarrow$, i.e., majority or minority spin) in magnetic lead Λ ($\Lambda = L$ or R) is equal to:

$$\sigma_\alpha^\Lambda = \int_{BZ} f^\Lambda(E_\alpha^\Lambda(\mathbf{k}))d^3k. \tag{6.1}$$

When not stated otherwise the calculations are performed for temperature $T = 4.6$ K.

The spin polarization of states in the lead Λ can be defined as:

$$\Pi^\Lambda = \frac{\sigma_\Updownarrow^\Lambda - \sigma_\updownarrow^\Lambda}{\sigma_\Updownarrow^\Lambda + \sigma_\updownarrow^\Lambda}. \tag{6.2}$$

In the free hole model the carrier transmission amplitude from left α spin state to right β spin state can be obtained by solving Schrödinger equation for tunneling:

$$t_{k_\alpha^L \to k_\beta^R}(E, \mathbf{k}_\parallel) = \frac{4}{\left(\frac{k^B}{k_\alpha^L} - \frac{k_\beta^R}{k^B}\right)^2 \mathrm{sh}^2(k^B a) + \left(1 + \frac{k_\beta^R}{k_\alpha^L}\right)^2 \mathrm{ch}^2(k^B a)}.$$

The transition probability is now equal to:

$$T_{k_\alpha^L \to k_\beta^R}(E, \mathbf{k}_\parallel) = |t_{k_\alpha^L \to k_\beta^R}(E, \mathbf{k}_\parallel)|^2 \frac{k_\beta^R}{k_\alpha^L}. \tag{6.3}$$

Using this equation together with (3.4) we can obtain the tunneling current $j_{\alpha\to\beta}$.

To calculate the TMR ratio we compare the tunneling currents in two configurations, i.e., with parallel (ferromagnetic – FM) and the antiparallel (antiferromagnetic – AFM) alignments of the magnetizations in the leads. We define the tunneling magnetoresistance (TMR) ratio as:

$$TMR = \frac{j_{FM} - j_{AFM}}{j_{AFM}}, \tag{6.4}$$

where j_{FM} and j_{AFM} are the tunneling currents in the FM and AFM configurations, respectively. As the tunneling process does not change the spin of a carrier, the total current j_{FM} in the ferromagnetic configuration of the device is equal to:

$$j_{FM} = j_{\Updownarrow\to\Updownarrow} + j_{\updownarrow\to\updownarrow}, \tag{6.5}$$

whereas the total current j_{AFM} in the antiferromagnetic configuration is equal to:

$$j_{AFM} = j_{\Updownarrow\to\updownarrow} + j_{\updownarrow\to\Updownarrow}, \tag{6.6}$$

where $\Updownarrow$ and $\updownarrow$ denote the majority and minority spin states, respectively.

6.7 One Dimensional Tunneling

In this section we simplify the model by assuming that the tunneling is one dimensional, i.e., $\mathbf{k}_\parallel = 0$. In such case (3.4) becomes:

$$j_{\alpha\to\beta}^{1D} = \frac{-e}{(2\pi)^3\hbar} \int dE \left[f^L(E - f^R(E)\right] T_{k_\alpha^L \to k_\beta^R}(E, \mathbf{0}). \tag{6.7}$$

Next, as $T_{k_\alpha^L \to k_\beta^R}(E, \mathbf{0})$ depends weakly on E we can do the following approximation:

$$j_{\alpha\to\beta}^{1D} \approx \frac{-e}{(2\pi)^3\hbar} T_{k_\alpha^L \to k_\beta^R}(0, \mathbf{0}) \int dE \left[f^L(E) - f^R(E)\right], \tag{6.8}$$

which leads to the following approximate formula for the TMR ratio:

$$TMR^{1D} \approx \frac{T_{k^L_{\Downarrow}\to k^R_{\Downarrow}}(0,\mathbf{0}) + T_{k^L_{\uparrow}\to k^R_{\uparrow}}(0,\mathbf{0}) - T_{k^L_{\Downarrow}\to k^R_{\uparrow}}(0,\mathbf{0}) - T_{k^L_{\uparrow}\to k^R_{\Downarrow}}(0,\mathbf{0})}{T_{k^L_{\Downarrow}\to k^R_{\uparrow}}(0,\mathbf{0}) + T_{k^L_{\uparrow}\to k^R_{\Downarrow}}(0,\mathbf{0})}. \tag{6.9}$$

Further, we note that our one dimensional free hole model in the limit of $T \to 0$ and $\Delta \to \infty$, i.e., in the limit when the spacer details do not play any role, is equivalent to the Jullière model. In the one dimensional case the number σ^Λ_α of spin-α states in lead Λ is equal to:

$$\sigma^\Lambda_\alpha = \int_{-\infty}^{\infty} f(E^\Lambda_\alpha(k))dk. \tag{6.10}$$

which, in the limit of $T \to 0$ equals to:

$$\sigma^\Lambda_\alpha = 2k^\Lambda_\alpha(0). \tag{6.11}$$

In this limit the spin polarization of states is given by:

$$\Pi^\Lambda = \frac{k^\Lambda_{\Downarrow} - k^\Lambda_{\uparrow}}{k^\Lambda_{\Downarrow} + k^\Lambda_{\uparrow}}. \tag{6.12}$$

Taking into account only the highest order term in Δ in $T_{k^L_\alpha \to k^R_\beta}(0,\mathbf{0})$ we obtain:

$$T_{k^L_\alpha \to k^R_\beta}(0,\mathbf{0}) \sim_{\Delta\to\infty} \frac{k^R_\beta}{k^L_\alpha} \frac{4}{\left(\frac{k^B}{k^L_\alpha}\right)^2 \mathrm{sh}^2(k^B a)}. \tag{6.13}$$

Plugging this into (6.9) we get:

$$\lim_{\Delta\to\infty} TMR^{1D} = \frac{k^R_{\Downarrow}k^L_{\Downarrow} + k^R_{\uparrow}k^L_{\uparrow} - k^R_{\uparrow}k^L_{\Downarrow} - k^R_{\Downarrow}k^L_{\uparrow}}{k^R_{\uparrow}k^L_{\Downarrow} + k^R_{\Downarrow}k^L_{\uparrow}}, \tag{6.14}$$

and after some algebra we finally obtain:

$$\lim_{\Delta\to\infty} TMR^{1D} = \frac{\Pi^R\Pi^L}{1 - \Pi^R\Pi^L}, \tag{6.15}$$

what is exactly the TMR ratio predicted by the Jullière model.

6.8 Comparison with the Tight-Binding Model

We check the validity of the free hole model by comparing its prediction with the results of the tight-binding model in the case of GaAs and AlAs barriers. To reproduce

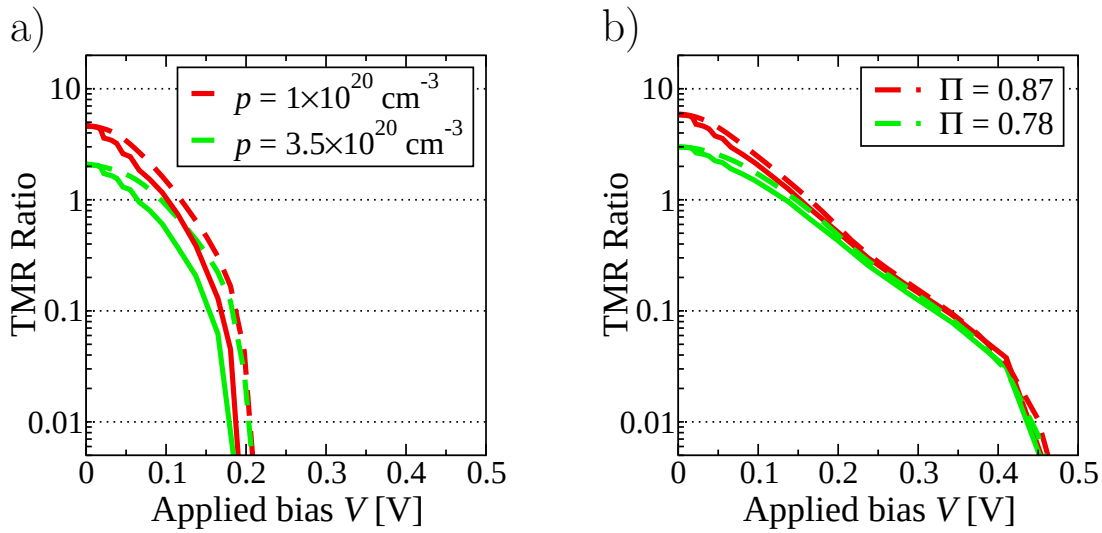

Figure 6.15: The TMR ratio in free hole model (dashed lines) fitted to the tight-binding results (cont. lines) in a) (Ga,Mn)As/$(GaAs)_4$/(Ga,Mn)As structure, b) (Ga,Mn)As/$(AlAs)_4$/(Ga,Mn)As structure. For GaAs spacer $\Delta = 0.23$ eV, whereas for AlAs spacer $\Delta = 0.55$ eV.

the TMR ratio obtained within the full tight-binding model in Ref. [59] (as presented in Fig. 6.15), we fit the free hole model parameters: Δ, which determines the band offset, and the spin polarization $\Pi = \Pi_L = \Pi_R$ in the magnetic contacts.

The value of Δ obtained from the fitting for the GaAs spacer is 0.23 eV and leads to a comparable band line-up that has been assumed in the tight-binding model [59]. Although the free hole model includes only two light hole bands, astonishingly, the fitted value of Δ for AlAs spacer (0.55 eV) is exactly equal to the band shift of the AlAs parametrization assumed in the tight-binding model. The spin polarizations Π in the (Ga,Mn)As magnetic leads are equal to 0.87 for $p = 1 \times 10^{20}$ cm^{-3} and 0.78 for $p = 3.5 \times 10^{20}$ cm^{-3}, in good agreement with the Zener model of ferromagnetism in (Ga,Mn)As [16].

6.9 Calculations for 3D Devices

In order to capture the key parameters that control the bias dependence of the TMR, we study a virtual structure consisting of two (Ga,Mn)As layers separated by four monolayers of a hypothetical spacer $\widetilde{\text{AlAs}}$, where $m^B = 0.15 m_e$, i.e., the effective mass is equal to the light hole mass in AlAs, but the band offset is varied. First, we assume that the spin polarization in both magnetic layers is the same and very high $\Pi_R = \Pi_L = 90\%$. In Fig. 6.16 a) the calculated TMR-ratios for different band-offset are shown.

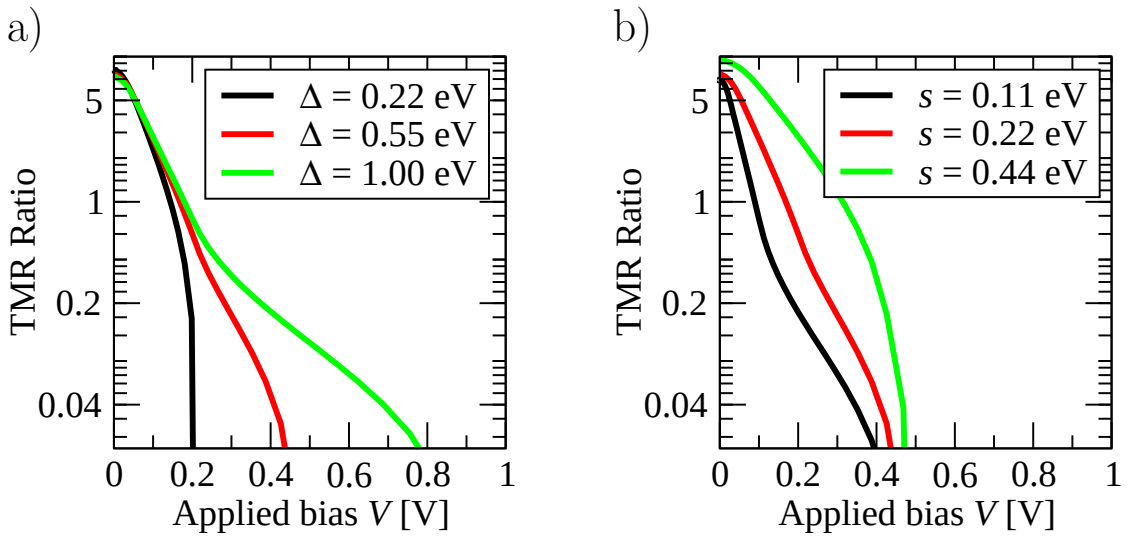

Figure 6.16: The simulated TMR-ratio for 3D tunneling in (Ga,Mn)As/$(\widetilde{\text{AlAs}})_4$/(Ga,Mn)As structure, where the band offset of the spacer material Δ is varied and $s = 0.22$ eV a) or the spin splitting $s = s_L = s_R$ in the magnetic leads is varied and $\Delta = 0.55$ eV b).

As one can see in Fig. 6.16, the decrease of the TMR-ratio with the bias occurs in two stages. In the first range, for $V \lessapprox s$, the decrease is almost independent on the value of Δ, whereas in the second range, for $V \gtrapprox s$, the decrease depends strongly on the value of Δ. For all studied band-offsets, the TMR-ratio tends to zero for $V \approx \Delta$. Next, we have calculated the bias dependence of the TMR-ratio for (Ga,Mn)As/$(\widetilde{\text{AlAs}})_4$/(Ga,Mn)As structure for different values of spin splitting $s_L = s_R = s$ in the magnetic leads, keeping the band-offset $\Delta = 0.55$ eV (Fig. 6.16 b)). Now it is clearly seen that in the first range the TMR dependence on bias is guided by the value of the spin splitting s, whereas in the second range the band offset plays the dominant role. Moreover, we note that the effective mass of the carriers in the spacer m^B should have a similar impact on the bias anomaly as Δ, what follows from the equation for k^B (see Table 6.1).

Now, let us study the impact of the spin polarization in the magnetic leads on the TMR value and the bias anomaly. As shown in Fig. 6.17, for $V = 0$ the higher the spin polarization the higher is the TMR ratio. On the other hand, higher Π results in faster decrease of TMR with the applied voltage and spin polarization has a very small impact on the bias for which the TMR disappears.

The situation changes, however, when we allow for different spin polarizations in the L and R leads, $\Pi_L \neq \Pi_R$.

In Fig. 6.18 the results obtained for different Π_L to Π_R ratios are presented and compared with the results for $\Pi_L = \Pi_R = 90\%$. The same spin splittings are assumed in all cases – thus, the different spin polarizations correspond to different

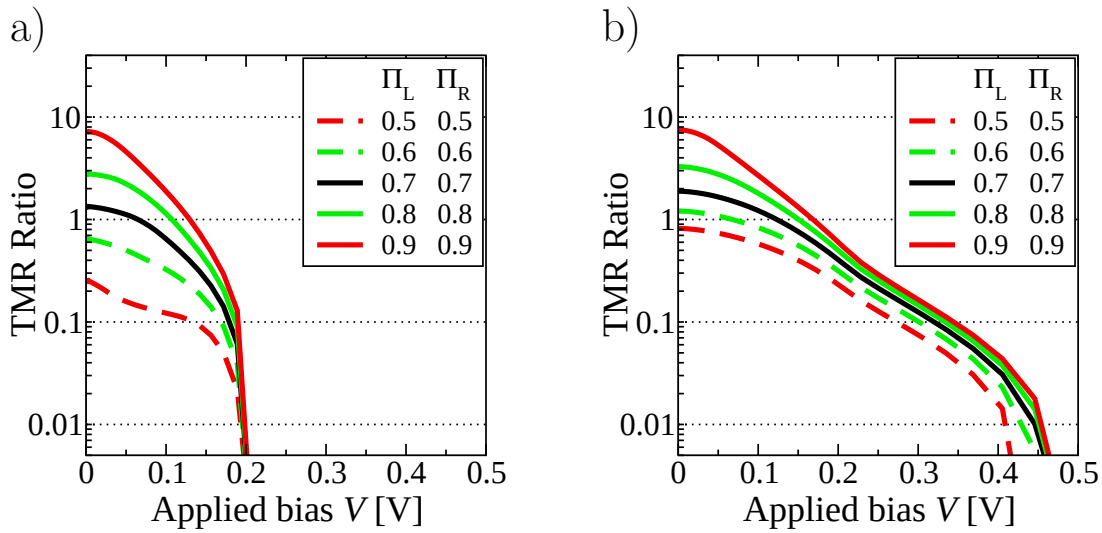

Figure 6.17: The TMR ratio in free hole model in a) (Ga,Mn)As/$(GaAs)_4$/(Ga,Mn)As structure, b) (Ga,Mn)As/$(AlAs)_4$/(Ga,Mn)As structure for the same spin polarizations in left and right leads. For GaAs spacer $\Delta = 0.23$ eV, for AlAs spacer $\Delta = 0.55$ eV, whereas $s = 0.22$ eV.

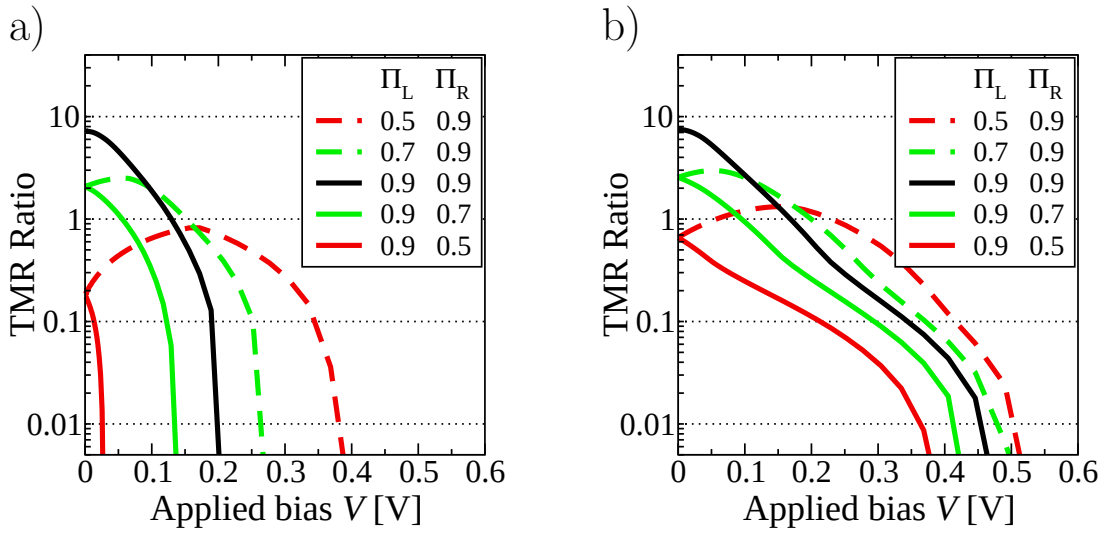

Figure 6.18: The TMR ratio calculated within the free hole model in a) (Ga,Mn)As/$(GaAs)_4$/(Ga,Mn)As structure, and b) (Ga,Mn)As/$(AlAs)_4$/(Ga,Mn)As structure for different spin polarizations in the left and right lead. The spin splitting in (Ga,Mn)As $s = 0.22$ eV, $\Delta = 0.22eV$ for the GaAs spacer, for AlAs $\Delta = 0.55eV$.

Fermi energies. First, we note that, as expected, a lower spin polarization even in one lead should result in lower TMR value for $V = 0$. However, a counter intuitive result that TMR ratio can grow with applied bias when $\Pi_L < \Pi_R$ can be seen in the figure. This result shows that the spin polarizations of the initial and final states are not the only important factors in spin tunneling. As can be seen in the formulae

for tunneling current the highest tunneling rates and spin transfer can be achieved when the **k** vectors at the Fermi levels in both leads are well matched. To explain the role played by the matching of **k** vectors in the above result, in Fig. 6.19 we present schematically the situation. For equal spin polarizations, the bands are best matched for $V = 0$ and hence the highest TMR value are obtained for zero bias (see Fig. 6.19 a)). Whereas, for $\Pi_L \neq \Pi_R$ the Fermi levels are different and the best match between the bands is obtained for such non-zero bias, which shifts appropriately the bands (see Fig. 6.19 b)).

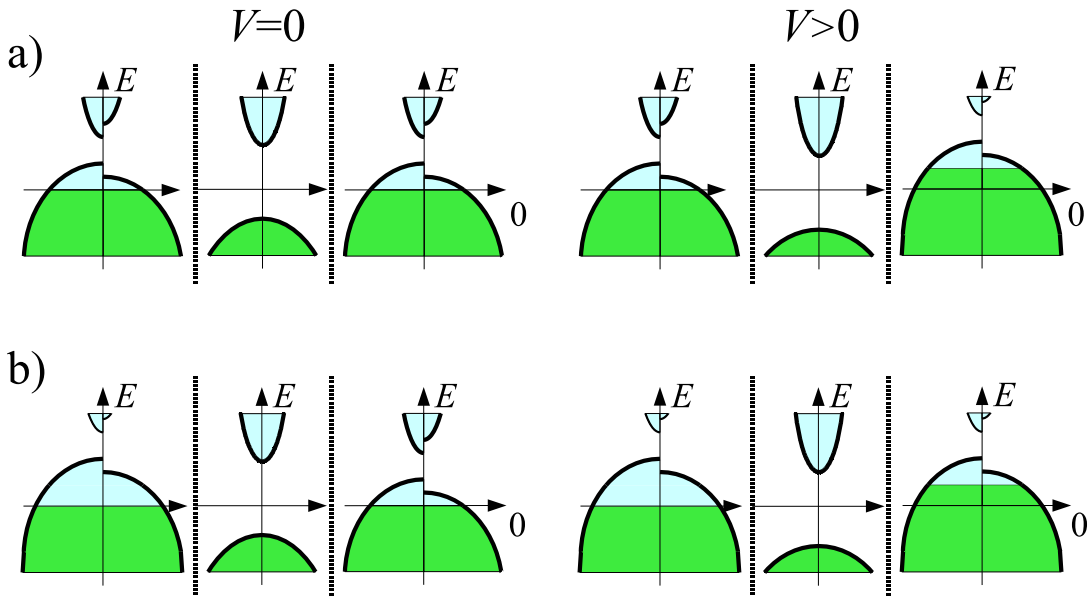

Figure 6.19: When $\Pi_L = \Pi_R$ the bands in both leads are well matched for $V = 0$ (a), whereas when $\Pi_L \neq \Pi_R$ the best matching is obtained for non-zero bias (b).

6.9.1 1D structures

Now, let us move to the case of one dimensional tunneling. The results are presented in Fig. 6.20.

In the 1D case, the decay of TMR-ratio with bias depends in a different way on the structure parameters. Namely, although here again the two different ranges of the TMR bias dependence can be observed, in the first range the decay is almost independent on s and Δ, whereas the second range it is now controlled by both of these important parameters.

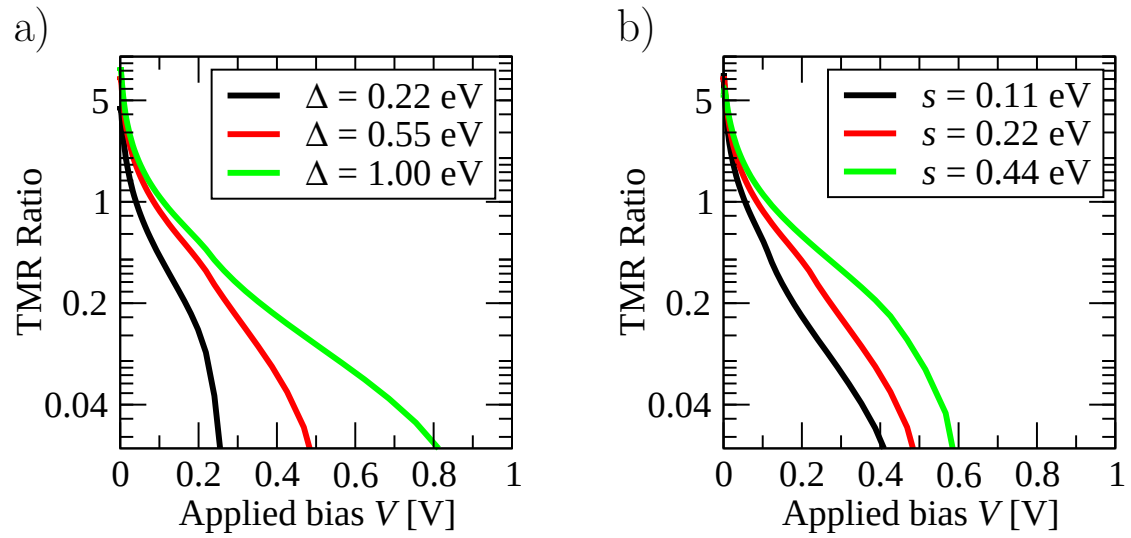

Figure 6.20: The simulated TMR-ratio for 1D tunneling in (Ga,Mn)As/$(\widetilde{\text{AlAs}})_4$/(Ga,Mn)As structure, where a) the band offset of the spacer material Δ is varied or b) the spin splitting $s = s_L = s_R$ in the magnetic leads is varied.

6.10 Comparison with the Jullière Model

The above results show that the height of the tunneling barrier in the spacer layer plays an indispensable role in the TMR bias anomaly effect. Moreover, not only the spin polarization of states in the magnetic layers, but also the appropriate matching of the **k** vectors in both leads decides about the TMR bias dependence. As shown in the previous section, Julliére model disregards the TMR dependence on the barrier height and can be obtained by assuming in the 1D free hole model an infinite barrier. Nor it takes into account the matching of the **k** vectors - Julliére model (Eq. (6.15)) predicts only a very strong dependence of TMR on the spin polarizations Π_L and Π_R. Still, we note that even according to the Julliére model the TMR-ratio depends on the applied bias. To show this dependence, we express the 3D TMR ratio in the limit of infinite barrier using the numbers of spin states in the leads, similarly to (6.14):

$$\lim_{\Delta\to\infty} TMR^{3D} = \frac{\sigma^R_{\Downarrow}\sigma^L_{\Downarrow} + \sigma^R_{\uparrow}\sigma^L_{\uparrow} - \sigma^R_{\uparrow}\sigma^L_{\Downarrow} - \sigma^R_{\Downarrow}\sigma^L_{\uparrow}}{\sigma^R_{\uparrow}\sigma^L_{\Downarrow} + \sigma^R_{\Downarrow}\sigma^L_{\uparrow}}. \tag{6.16}$$

As follows from (6.16) even in the limit of infinite barrier, the bias changes the number of spin polarized states in right lead and the TMR ratio decreases with bias. This is shown in Fig. 6.21 by the black line. Taking into account the finite height of the barrier, essentially leads to lower values of TMR and its much faster decay with the applied voltage (see Fig. 6.21). Still, for a proper choice of different spin polarizations in the magnetic leads, the applied bias can increase the **k**-vector matching and thus the TMR value.

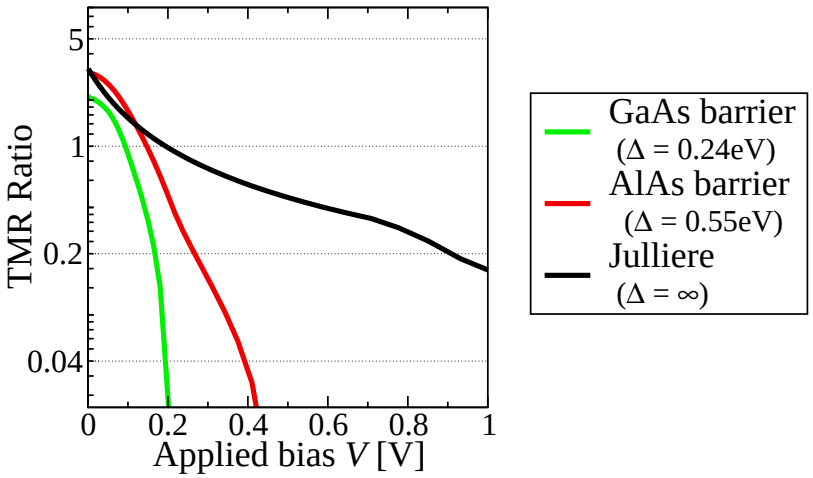

Figure 6.21: The simulated TMR-ratio for 3D tunneling in (Ga,Mn)As/$(GaAs)_4$/(Ga,Mn)As structure, (Ga,Mn)As/$(AlAs)_4$/(Ga,Mn)As structure together with the predictions of the Julliére model. The assumed spin polarization in the leads is $\Pi = 0.87$.

6.11 Nonsymmetric Leads in Tight-binding Model

We have seen that the free hole model predicts that the decrease of TMR with bias can be improved when polarizations in both lead are nonsymmetric (Fig. 6.18). This prediction can be verified with the use of the tight-binding model as shown on Fig. 6.22.

Here, again we see exactly the same trends, i.e., the inequality of the polarizations can shift the dependence in the bias regime.

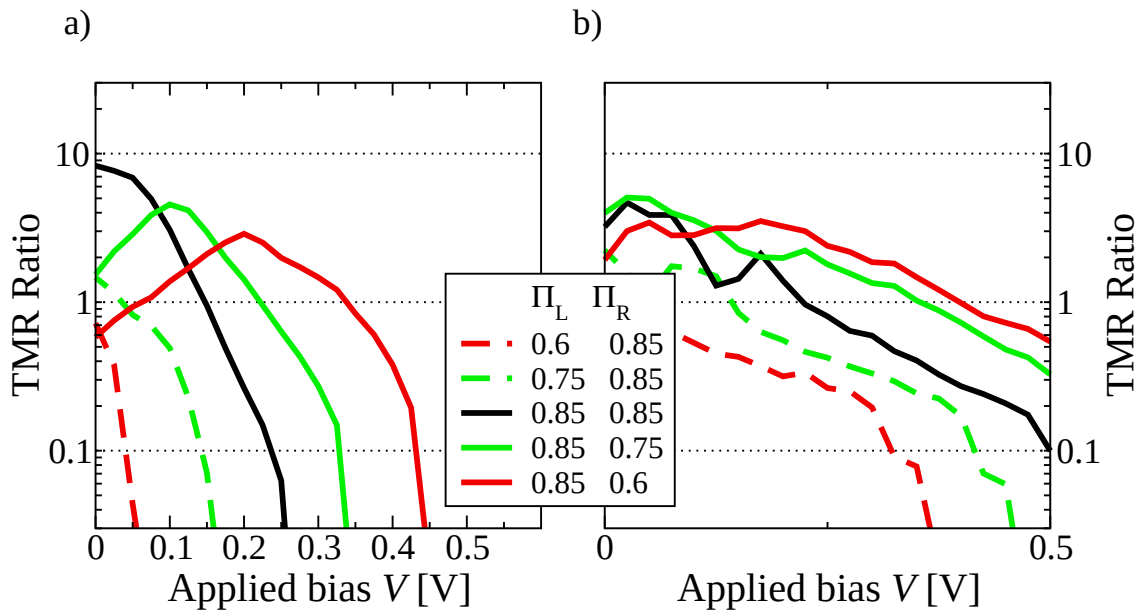

Figure 6.22: The TMR ratio calculated within the tight-binding model in a) (Ga,Mn)As/$(GaAs)_4$/(Ga,Mn)As structure, and b) (Ga,Mn)As/$(AlAs)_4$/(Ga,Mn)As structure for different spin polarizations in the left and right lead. The Mn concentration is assumed to be 8%.

Chapter 7

Summary

In conclusion, we have studied, within a tight binding model, the sensitivity of the band structure of (Ga,Mn)As-based SL to the spin configuration in successive DMS layers. Such effects describe correctly the AFM IEC between the FM layers in EuS/PbS and EuS/YbSe and are, up to now, the only effective mechanism capable to explain the origin of interlayer correlations in AFM EuTe/PbTe SL. We have shown that by this mechanism also the FM interlayer coupling in (Ga,Mn)As/GaAs SL can be described. Moreover, the model points to a possibility of engineering (Ga,Mn)As-based multilayers for obtaining an AFM interlayer coupling.

We have developed the model of quantum transport in spatially modulated structures of hole-controlled diluted ferromagnetic semiconductors, taking into account relevant features of the band structure within the tight-binding approximation. The model disregards disorder and effects of carrier–carrier interactions, so that it is applicable to the carrier density range and length scales, where localization effects are unimportant. However, the model allows for self-consistent simulations. Within the model we have analyzed the spin polarization of the injected current in a (Ga,Mn)As/(Al,Ga)As spin-LED. Our studies explain quantitatively the large spin polarization of the injected current and its strong dependence on the applied voltage, as has been recently observed in experiments. Our simulations point to an enhanced tunneling from the depleted (Ga,Mn)As and non-magnetic GaAs regions and an increase of the energy window where tunneling is allowed. The results of the tight-binding calculations of coherent tunneling indicate that the enhanced energy window of tunneling at higher bias leads to an increase of the relative contribution of the minority spin electrons in the tunnel current due to the better match of their group velocity with the group velocity of the conduction band states. Furthermore, the theory describes quantitatively a fast decay of TMR with the bias voltage without invoking inelastic processes. However, these processes together with heating of Mn spin subsystem may become crucial in the highest bias regime. The detail studies of anisotropy effects reveal the presence of C_{2v} symmetry in the magnitude of current

spin polarization in the Zener-Esaki diode. This indicates a noticeable importance of inversion asymmetry terms specific to interfaces and zinc-blende structure in tunneling structures. These effects are not taken into account within the standard kp-type approaches. According to our findings, if strain is not excessively large, the dominant anisotropy appears when the direction of magnetization changes from parallel to perpendicular to the current, in a full analogy to AMR. Finally, we have used the model to predict theoretical conditions for improving the performance of the studied devices. Our results indicate that an attempt to increase the electron concentration in the n-GaAs layer of the Zener-Esaki tunnel junction should pay off in an increase of the spin polarization of the current. For the trilayers, the calculations suggest that reducing barrier thickness and increasing barrier height may result in higher values of TMR and its slower decay with the applied bias. Moreover, we have shown that interface roughness, that cannot be avoided in the real devices should not have negative impact on the effect and might even increase TMR ratio due to effective reduction of the spacer width.

Finally, we have shown that the TMR bias anomaly in the ferromagnetic semiconductor structures can be described and understood correctly within the simple two band free hole model. This model is a convenient tool for predicting the behavior of the TMR in various structures with hole-mediated ferromagnetism in the magnetic layers. Our results show that two parameters – spin splitting in the magnetic layers and spacer barrier height – define the two range decay of TMR with bias. It is shown that the higher is the barrier in the spacer layer and the bigger is the spin-splitting in the magnetic layers the slower is the decay of the TMR ratio with the applied voltage. Additionally, we predict that the TMR decay can be reduced when asymmetric polarizations in the leads are introduced. The indispensable role played by the barrier height and $\mathbf{k}$-vector matching in the bias anomaly was further confirmed by the comparison with the Julliére model, which neglected these dependencies. Moreover, using the free hole model we have investigated the impact of the dimension of the tunneling structure on the TMR effect.

Bibliography

[1] N. Akiba, F. Matsukura, A. Shen, Y. Ohno, H. Ohno, A. Oiwa, S. Katsumoto, and Y. Iye. Interlayer exchange in (ga,mn)as/(al,ga)as/(ga,mn)as semiconducting ferromagnet/nonmagnet/ferromagnet trilayer structures. *Applied Physics Letters*, 73(15):2122–2124, 1998.

[2] M. N. Baibich, J. M. Broto, A. Fert, F. Nguyen Van Dau, F. Petroff, P. Etienne, G. Creuzet, A. Friederich, and J. Chazelas. Giant magnetoresistance of (001)fe/(001)cr magnetic superlattices. *Phys. Rev. Lett.*, 61(21):2472–2475, Nov 1988.

[3] David V. Baxter, Dmitry Ruzmetov, Julia Scherschligt, Y. Sasaki, X. Liu, J. K. Furdyna, and C. H. Mielke. Anisotropic magnetoresistance in $ga1 - xmnxas$. *Phys. Rev. B*, 65(21):212407, May 2002.

[4] J. Blinowski and P. Kacman. Interlayer exchange coupling mediated by valence-band electrons. *Phys. Rev. B*, 64(4):045302, Jun 2001.

[5] M. Bode, M. Getzlaff, and R. Wiesendanger. Spin-polarized vacuum tunneling into the exchange-split surface state of gd(0001). *Phys. Rev. Lett.*, 81(19):4256–4259, Nov 1998.

[6] M. A. Boselli, I. C. da Cunha Lima, and A. Ghazali. Indirect exchange in (ga,mn)as bilayers via the spin-polarized inhomogeneous hole gas: Monte carlo simulation. *Phys. Rev. B*, 68(8):085319, Aug 2003.

[7] L. Brey, J. Fernández-Rossier, and C. Tejedor. Spin depolarization in the transport of holes across $gaxmn1 - xas?gayal1 - yas?p - gaas$. *Phys. Rev. B*, 70(23):235334, Dec 2004.

[8] L. Brey, C. Tejedor, and J. Fernández-Rossier. Tunnel magnetoresistance in gamnas: Going beyond julli[e-grave]re formula. *Applied Physics Letters*, 85(11):1996–1998, 2004.

[9] P. Bruno. Theory of interlayer magnetic coupling. *Phys. Rev. B*, 52(1):411–439, Jul 1995.

[10] A Di Carlo. Microscopic theory of nanostructured semiconductor devices: beyond the envelope-function approximation. *Semiconductor Science and Technology*, 18(1):R1–R31, 2003.

[11] M. Chernyshova, L. Kowalczyk, M. Baran, A. Szczerbakow, T. Story, C.J.P. Smits, A.T. Filip, H.J.M. Swagten, W.J.M. de Jonge, and A.Yu. Sipatov. Temperature dependence of antiferromagnetic interlayer exchange coupling in eus–pbs multilayers. *Acta Phys. Polon. A*, 105:599–606, 2004.

[12] D. Chiba, N. Akiba, F. Matsukura, Y. Ohno, and H. Ohno. Magnetoresistance effect and interlayer coupling of (ga, mn)as trilayer structures. *Applied Physics Letters*, 77(12):1873–1875, 2000.

[13] D. Chiba, F. Matsukura, and H. Ohno. Tunneling magnetoresistance in (ga,mn)as-based heterostructures with a gaas barrier. *Physica E*, 21(2-4):966–969, march 2004.

[14] S. J. Chung, S. Lee, I. W. Park, X. Liu, and J. K. Furdyna. Possible indication of interlayer exchange coupling in gamnas/gaas ferromagnetic semiconductor superlattices. In *J. Appl. Phys. (Proceedings of the 9th Joint MMM/Intermag Conference)*, volume 95(11), pages 7402–7404. AIP, 2004.

[15] Aldo Di Carlo, P. Vogl, and W. Pötz. Theory of zener tunneling and wannier-stark states in semiconductors. *Phys. Rev. B*, 50(12):8358–8377, Sep 1994.

[16] T. Dietl, H. Ohno, and F. Matsukura. Hole-mediated ferromagnetism in tetrahedrally coordinated semiconductors. *Phys. Rev. B*, 63(19):195205, Apr 2001.

[17] H. F. Ding, W. Wulfhekel, J. Henk, P. Bruno, and J. Kirschner. Absence of zero-bias anomaly in spin-polarized vacuum tunneling in co(0001). *Phys. Rev. Lett.*, 90(11):116603, Mar 2003.

[18] P. Van Dorpe, Z. Liu, W. Van Roy, V. F. Motsnyi, M. Sawicki, G. Borghs, and J. De Boeck. Very high spin polarization in gaas by injection from a (ga,mn)as zener diode. *Applied Physics Letters*, 84(18):3495–3497, 2004.

[19] P. Van Dorpe, W. Van Roy, J. De Boeck, G. Borghs, P. Sankowski, P. Kacman, J. A. Majewski, and T. Dietl. Voltage-controlled spin injection in a (ga,mn)as/(al,ga)as zener diode. *Physical Review B (Condensed Matter and Materials Physics)*, 72(20):205322, 2005.

[20] K. W. Edmonds, K. Y. Wang, R. P. Campion, A. C. Neumann, C. T. Foxon, B. L. Gallagher, and P. C. Main. Hall effect and hole densities in ga[sub 1 - x]mn[sub x]as. *Applied Physics Letters*, 81(16):3010–3012, 2002.

[21] M. Elsen, O. Boulle, J.-M. George, H. Jaffrès, R. Mattana, V. Cros, A. Fert, A. Lemaitre, R. Giraud, and G. Faini. Spin transfer experiments on (ga,mn)as/(in,ga)as/(ga,mn)as tunnel junctions. *Physical Review B (Condensed Matter and Materials Physics)*, 73(3):035303, 2006.

[22] A. D. Giddings, M. N. Khalid, T. Jungwirth, J. Wunderlich, S. Yasin, R. P. Campion, K. W. Edmonds, J. Sinova, K. Ito, K.-Y. Wang, D. Williams, B. L. Gallagher, and C. T. Foxon. Large tunneling anisotropic magnetoresistance in (ga,mn)as nanoconstrictions. *Physical Review Letters*, 94(12):127202, 2005.

[23] R. Giraud, M. Gryglas, L. Thevenard, A. Lemaître, and G. Faini. Voltage-controlled tunneling anisotropic magnetoresistance of a ferromagnetic p[sup ++]-(ga,mn)as/n[sup +]-gaas zener-esaki diode. *Applied Physics Letters*, 87(24):242505, 2005.

[24] C. Gould, C. Rüster, T. Jungwirth, E. Girgis, G. M. Schott, R. Giraud, K. Brunner, G. Schmidt, and L. W. Molenkamp. Tunneling anisotropic magnetoresistance: A spin-valve-like tunnel magnetoresistance using a single magnetic layer. *Phys. Rev. Lett.*, 93(11):117203, Sep 2004.

[25] P. Grünberg, R. Schreiber, Y. Pang, M. B. Brodsky, and H. Sowers. Layered magnetic structures: Evidence for antiferromagnetic coupling of fe layers across cr interlayers. *Phys. Rev. Lett.*, 57(19):2442–2445, Nov 1986.

[26] Walter A. Harrision. *Electronic Structure and the Properties of Solids: The Physics of the Chemical Bond*. San Francisco: Freeman, 1980.

[27] Ioffe Physico-Technical Institute. http://www.ioffe.ru/sva/nsm/semicond/algaas/index.html.

[28] Jean-Marc Jancu, Reinhard Scholz, Fabio Beltram, and Franco Bassani. Empirical *spds** tight-binding calculation for cubic semiconductors: General method and material parameters. *Phys. Rev. B*, 57(11):6493–6507, Mar 1998.

[29] E. Johnston-Halperin, D. Lofgreen, R. K. Kawakami, D. K. Young, L. Coldren, A. C. Gossard, and D. D. Awschalom. Spin-polarized zener tunneling in (ga,mn)as. *Phys. Rev. B*, 65(4):041306, Jan 2002.

[30] E. Johnston-Halperin, D. Lofgreen, R. K. Kawakami, D. K. Young, L. Coldren, A. C. Gossard, and D. D. Awschalom. Spin-polarized zener tunneling in (ga,mn)as. *Phys. Rev. B*, 65(4):041306, Jan 2002.

[31] M. Julliere. Tunneling between ferromagnetic films. *Phys. Lett. A*, 54:225–226, 1975.

[32] T. Jungwirth, W. A. Atkinson, B. H. Lee, and A. H. MacDonald. Interlayer coupling in ferromagnetic semiconductor superlattices. *Phys. Rev. B*, 59(15):9818–9821, Apr 1999.

[33] T. Jungwirth, Jairo Sinova, K. Y. Wang, K. W. Edmonds, R. P. Campion, B. L. Gallagher, C. T. Foxon, Qian Niu, and A. H. MacDonald. Dc-transport properties of ferromagnetic (ga,mn)as semiconductors. *Applied Physics Letters*, 83(2):320–322, 2003.

[34] H. Kępa, P. Sankowski, P. Kacman, A. Yu. Sipatov, C.F. Majkrzak, and T.M. Giebultowicz. Antiferromagnetic interlayer coupling in eus/ybse superlattices. *J. Mag. Mag. Mat.*, 272-276:323–324, 2004.

[35] H. Kepa, J. Kutner-Pielaszek, J. Blinowski, A. Twardowski, C. F. Majkrzak, T. Story, P. Kacman, R. R. Galazka, K. Ha, H. J. M. Swagten, W. J. M. de Jonge abd A. Yu. Sipatov, V. Volobuev, and T. M. Giebultowicz. Antiferromagnetic interlayer coupling in ferromagnetic semiconductor eus/pbs(001) superlattices. *Europhys. Lett.*, 56(1):54–60, 2001.

[36] H. Kępa, J. Kutner-Pielaszek, A. Twardowski, C. F. Majkrzak, J. Sadowski, T. Story, and T. M. Giebultowicz. Ferromagnetism of gamnas studied by polarized neutron reflectometry. *Phys. Rev. B*, 64(12):121302, Sep 2001.

[37] H. Kępa, G. Springholz, T. M. Giebultowicz, K. I. Goldman, C. F. Majkrzak, P. Kacman, J. Blinowski, S. Holl, H. Krenn, and G. Bauer. Magnetic interactions in eute epitaxial layers and eute/pbte superlattices. *Phys. Rev. B*, 68(2):024419, Jul 2003.

[38] M. Kohda, T. Kita, Y. Ohno, F. Matsukura, and H. Ohno. Bias voltage dependence of the electron spin injection studied in a three-terminal device based on a (ga,mn)as/n[sup +]-gaas esaki diode. *Applied Physics Letters*, 89(1):012103, 2006.

[39] M. Kohda, Y. Ohno, F. Matsukura, and H. Ohno. Effect of n^+-gaas thickness and doping density on spin injection of gamnas/n^+-gaas esaki tunnel junction. *Physica E*, 32(1-2):438–441, May 2006.

[40] M. Kohda, Y. Ohno, K. Takamura, F. Matsukura, and H. Ohno. A spin esaki diode. *Japn. J. Appl. Phys.*, 40(2):L1274, 2001.

[41] M. Kohda, Y. Ohno, K. Takamura, F. Matsukura, and H. Ohno. A spin esaki diode. *Jpn. J. Appl. Phys.*, 40:L1274, 2001.

[42] Per-Olov Löwdin. On the non-orthogonality problem connected with the use of atomic wave functions in the theory of molecules and crystals. *The Journal of Chemical Physics*, 18(3):365–375, 1950.

[43] Paolo Lugli, Aldo Di Carlo, and Andrea Reale. Modelling of semiconductor nanostructured devices within the tight-binding approach. *Journal of Physics: Condensed Matter*, 11(31):6035–6043, 1999.

[44] F. Matsukura, H. Ohno, and T. Dietl (edited by K. H. J. Buschow). *Handbook of Magnetic Materials*, volume 14. North-Holland, Amsterdam, 2002.

[45] R. Mattana, J.-M. George, H. Jaffrès, F. Nguyen Van Dau, A. Fert, B. Lépine, A. Guivarc'h, and G. Jézéquel. Electrical detection of spin accumulation in a p-type gaas quantum well. *Phys. Rev. Lett.*, 90(16):166601, Apr 2003.

[46] A. Mikkelsen, L. Ouattara, H. Davidsson, E. Lundgren, J. Sadowski, and O. Pacherova. Mn diffusion in ga[sub 1 - x]mn[sub x]as/gaas superlattices. *Applied Physics Letters*, 85(20):4660–4662, 2004.

[47] J. S. Moodera, Lisa R. Kinder, Terrilyn M. Wong, and R. Meservey. Large magnetoresistance at room temperature in ferromagnetic thin film tunnel junctions. *Phys. Rev. Lett.*, 74(16):3273–3276, Apr 1995.

[48] H. Ohno, N. Akiba, F. Matsukura, A. Shen, K. Ohtani, and Y. Ohno. Spontaneous splitting of ferromagnetic (ga, mn)as valence band observed by resonant tunneling spectroscopy. *Applied Physics Letters*, 73(3):363–365, 1998.

[49] Y. Ohno, D. K. Young, B. Beschoten, F. Matsukura, H. Ohno, and D. D. Awschalom. Electrical spin injection in a ferromagnetic semiconductor heterostructure. *Nature*, 402:790–792, December 1999.

[50] J. Okabayashi, A. Kimura, O. Rader, T. Mizokawa, A. Fujimori, T. Hayashi, and M. Tanaka. Electronic structure of ga1-xmnxas studied by angle-resolved photoemission spectroscopy. *Physica E*, 10(1-3):192–195, may 2001.

[51] V. Osinniy, K. Dybko, A. Jedrzejczak, M. Arciszewska, W. Dobrowolski, T. Story, M. V. Radchenko, V. I. Sichkovskiy, G. V. Lashkarev, S. M. Olsthoorn, and J. Sadowski. Thermoelectric studies of electronic properties of ferromagnetic GaMnAs layers. *ArXiv Condensed Matter e-prints*, September 2004.

[52] S. S. P. Parkin. Systematic variation of the strength and oscillation period of indirect magnetic exchange coupling through the 3d, 4d, and 5d transition metals. *Phys. Rev. Lett.*, 67(25):3598–3601, Dec 1991.

[53] A. G. Petukhov, A. N. Chantis, and D. O. Demchenko. Resonant enhancement of tunneling magnetoresistance in double-barrier magnetic heterostructures. *Phys. Rev. Lett.*, 89(10):107205, Aug 2002.

[54] C. L. Platt, B. Dieny, and A. E. Berkowitz. Spin-dependent tunneling in hfo[sub 2] tunnel junctions. *Applied Physics Letters*, 69(15):2291–2293, 1996.

[55] C. Rüster, C. Gould, T. Jungwirth, J. Sinova, G. M. Schott, R. Giraud, K. Brunner, G. Schmidt, and L. W. Molenkamp. Very large tunneling anisotropic magnetoresistance of a (ga,mn)as/gaas/(ga,mn)as stack. *Physical Review Letters*, 94(2):027203, 2005.

[56] C. Rüster, C. Gould, T. Jungwirth, J. Sinova, G. M. Schott, R. Giraud, K. Brunner, G. Schmidt, and L. W. Molenkamp. Very large tunneling anisotropic magnetoresistance of a (ga,mn)as/gaas/(ga,mn)as stack. *Physical Review Letters*, 94(2):027203, 2005.

[57] H. Saito, S. Yuasa, and K. Ando. Origin of the tunnel anisotropic magnetoresistance in ga[sub 1-x]mn[sub x]as/znse/ga[sub 1-x]mn[sub x]as magnetic tunnel junctions of ii-vi/iii-v heterostructures. *Physical Review Letters*, 95(8):086604, 2005.

[58] P. Sankowski and P. Kacman. Interlayer coupling in eus-based superlattices (dependence on the energy structure of non-magnetic layer). *Acta Phys. Pol. A*, 103:621–628, 2003.

[59] P. Sankowski, P. Kacman, J. A. Majewski, and T. Dietl. Spin-dependent tunneling in modulated structures of (ga,mn)as. *Physical Review B (Condensed Matter and Materials Physics)*, 75(4):045306, 2007.

[60] Paulo V. Santos, M. Willatzen, M. Cardona, and A. Cantarero. Tight-binding calculation of spin splittings in semiconductor superlattices. *Phys. Rev. B*, 51(8):5121–5129, Feb 1995.

[61] M. Sawicki, F. Matsukura, A. Idziaszek, T. Dietl, G. M. Schott, C. Ruester, C. Gould, G. Karczewski, G. Schmidt, and L. W. Molenkamp. Temperature dependent magnetic anisotropy in (ga,mn)as layers. *Phys. Rev. B*, 70(24):245325, Dec 2004.

[62] M. Sawicki, K.-Y. Wang, K. W. Edmonds, R. P. Campion, C. R. Staddon, N. R. S. Farley, C. T. Foxon, E. Papis, E. Kamińska, A. Piotrowska, T. Dietl, and B. L. Gallagher. In-plane uniaxial anisotropy rotations in (ga,mn)as thin films. *Physical Review B (Condensed Matter and Materials Physics)*, 71(12):121302, 2005.

[63] J. C. Slater and G. F. Koster. Simplified lcao method for the periodic potential problem. *Phys. Rev.*, 94(6):1498–1524, Jun 1954.

[64] J. C. Slonczewski. Conductance and exchange coupling of two ferromagnets separated by a tunneling barrier. *Phys. Rev. B*, 39(10):6995–7002, Apr 1989.

[65] C. J. P. Smits, A. T. Filip, H. J. M. Swagten, B. Koopmans, W. J. M. de Jonge, M. Chernyshova, L. Kowalczyk, K. Grasza, A. Szczerbakow, T. Story, W. Palosz, and A. Yu. Sipatov. Antiferromagnetic interlayer exchange coupling in all-semiconducting *eus?pbs?eus* trilayers. *Phys. Rev. B*, 69(22):224410, Jun 2004.

[66] C. Strahberger and P. Vogl. Model of room-temperature resonant-tunneling current in metal/insulator and insulator/insulator heterostructures. *Phys. Rev. B*, 62(11):7289–7297, Sep 2000.

[67] W. Szuszkiewicz, E. Dynowska, B. Hennion, F. Ott, M. Jouanne, and J.F. Morhange. Interlayer exchange coupling in short period gamnas/gaas superlattices. *Acta Phys. Pol. A*, 100:335–342, 2001.

[68] M. Tanaka and Y. Higo. Large tunneling magnetoresistance in gamnas /alas /gamnas ferromagnetic semiconductor tunnel junctions. *Phys. Rev. Lett.*, 87(2):026602, Jun 2001.

[69] P. M. Tedrow and R. Meservey. Spin-dependent tunneling into ferromagnetic nickel. *Phys. Rev. Lett.*, 26(4):192–195, Jan 1971.

[70] K. Y. Wang, R. P. Campion, K. W. Edmonds, M. Sawicki, T. Dietl, C. T. Foxon, and B. L. Gallagher. Magnetism in (ga,mn)as thin films with tc up to 173k. 2004.

[71] Wulf Wulfhekel and Jürgen Kirschner. Spin-polarized scanning tunneling microscopy on ferromagnets. *Applied Physics Letters*, 75(13):1944–1946, 1999.

[72] Y. Yafet. Ruderman-kittel-kasuya-yosida range function of a one-dimensional free-electron gas. *Phys. Rev. B*, 36(7):3948–3949, Sep 1987.

[73] K. M. Yu, W. Walukiewicz, T. Wojtowicz, W. L. Lim, X. Liu, Y. Sasaki, M. Dobrowolska, and J. K. Furdyna. Determination of free hole concentration in ferromagnetic ga[sub 1 - x]mn[sub x]as using electrochemical capacitance–voltage profiling. *Applied Physics Letters*, 81(5):844–846, 2002.